UNDERSTANDING HYDROGEOMORPHIC INFLUENCES ON STREAM NETWORK DENITRIFICATION AND TEMPERATURE DYNAMICS

by

Samuel Paul Carlson

A dissertation submitted in partial fulfillment
of the requirements for the degree

of

Doctor of Philosophy

in

Ecology and Environmental Science

MONTANA STATE UNIVERSITY
Bozeman, Montana

April 2020

ACKNOWLEDGEMENTS

I would like to thank the numerous people who have helped and supported me throughout the development and refinement of the work specified here, including Dr. Geoff Poole, Dr. Robert Payn, Dr. Stephanie Ewing, Dr. Wyatt Cross, Dr. Robert Hall, Hannah Rasker, Dave & Mary Lou Carlson, and Oscar Raskelson. Funding for this work was provided by NSF grant # 1145616, with additional support from the MSU Grad School, and the Department of Land Resources and Environmental Sciences.

TABLE OF CONTENTS

TABLE OF CONTENTS – CONTINUED

TABLE OF CONTENTS – CONTINUED

LIST OF TABLES

LIST OF TABLES – CONTINUED

Table Page

LIST OF FIGURES

LIST OF FIGURES – CONTINUED

Figure Page

LIST OF FIGURES – CONTINUED

Figure Page

LIST OF FIGURES – CONTINUED

Figure Page

ABSTRACT

The removal of nitrate from stream networks through the process of denitrification is an important component of local and regional nutrient cycles, but the controls on stream network denitrification rates remain poorly understood. Previous work has demonstrated general effects of stream channel size and nitrate loading rates on network-scale denitrification rates, but has been unable to elucidate connections between the complex environmental template of streams, and resulting denitrification rates. Understanding links between land use and management practices, physical characteristics of streams, and stream denitrification rates is critical to interpreting observed patterns of nitrate in freshwater systems and forming holistic management strategies for reducing the negative effects of elevated nitrate concentrations. To address these critical uncertainties, I developed a stream network simulation model that incorporates the effects of whole-stream aerobic respiration on biotic denitrification demand. This model is applied to a small, subalpine stream network under scenarios designed to explore: 1) the implications of temperature-controlled, network scale patterns of respiration rates on the distribution and overall magnitude of stream network denitrification, and 2) the effect of logging-induced channel simplification on whole network denitrification rates. The first analysis is complimented by an evaluation of controls on stream temperature across this network, revealing the spatially and temporally variable influence of in-network lakes on stream temperatures. Results from the first analysis suggest that reach- and network-scale denitrification rates are strongly influenced by respiration rate and temperature when nitrate supplies are high relative to removal rates, indicating an increased contribution of lower, warmer streams to whole-network denitrification. The second analysis reveals that historical logging has caused a $\sim$30% loss of stream network denitrification capacity, which is manifested as a corresponding reduction in whole-network denitrification rates when nitrate supplies are not limiting. In sum, this work emphasizes the diverse set of factors that influence reach- and watershed-scale biogeochemical characteristics and processes, and suggests that land management actions which influence stream morphology may also alter stream denitrification rates.

1

INTRODUCTION

Anthropogenic alterations of nutrient cycles arise from both the production and distribution of nutrients, and from alterations to the environmental conditions in which nutrient cycling occurs. Although the cycles of many nutrients have been altered by human activity to some degree, the alteration of nitrogen (N) cycles is especially widespread and consequential [Galloway et al., 2004, Vitousek et al., 1997], due to the synthetic production of reactive N for fertilizer and the incidental production of reactive N through the combustion of fossil fuels. Together, these processes have approximately doubled the global rate of reactive N production [Galloway et al., 1995]. N budgets of terrestrial and marine systems are both affected by N deposition, while only terrestrial systems are directly impacted by fertilizer inputs [Fowler et al., 2013]. Elevated N concentrations in terrestrial systems result in increased N losses to groundwater, streams, and lakes [Aber et al., 1989]. Terrestrial N cycles are therefore linked to freshwater N cycles, and further linked to marine N cycles by N transport in streams in rivers. However, the N budgets of freshwater systems are not a simple function of N inputs, as N can be assimilated into biomass, released from biomass, and removed from the system entirely through the process of denitrification. Understanding the transport, retention, and removal of N in freshwater systems is therefore critical to interpreting and managing N pollution globally.

The behavior of N in streams and rivers is constrained by the physical, chemical, hydrological, and geomorphic characteristics of these systems [Groffman et al., 2005, Dodds, 2006, Wollheim et al., 2006, Craig et al., 2008, Alexander et al., 2009, Briggs et al., 2014, Helton et al., 2018]. Although the large-scale implications

of these constraints remain poorly understood [Boyer et al., 2006, Helton et al., 2011], anthropogenic alterations of stream characteristics are likely to substantially alter N removal from stream systems. My work addresses the potential effect of anthroprogenic alterations of stream characteristics on stream N removal through the development and application of a simulation model capable of explicitly representing connections among stream hydrogeomorphology, temperature, aerobic respiration rate, and denitrification rate. I introduce my work with a summary of stream N cycling concepts, previous approaches for quantifying stream denitrification rates, and the current understanding of controls on network-scale denitrification rates. Subsequently, in combination with an examination of the spatially and temporally variable controls on water temperature across a stream-lake network documented in Ch. 2, I develop a simulation model to explore the effects of hypothetical temperature-driven patterns of respiration on the overall magnitude and spatial distribution of denitrification across a montaine stream network in Ch. 3. Finally, I use this simulation model to analyze the loss of network-scale denitrification capacity that results from hydrogeomorphic simplification associated with historical logging in Ch. 4.

The radical alteration of the global N cycle has cascading effects on ecosystems and human communities [Galloway et al., 2003]. Elevated N levels are linked to increased primary productivity in freshwater systems, estuaries, and coastal regions (eutrophication), ultimately leading to the depletion dissolved oxygen during the decomposition of algal or plant biomass, and dramatic alterations of benthic and palegic community structure [Rabalais et al., 2002, Diaz and Rosenberg, 2008]. While elevated concentration of other nutrients may also contribute these varied effects of eutrophication [Anderson et al., 2002], nitrate is suggested to be a primary to the eutrophic 'dead zone' in the Gulf of Mexico [Dodds, 2006, Howarth and

Marino, 2006]. Additionally, elevated nitrate levels in drinking water is known to cause or contribute to a variety of serious human health concerns, including infant methemoglobinemia, specific birth defects and cancers, and thyroid disease, even when nitrate concentrations were below regulatory thresholds [Ward et al., 2018].

Despite the extensive impacts of elevated N, substantial reduction or elimination of anthropogenic sources of N is impractical due to the integration of N sources into human food production, manufacturing, and transportation. Optimal management of N therefore requires a quantitative understanding of the numerous anthropogenic and natural source and sink pathways [Mitsch et al., 2001, Driscoll et al., 2003]. However, observing the magnitude of these pathways is complicated by the spatial and temporal variability of N sources, and the challenge of separating denitrification from temporary N sinks, such as biotic assimilation, that do not remove N from the stream system.

Stream Nitrogen Cycling

As in terrestrial, marine, and other freshwater systems, nitrogen cycling in streams is characterized by biologically mediated transformations among multiple inorganic and organic forms. Streams receive N in organic form from terrestrial systems as detritus, dissolved organic matter, and biomass, and receive inorganic N as dissolved nitrate, nitrite, and ammonium through groundwater contributions and atmospheric deposition. Additionally, inorganic dinitrogen (N_2) gas is is exchanged between the atmosphere and dissolved form in streamwater. In addition to exporting N in all of these forms to downstream lakes, estuaries, and oceans, streams lose N through the process of denitrification, which transforms inorganic nitrate into dinitrogen gas.

Nitrate, nitrite, and ammonium are reactive forms of inorganic N that are

available for biotic use, while inorganic dinitrogen gas is considered nonreactive and unavailable to biota (except for nitrogen fixers). Dinitrogen gas is ubiquitous in the atmosphere, and is therefore present in dissolved form in streamwater. However, dinitrogen is made available only through the the energetically intensive process of N fixation, which transforms dinitrogen to ammonia and ammonium. N fixation processes, both biotic and abiotic, largely take place outside of streams, and drive the global availability of reactive N species. Biotic N fixation in streams is not typically a substantial portion of the overall N budgets of most streams and stream networks. However, substantial rates of N fixation have been documented for specific streams, microhabitats, or moments in time for which available forms of N are limiting, and environmental conditions are conducive to N fixation [Stewart, 1970, Horne, 1975, Grimm and Fisher, 1986, Kunza and Hall, 2014]. Thus, most reactive inorganic N in streams is either sourced from external inputs or from the decomposition of organic matter which commonly yields ammonium. Under the typically well-oxygenated conditions in stream waters, ammonium is often rapidly transformed into nitrate via nitrification. As a result of the favorability of nitrification, the majority of inorganic reactive N in streams is commonly present as nitrate.

Nitrate can be removed from stream water through the process of denitrification, although denitrification is only favorable under anoxic conditions. Nitrification and denitrification are both multi-step processes with numerous intermediate compounds, and can evolve small amounts of other products, including nitrous oxide and NO_X species. While the production of partially oxidized species of nitrogen has global significance due to the atmospheric residence time and greenhouse potential of nitrous oxide in particular, analysis of isotopic tracers suggests that less than 1% of the total mass of N denitrified in streams ends up as nitrous oxide [Beaulieu et al., 2010]. Denitrification using organic carbon as an energy source is often assumed to be the

main pathway by which nitrate is lost from stream systems, although other pathways, including iron-driven denitrification, sulfur-driven nitrate reduction, and anammox, may result in similar gaseous losses [Burgin and Hamilton, 2007].

Organic forms of N include N in biomass, and N in organic molecules freed by decomposition or excretion biotic processes. N is assimilated into autotrophic biomass through the uptake of available inorganic N. Therefore, rates of inorganic N uptake are coupled with rates of primary production [Fellows et al., 2006]. In contrast, heterotrophic organisms can acquire N in organic form.

Dissolved forms of N in streams move with streamwater, while N that is assimilated into biomass is likely to be static. Therefore, the cycling of N between dissolved inorganic, dissolved organic, and assimilated forms takes on a longitudnal dimension, and is commonly conceptualized as as a nutrient spiral [Newbold et al., 1981]. For processes that are assumed to occur primarily in the stream benthos, the influence of uptake on N spirals can be quantified as the areal uptake rate U (i.e., flux), the uptake velocity v_f, (i.e., the ratio of the areal uptake rate to the stream concentration), and the mean downstream transit distance before uptake, S_w. Denitrification rates are generally tied to the activity of biota associated with the stream bed or benthic region [Inwood et al., 2007, Böhlke et al., 2009], and can therefore be intuitively described in terms of U, V_f, and S_w.

The N content of a stream at a given location results from N inputs from that stream's watershed, as modified by upstream N cycling and removal. By providing an integrated measure of the aqueous export, the analysis of a stream provides a convenient perspective on the nutrient losses of a small watershed [Bormann and Likens, 1967]. However, given the diversity of forms and pathways of stream N cycles, it is unsurprising that watershed scale N budgets fail to explain stream N concentrations [Campbell et al., 2004]. Instead, stream nitrate export is often

substantially lower than total watershed nitrate inputs due to the storage or removal of nitrate across a stream network [Boyer et al., 2002]. This nitrate retention can change over time with changing stream characteristics, leading to trends in stream nitrate concentrations that are uncoupled from trends in nitrate loading from upland sources [Bernhardt et al., 2005]. In-stream processes can also attenuate pulse releases of N from from upland systems [Bernhardt et al., 2003], especially under conditions where disturbances effecting the release of N from upland systems also affect in-stream demand for N [Hall, 2003]. The extent to which in-stream processes are capable of altering watershed N export may diminish when sufficiently large N concentrations cause the saturation of N uptake and removal pathways, thus leading to a closer connection between stream N loading and watershed export under some conditions [Bernot and Dodds, 2005]. A detailed understanding of the controls on stream N retention and removal is critical to understanding how N loads are affected by in-stream N processing, and therefore how N exports are controlled by both N loads and in-stream processes [Helton et al., 2011].

Examination of spatial patterns of nitrate loads and stream nitrate concentrations reveals unequivocal evidence of nitrate removal across stream networks, likely due to stream denitrification [Burns, 1998, Smith et al., 1997, van Breemen et al., 2002]. Although denitrification does not restore nitrate concentrations down to pre-industrial levels [Galloway et al., 2004], stream denitrification plays an important role in the regulating the aquatic impacts of elevated reactive N production, and is therefore a necessary component of holistic approaches for managing N pollution [Mitsch et al., 2001, Driscoll et al., 2003]. However, direct observation of the extent to which stream denitrification reduces stream nitrate concentrations is made difficult by the spatial and temporal variability in N sources, along with the variety of in-stream processes that produce or consume nitrate. This work uses a simulation modeling

approach to explore how stream characteristics may constrain the magnitude of network-scale denitrification, as well as the distribution of denitrification rates across stream networks.

Measuring Stream Denitrification Rates

Existing methods for measuring denitrification are only practical at specific scales, and are limited in their ability to provide direct estimates of denitrification rates across large and heterogenious stream networks. Stream denitrification rates can be estimated through ex-situ experiments that contain a small volume of stream water and/or benthic substrate within a chamber, and through in-situ observations that attempt to quantify dinitrogen production across a stream reach [Groffman et al., 2006]. Ex-situ experiments can produce precise measures of realized denitrification rates, and can be used to experimentally identify correlates of and controls on denitrification rates, however extrapolation from ex-situ measurements to whole-stream denitrification rates introduces numerous challenges and sources of error. In contrast, in-situ estimates of stream denitrification directly represent whole-stream rates without the need for extrapolation, but are more expensive than ex-situ methods, and have greater associated uncertainty.

Ex-situ measurement of stream denitrification

Methods for ex-situ experiments often leverage the controlled environment of a sealed chamber to track denitrification through measurements of changes in dissolved and headspace gasses. This approach allows for the direct quantification of the products of denitrification, including dinitrogen gas, nitrous oxide, and NO_X species. Measurement uncertainty of this approach can be further reduced by measuring changes in the molecular ratio of N_2:Ar, instead of or in addition to measuring

absolute changes in dintirogen concentration [Groffman et al., 2006]. Additionally, the denitrification process can be altered in experimental chambers by the introduction of acetylene into the chamber environment, which suppresses the final chemical transformation of denitrification and results in the production of nitrous oxide instead of dinitrogen gas. As nitrous oxide is rare in stream environments, the production of nitrous oxide can be measured with greater accuracy [Christensen et al., 1990, Martin et al., 2001, Arango et al., 2007]. These chamber scale budget approaches can be combined with measurements of other indicators or correlates of denitrification. Combined measurements of the production of dinitrogen gas and the consumption of oxygen through the process of respiration give insight into the association between these two metabolic processes [Madinger and Hall, 2019]. Additionally, measurements of denitrification enzyme activities associated with benthic sediments in incubatated samples taken from different geomorphic structures suggest a context-dependant relationship between activity of denitrification enzymes, and the organic content of the incubated sample [Groffman et al., 2005].

Ex-situ experiments represent samples taken from a specific environment within a stream, while stream denitrification occurs at varied rates across water column, benthic, and hyporheic environments [Reisinger et al., 2016]. Further, ex-situ experiments necessarily isolate the observed microcosm from important stream processes, such as upwelling or downwelling across across water-sediment interfaces, and the production and delivery of oxygen, nitrate, and organic carbon. Therefore, observed denitrification rates in ex-situ experiments cannot be assumed to be equal to rates for equivalent stream environments. Ex-situ experiments have strong potential for revealing fine-scale correlates of and controls on denitrification rates within specific stream environments, but whole-stream denitrification rates can not be accurately determined from ex-situ experiments.

In-situ measurement of stream denitrification

In-situ approaches provide a direct estimate of denitrification rates across heterogeneous stream reaches containing numerous hydrological and metabolic processes, yet ongoing gas exchange between stream water and atmosphere limit the accuracy of N budget approaches. Rates of whole-stream aerobic respiration can be inferred from observed rates of production and consumption of dissolved oxygen, after accounting for atmospheric gas exchange [Appling et al., 2018]. A similar approach might be considered for denitrification rates by measuring the production of dinitrogen gas. However, the uncertainty associated with this budget approach is substantially greater for denitrification than for aerobic respiration, due to the tiny magnitude of dinitrogen production relative to the stream and atmospheric dinitrogen content. Such N budget approaches are capable of detecting high rates of denitrification under some circumstances, but are incapable of detecting denitrification when rates are low, or when groundwater contributions of nitrate or dinitrogen are large [Böhlke et al., 2009]. At sufficiently large scales, N budget approaches tracking only the depletion of transported N can provide estimates of denitrification rates [Smith et al., 1997], although such approaches include substantial uncertainty associated with the N yield of terrestrial systems. Further, such large scale approaches cannot distinguish between N assimilation, denitrification, or other processes which remove N from stream systems.

Many of the challenges associated with in-situ approaches for estimating denitrification rates can be overcome though the release and collection of isotopically labeled N [Groffman et al., 2006, Mulholland et al., 2009]. This process typically consists of the release of 15N-nitrate in sufficient quantity to enrich the isotopic composition of the stream nitrate pool, without substantially altering stream nitrate concentrations. Thereafter, different forms of stream N are sampled, and the rates of transformation

of N into these different forms are inferred from the isotopic composition of the samples. This approach allows for the quantification of denitrification-associated depletion of stream nitrate, and dinitrogen production, despite the presence of multiple other fluxes which alter stream nitrate and dinitrogen content [Böhlke et al., 2004, Mulholland et al., 2009]. However, this approach is limited in scale to stream reaches that are of sufficient length to show measurable isotopic enrichment of dissolved dinitrogen gas, while also short enough to minimize the dilution of the 15N-nitrate pool due to the contribution of nitrate from lateral terrestrial or groundwater sources.

Observed Controls on Denitrification Rates

While methods for measuring stream denitrification rates are limited to point or reach scales, understanding the cascading effects of elevated nitrate levels requires approaches for extending measured denitrification rates to unmeasured locations and scales. Approaches for extending measurements from reach to network scales generally rely on identifying controls on or correlates of observed denitrification rates in order to predict denitrification rates based on more easily measured or remotely sensed properties. While there a large number of controls on denitrification rates have been observed across a variety of ex- and in-situ measurements, incorporating all known controls into the extrapolation of denitrification rates is not feasible due to the biogeochemical complexity of stream environments. Instead, approaches that selectively incorporate empirically based and mechanistically reasonable controls on denitrification rates provide an optimal approach that provides reasonable predictive power while avoiding excessive complexity [Boyer et al., 2006]. Observed controls on denitrification rates that may provide an optimal predictive model include the concentrations of nitrate and oxygen in streamwater, stream temperature, benthic

organic carbon content, and stream aerobic respiration rates.

Numerous studies have identified an association between stream nitrate concentrations and stream denitrification rates. Ex-situ approaches have documented an association between denitrification rates and nitrate concentrations under conditions where carbon is not limiting, although this association has been less clear under nitrate saturated, carbon poor conditions [Inwood et al., 2007]. In-situ approaches have identified a similar association, that is quantified as a positive, yet less than compensatory, correlation between stream nitrate concentrations and denitrification uptake rates [Böhlke et al., 2009, Mulholland et al., 2008]. This relationship between stream nitrate concentration and denitrification rate is entirely reasonable from a mechanistic perspective, as it differs little from the Michaelis–Menten kinetics used to describe the relationship between the concentration of a substrate, and the rate of an enzymatically-catalyzed reaction.

The concentration of dissolved oxygen is another factor that has been shown to correspond with denitrification rates. For ex-situ incubations, denitrification rates appear to be inversely related to oxygen concentrations, suggesting that denitrification rates may be limited by the depth to which oxic conditions extend into benthic substrates [Christensen et al., 1990]. This effect further suggests a diel pattern in denitrification rates, with photosynthetic oxygen production limiting denitrification in upper benthic environments during the daytime. Due to the biotic production and consumption of oxygen, oxygen concentrations are highly variable across the water column, benthic, and hyporheic components of a stream. Thus, in-situ approaches have not identified correlations between water-column oxygen concentrations and whole-stream denitrification rates [Mulholland et al., 2009]. Although denitrificaiton under oxic conditions has been observed [Marchant et al., 2017], thermodynamic principles suggest that aerobic respiration would be favored over denitrification when

oxygen concentrations are sufficient. The relationship between oxygen concentrations and denitrification rates therefore makes mechanistic sense at the scale of a single micro-environment, but may be confounded by spatial and temporal heterogeneity in attempts to apply it to whole stream reaches or networks.

Because denitrification is typically fueled by organic carbon, the amount of organic carbon present is unsurprisingly found to correlate with denitrification rates when other factors are not limiting. The carbon content of sediment cores has been found to correspond to denitrification rates in ex-situ incubation experiments [Arango et al., 2007, Böhlke et al., 2009, Inwood et al., 2007], while fine benthic organic matter has been identified as a weak correlate of whole stream denitrification rates [Mulholland et al., 2009]. However, not all forms of organic carbon are equivalent in their availability to fuel denitrification, and the availability of organic carbon for a specific metabolic process is difficult to directly quantify at the scale of a stream reach. Further, as denitrification consumes organic carbon, denitrification rates of a particular stream environment could be correlated with the delivery of carbon to that stream environment, rather than storage of carbon in that environment, at some scales. The relationship between denitrification rate and the availability of organic carbon is therefore mechanistically clear, although limited in it applicability due to the challenges in quantifying carbon availability.

While the distribution and role of oxygen depleted and organic carbon rich microzones across stream reaches is poorly understood, estimates of whole-stream aerobic respiration rate may provide some indication of both conditions. Because aerobic respiration consumes oxygen, and requires available organic carbon, streams with low aerobic respiration rates may be expected to have low denitrification rates due to a lack of available organic carbon, while streams with high aerobic respiration rates may be expected to have higher quantities of available carbon and to be

associated with oxygen depleted microzones when water velocities (and thus the rate of dissolved oxygen supply) are low. This relationship between aerobic respiration rate and denitrification rate may therefore provide a coherent integration of the effects of oxygen concentration and carbon availability on respiration rate, although it may break down under conditions where aerobic respiration rates are strongly limited by the availability of organic carbon, thus resulting in the depletion of carbon but not oxygen. Reach-scale observations reveal a clear relationship between whole-stream aerobic respiration rates and denitrification rates [Mulholland et al., 2009], with respiration rates proving to be the second strongest correlate (after nitrate concentration) of biotic demand for denitrification. Additionally, a strong relationship has been observed between measures of whole-stream aerobic respiration rates, and chamber-scale measures of denitrification rates [Madinger and Hall, 2019], suggesting that the relationship between aerobic respiration rate and denitrificaiton rate indicates stream characteristics favorable for both processes.

Temperature is known to influence the rates of many biotic processes, therefore, stream temperatures may be expected to modulate rates of both denitrification and aerobic respiration. Temperature dependence of denitrification rates have been observed in experimental incubations when denitrificaiton is not limited by other factors, and is suggested to contribute to seasonal variation in network-scale nitrate removal [Alexander et al., 2009]. Further, watershed-scale N budgets suggest that temperature differences may modulate network-scale denitrificaiton rates [Schaefer and Alber, 2007].

Denitrification rates of stream reaches and networks may also be constrained by stream hydrogeomorphology in a number of ways. Stream width and velocity directly control the exposure of stream nitrate to benthic environments, and may further alter the volume and character of the stream benthos. Stream velocity alters

the fractional removal of nitrate across a stream reach, even if denitrification rates remain constant [Newbold et al., 1981, Dodds, 2006]. Additionally, if biotic demand is held constant, a deeper and wider stream reach removes more nitrate than a shallower and narrower, but otherwise identical stream reach. The general relationship between streamflow, velocity, and width [Leopold and Maddock Jr., 1953] therefore implies an underlying network-scale pattern of fractional nitrate removal, suggesting greater fractional removal from high order streams with lower gradients, slower velocities, and larger widths [Wollheim et al., 2006]. However, links between variations in surface hydrology and the magnitude of hyporheic exchange [Hall et al., 2009], along with non-constant denitrification rates [Mulholland et al., 2008] may overwhelm these fundamental effects in some cases. Distributions of the fractional removal of nitrate due to denitrification across stream networks are therefore influenced by stream hydrogeomorphology and factors which influence denitrification rates, as well as any interactions between the two.

Understanding Network Scale Denitrification

N budget approaches have demonstrated the significance of nitrate removal across stream networks [Burns, 1998, Smith et al., 1997, van Breemen et al., 2002, Galloway et al., 2003, Schaefer and Alber, 2007], but the uncertainty associated with quantifying all nitrate sources and sinks limits the accuracy of these approaches and other large-scale measurements of denitrification rates [Groffman et al., 2006]. Models offer an alternative approach to explore how reach-scale measurements may extrapolate to network scales, and can be used to infer primary controls on the magnitude and distribution of network-scale denitrification. Spatially explicit simulation modeling approaches are beneficial for scaling from reach to network scales, as they can simulate both the serial processing of nitrate, and the distributed

inputs of water and nitrate across a stream network. Modeling approaches that selectively incorporate empirically supported and mechanistically reasonable controls on denitrification can facilitate an exploration of the primary controls on network-scale denitrification and our ability to explain patterns in the variation of observed stream nitrate concentrations [Helton et al., 2011].

Previous modeling approaches have incorporated some hydrogeomorphic controls on reach-scale denitrification, along with a relationship between nitrate concentrations and denitrification rate. Using an empirical dataset describing the decay in transported nitrate between nested watersheds [Smith et al., 1997], regional-scale simulations conducted by Alexander et al. [2000] suggest effects of streamflow and channel size on denitrification fractions. Additionally, these simulations suggest that a greater portion of the nitrate entering a stream network in smaller streams that are more distant from the outflow is denitrified, and that a smaller portion of the nitrate loads entering larger streams is denitrified. A further development of this model incorporated the effects of seasonal variations in streamflow and nitrate loads, and suggested that nitrate removal rates are highest during late summer time periods [Alexander et al., 2009]. A separate model developed by Mulholland et al. [2008] explicitly accounts for the relationship between nitrate concentration and denitrification rates along with the effects of streamflow and channel width, and demonstrates the response of whole-network denitrification to varied nitrate loading rates, suggesting a disproportionate contribution of small streams to whole-network denitrification.

These previous models provide substantial insight into the potential magnitudes of stream network denitrification across a range of nitrate loading conditions, and suggest generalized hydrogeomorphic controls on the distribution of denitrification across a stream network. However, the ability of these models to explain observed

patterns of stream nitrate concentrations may be limited by the lack of simulated heterogeneity in stream conditions, and thus denitrification rates [Groffman et al., 2009]. Further, these models have a minimal ability to represent the consequences of land use and management actions for stream network denitrification, thus limiting their applicability to the management of N pollution [Mitsch et al., 2001].

While many factors could be incorporated into network scale denitrification models to improve their precision, accuracy, or realism, the work presented here focuses on the effects of aerobic respiration rate on denitrification rate, and implications of altered channel hydrogeomorphology associated with historical logging. Aerobic respiration rate is emphasized due to the strength and coherence of the relationship between respiration and denitrification [Mulholland et al., 2009], and the implication of this relationship for estimating network-scale denitrification is examined in Ch. 3. Effects of altered channel hydrogeomorphology associated with logging on both respiration and network-scale denitrification are subsequently considered in Ch. 4 due to the well-documented effects of large wood on the channel complexity, sediment transport, stability, and ecology of stream systems [Gurnell et al., 2002, Wohl, 2014, Beckman and Wohl, 2014a, Venarsky et al., 2018].

Aerobic Respiration Rate

The relationship between denitrification rate and aerobic respiration rate suggests a number of indirect linkages between a variety of stream characteristics and denitrificaiton rates. The fundamental connection between respiration rates and rates of primary production has been observed at scales varying from ex-situ chambers to stream reaches [Bernhardt et al., 2018, Bott et al., 1985, Beaulieu et al., 2013, Demars et al., 2011b, Bernot et al., 2010], and suggests that factors such as the availability of light and nutrients can indirectly affect aerobic respiration rates [Peterson et al.,

1985, Kominoski et al., 2018].

Along with the influence of primary production, stream temperature and carbon availability are known correlates of aerobic respiration rates. Ex-situ incubations suggest that aerobic respiration rates are modulated by temperature when other factors are not limiting [Acuña et al., 2008], consistent with the general description of the effects of temperature on many biological processes [Arrhenius, 1915]. In-situ observations find evidence for thermal control of respiration rates in a wide variety of streams and rivers [Demars et al., 2011b,a, Perkins et al., 2012], although other factors such as stream velocity may obscure this effect in smaller streams [Bott et al., 1985]. Connections between respiration rates and organic carbon have been observed at the reach scale [Bernot et al., 2010], although this relationship may be clouded by the uncertainty surrounding the availability of organic carbon sources [Mulholland et al., 2009]. The mechanisms linking stream temperature and carbon availability to respiration rate are also applicable to denitrification rates, therefore variations in carbon availability and stream temperature are likely to constrain rates of respiration and denitrification across stream networks.

Temperature Increasing surface residence time and decreasing elevation typically cause stream temperatures to increase in a downstream direction, although complex temperature patterns have also been observed [Fullerton et al., 2015]. In headwater streams, water temperatures are strongly influenced by groundwater temperatures due to the short surface residence time of the stream water. In larger streams, the influence of atmospheric heat exchange on water temperatures is more significant. Stream water therefore transitions from groundwater temperatures toward equilibrium with current atmospheric conditions with increasing mean surface residence time in a downstream direction [Caissie, 2006]. This effect is commonly manifested

as an asymptotic downstream increase in stream temperature, although downstream decreases are possible under conditions where groundwater temperatures are warmer than the atmospheric equilibrium temperature. For moderate and large streams, atmospheric equilibrium alone is a reasonable descriptor of stream temperatures, although disequilibrium conditions can arise from longitudinal changes in shading and wind shelter, or reductions in the mean surface residence time associated with high rates of hydrologic gain[Cluis, 1972, Crisp and Howson, 1982, Bogan et al., 2003, Caissie et al., 2007]. Downstream decreases in stream elevation are commonly associated with increased air temperatures, and therefore increased equilibrium water temperatures, although this pattern may not apply to low gradient streams or streams which pass through regions with different climactic conditions. In the absence of other factors, this downstream increase in surface residence time and air temperature typically results in rapid increases in stream temperature in headwater streams because of the rapid longitudinal decrease in the role of groundwater temperature, and more gradual increases in larger streams, where there is less longitudinal variability in groundwater influence.

Factors which cause complexity in stream temperature patterns warrant attention, as heterogeneous stream temperatures may potentially lead to variability in rates of aerobic respiration and denitrification. Dense canopies over streams are one such factor that may cause a perceived cooling effect, which may in practice arise from the reduction in solar heating applied to cooler waters flowing into canopied reaches at night or early in the morning [Garner et al., 2014]. Thus, by limiting solar heating, dense canopies may reduce the diel temperature range and the mean temperature of streamwater [Hannah et al., 2008]. The mixing of waters with distinct thermal histories can also lead to complex stream temperature patterns [Fullerton et al., 2015]. Glacial runoff is consistently cooler than groundwater and can lead

to spatial heterogeneity in stream temperatures across small networks [Brown and Hannah, 2008]. Lake temperatures may also be distinct from stream temperatures due to their high surface area and residence time, and the extent to which lakes to impart complexity into temperature patterns of stream-lake networks across seasons is analyzed in Ch. 2. Temporal changes in stream temperatures are also relevant to seasonal denitrification rates, with the co-occurrence of warm temperatures and low flows potentially maximizing late-summer denitrification rates [Alexander et al., 2009, Arismendi et al., 2012].

Historical Logging

Many natural and anthropogenic factors shape the hydrogeomorphology of streams, with resulting effects on the accumulation and export of stream carbon [Wohl et al., 2017]. Such factors may influence denitrification rates by altering both the hydrogeomorphic character of stream reaches, but also the carbon-fueled biotic demand. As carbon rich benthic habitat is an ideal environment for denitrification activity [Inwood et al., 2007, Hill et al., 2000], factors which influence the area, volume, or carbon content of stream benthos are also likely to influence whole-stream denitrification rates. Benthic conditions ideal for denitrification are formed under low-velocity conditions where fine particles of organic carbon are deposited [Böhlke et al., 2009], while higher stream velocities may disturb benthic communities and scour fine benthic substrates [Dodds, 2006, Groffman et al., 2005]. Therefore, high denitrification rates may occur in areas of streams that are sheltered from high velocity events such as vernal pools [Capps et al., 2014], or pools formed by channel spanning structures [Groffman et al., 2005]. Large wood and channel spanning structures have also been observed to correlate with high rates of aerobic respiration, likely due to the deposition of organic substrate on slow moving pools [Houser et al.,

2005, Briggs et al., 2014]. Historical logging practices have substantially reduced the occurrence of large wood and channel-spanning logjams, with persistent effects on channel hydrogeomorphology, and potential implications for rates of respiration and denitrification that are examined in Ch. 4. Although beyond the scope of my dissertation, the broad similarity between channel-spanning logjams and beaver dams suggests that the removal of beaver from North American and Eurasian streams may have similar implications for the retention of fine sediment and organic carbon [Anderson and Rosemond, 2007], and thus local denitrification rates [Briggs et al., 2013].

Historical logging is associated with a reduction in the quantity of large wood deposited into streams and rivers, with substantial and persistent effects on channel planform, channel stability, stream sediment retention, and the formation of logjams [Gurnell et al., 2002, Wohl, 2014]. While logjams are often comprised of multiple sizes of logs, the formation of a logjam often requires both the presence of a log of sufficient size to resist downstream transport, and the accumulation of smaller logs transported from upstream sources [Abbe and Montgomery, 2003]. Survey data of a coastal Oregon watershed suggests that smaller from young-growth forests (<50 years old) contribute little to the formation of new logjams, while jams formed from larger, older logs are highly persistent [Andrus et al., 1988]. Similarly, Colorado front range watersheds with old-growth forests are associated with greater longitudinal densities of logjams [Beckman and Wohl, 2014b], a difference which is most prominent in geomorphically unconfined reaches [Livers and Wohl, 2016] where stream power may be distributed across the floodplain during high flow events. Large wood and jams are also associated with the formation and maintenance of multi-channel reaches [Harwood and Brown, 1993], an effect which leads to a disparity between the total channel bed area of streams in unlogged and logged areas [Livers et al., 2017].

Additionally, logjams create low-velocity pools that trap fine sediments and organic carbon [Gurnell et al., 2002, Beckman and Wohl, 2014a], leading to substantially increased benthic carbon stocks in stream networks draining unlogged watersheds [Wohl et al., 2017]. Historical logging therefore leads to a simplification of stream network hydrogeomorphology, characterized by a loss of in-stream wood, logjams, and multi-channel reaches, and decreased retention and storage of carbon and fine sediments. This simplification likely has implications for the magnitude of multiple biogeochemical processes including aerobic respiration and denitrification [Wohl and Beckman, 2011, Craig et al., 2008], although such effects have not been previously quantified.

Dissertation Scope

The work presented here builds on previous efforts to understand biotic and hydrogeomorphic controls on network-scale denitrification through the development of a stream network denitrification model incorporating a relationship between aerobic respiration rates and biotic demand for denitrification. Additionally, this work provides a novel look at spatial and temporal influences of lakes on stream temperatures. Through application of the stream network denitrification model to scenarios representing reasonable yet simplistic warm and cool stream temperature patterns, the effects of variable biotic demand on the distribution and magnitude of whole network denitrification are explored across a range of N loading conditions. The model is further used to examine the combined biotic and hydrogeomorphic effects of logging-induced channel simplification (loss of logjams and side channels) on the magnitude of whole-network denitrification. By incorporating landscape-scale drivers of heterogeneity in the physical and biotic controls on stream denitrification, this work enhances our understanding of the stream network's ability to remove nitrate

before its export from watersheds.

DESCRIBING ALPINE LAKE INFLUENCE ON STREAM NETWORK TEMPERATURES: A STATISTICAL MODELING APPROACH

Introduction

Across stream networks, channel temperature is commonly found to be correlated with air temperature [Crisp and Howson, 1982, Stefan and Preud'homme, 1993, Erickson and Stefan, 2000], or with watershed characteristics such as morphologic structure or hydrologic processes [Scott et al., 2002, Brown and Hannah, 2008, Poole and Berman, 2001]. As groundwater influence decreases with increasing surface residence time in a downstream direction, heat exchange with the atmosphere typically becomes the dominant determinant of stream temperature. Thus, systematic spatial variation in groundwater influence and atmospheric conditions often yields an asymptotic change in stream temperature in a downstream direction [Vannote et al., 1980, Bogan et al., 2003, Caissie, 2006]. However, this pattern is not always consistent with field observations [Fullerton et al., 2015]. Previous studies have identified variations in riparian canopy cover [Garner et al., 2014, Monk et al., 2013] and thermally distinct water sources such as upstream lakes or glaciers [Mellina et al., 2002, Leach et al., 2017, Brown and Hannah, 2008] as confounding factors which may alter typical longitudinal stream temperature profiles. Such confounding factors may obscure underlying longitudinal trends driven by diffuse groundwater input and atmospheric heat exchange. Understanding complex longitudinal patterns in stream temperature therefore requires an approach that accounts for both expected trends with loss of elevation as well as other discontinuous localized factors.

Water temperatures in both streams and lakes are influenced by atmospheric heat fluxes as well as groundwater inputs or exchanges [Webb and Zhang, 1997, Caissie, 2006]. However, the effects of these heat exchanges on water temperature

are determined by hydrologic differences between small streams, large streams, and lakes [Hebert et al., 2011, Richards et al., 2012]. Turbulent flow in stream channels results in a well-mixed water column that integrates atmospheric and groundwater influences. In contrast, slow water velocity in lakes often allows for stratification, which concentrates the direct influence of atmospheric heat exchange on the epilimnion, which is often the source of outflow from the lake into receiving streams [Wotton, 1995]. Additionally, the large surface area of lakes limits the possible extent of canopy shading, and longer hydrologic residence times further magnify the influence of atmospheric heat fluxes on lake surface water temperature. Consequently, the temperature dynamics of lake outlet streams differ from streams that are independent of lake influence, contributing to discontinuous or complex profiles in stream network temperature [Jones, 2010, Fullerton et al., 2015, Poole, 2002].

The potential influence of lakes on stream temperature is determined by the proportion of stream water that has flowed through one or more lakes. Lake influence on stream temperature will be substantial where a large portion of stream water has originated from an upstream lake, but entirely absent where no upstream lakes are present. However, lake-sourced contributions to streamflow at any single point may be variable over time due to the differing runoff potential of contributing areas [Leach et al., 2017], and lake influences on stream temperature are only meaningful if lake temperature differs from inlet stream temperature. Therefore, the relative influence of lakes on stream temperature within a stream-lake network may vary over space and time.

Accordingly, we hypothesize that the influence of lakes on stream temperature varies spatially across a stream-lake network in proportion with the fraction of stream discharge sourced from one or more upstream lakes. Therefore, we expect stream

elevation, stream drainage area, upstream lake temperature, and the fraction of stream flow derived from lakes to explain complex longitudinal patterns in stream temperature. We analyze the performance of a generalized linear regression model applied to a dataset describing stream temperatures across a montane stream network with numerous lakes. By applying the regression model across seasons, we assess the temporal consistency of lake-induced complexity in describing the spatial variance in stream temperature data collected at a variety of elevations within a stream network.

Methods

Study Area

The upper North Saint Vrain (NSV) River and Glacier Creek (GC) are adjacent high elevation, snowmelt dominated stream networks located in Rocky Mountain National Park, Colorado, USA (figure 2.1). The NSV and GC watersheds encompass 113 km^2 of mountainous topography ranging in elevation from 2550 to 4300 m, with streams present as high as ca. 3600 m. Many headwater (first order) streams originate from alpine lakes and lakes located within the stream network are common features above 3000 m. The study area experiences strong seasonality of precipitation, streamflow, and air temperature. Precipitation near the study site is greatest in the springtime, although small precipitation events are common year round. Streamflow follows a pattern typical of snowmelt-dominated systems, with maximal flow occurring in early summer, followed by a decline through the summer and fall to a wintertime minimum. Air temperature follows a seasonal pattern, with mean summertime temperatures of around 10°C and mean wintertime temperatures of around -5°C.

Figure 2.1: Locations of streams, lakes, and temperature sampling points within the North Saint Vrain (NSV) and Glacier Creek (GC) watersheds, Rocky Mountain National Park, Colorado, USA. Base map ©2017 Google.

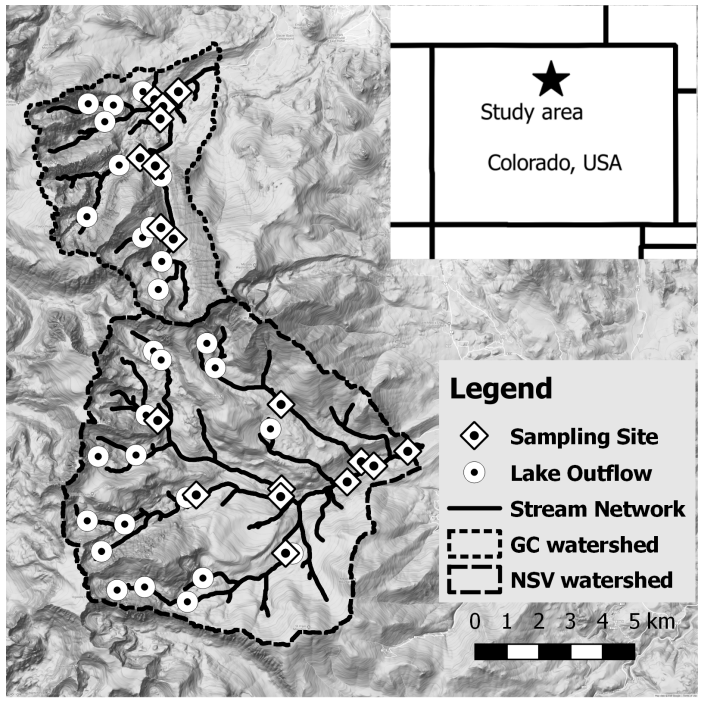

Watershed Characterization

We used a digital elevation model (DEM) with 1/3 arc-second resolution (~10 x 10 m pixel resolution) from the National Elevation Dataset (data available from the U.S. Geological Survey) to delineate streams and watershed boundaries using the GRASS [GRASS Development Team, 2018] r.watershed module, specifying a minimum basin size of 0.5 km^2, and using the default Multiple Flow Direction option, with the default convergence factor of 5. We divided the stream network into segments delimited by tributary junctions and, to facilitate unbiased characterization of the entire network, we subdivided each segment into n equal-length reaches such that:

$$n_i = \left\lceil \frac{l_i}{r_{max}} \right\rceil, \tag{2.1}$$

where i denotes a segment, l is the segment length (km), r_{max} is the maximum allowed reach length (km), and asymmetrical brackets denote rounding up to the nearest integer. We chose $r_{max} = 0.6$, yielding stream reaches that were typically between 0.5 and 0.6 km in length. From the DEM, we determined stream reach elevation and contributing basin area ("upstream accumulated area"; UAA) for the downstream end of each reach.

We digitized outflow points of lakes that were larger than 0.1 km^2 visible in Google satellite imagery (Sources: DigitalGlobe, Landsat / Copernicus, U.S. Geological Survey, USDA Farm Service Agency). The elevation of each lake was then determined from the DEM. We used the GRASS r.water.outlet module, in combination with flow directions determined by the r.watershed module, to delineate the sub-watershed draining to each stream sampling point and lake outflow point.

Sampling Points and Data Collection

From the population of accessible stream reaches within the study area, we selected 18 sampling points (figure 2.1) representative of the observed distribution of UAA and elevation (figure 2.2). At each sampling point, we deployed Onset "HOBO pendant temp" self-contained temperature loggers with an advertised precision of ±0.14°C and accuracy of ±0.53°C. Temperatures were recorded at 30 minute intervals. Loggers were contained within ˜3.2 cm internal diameter PVC housings (open at each end) that were anchored to submerged logs in the main flow of the channel, and were deployed from August 2014 to August 2015. Variation in stream discharge or shifting of logs to which loggers were attached during high flow caused some loggers to be out of the water for part of the study period. Therefore, we compared temperature data between all sampling points and concurrent stream temperature records from the nearby U.S. Geological Survey Big Thomson Moraine Park gage

[U.S. Geological Survey, 2016]. For each sampling point, we identified inactive (out of water) periods when temperature signals exhibited unreasonable patterns relative to the Big Thomson Moraine Park temperature record (e.g., extreme maxima or minima, high rate of change), and disregarded these data as times when the temperature sensor may not have been immersed in stream water. Thus, the number of active sampling points varies over the period of deployment (figure 2.4).

Additional data were compiled to provide a contextual description of local weather patterns and seasonal changes during the study period. Stream flow data were also obtained from the Big Thompson Moraine Park stream gage. Precipitation and air temperature data were provided by the NSF supported Niwot Ridge Long-Term Ecological Research project and the University of Colorado Mountain Research Station [Losleben, 2007b,a], located ˜15km south of the study area.

Characterization of Lake Influence

We posit that water passing through a lake takes on the temperature of the lake surface, and therefore view each lake as a potential serial discontinuity [Ward and Stanford, 1995] in the longitudinal stream temperature pattern. Thus, if multiple lakes are arranged serially upstream of a stream temperature sampling point, only the downstream-most lake in the series will affect the temperature of a downstream sampling point. A sampling point below a stream confluence may be influenced by the downstream-most lake from multiple series. We refer to the downstream-most lake of each longitudinal series of lakes above a sampling point as the "lakes of influence" (LoIs) for a sampling point (figure 2.3). Any lakes further upstream from the lake of influence were assumed to have negligible effect on temperature downstream of the lake of influence.

Stream water at a sampling point is a mixture of water that has passed through

Figure 2.2: Upstream accumulated area (UAA, km^2) and elevation (m) of stream reaches and temperature sampling points across the NSV and GC watersheds.

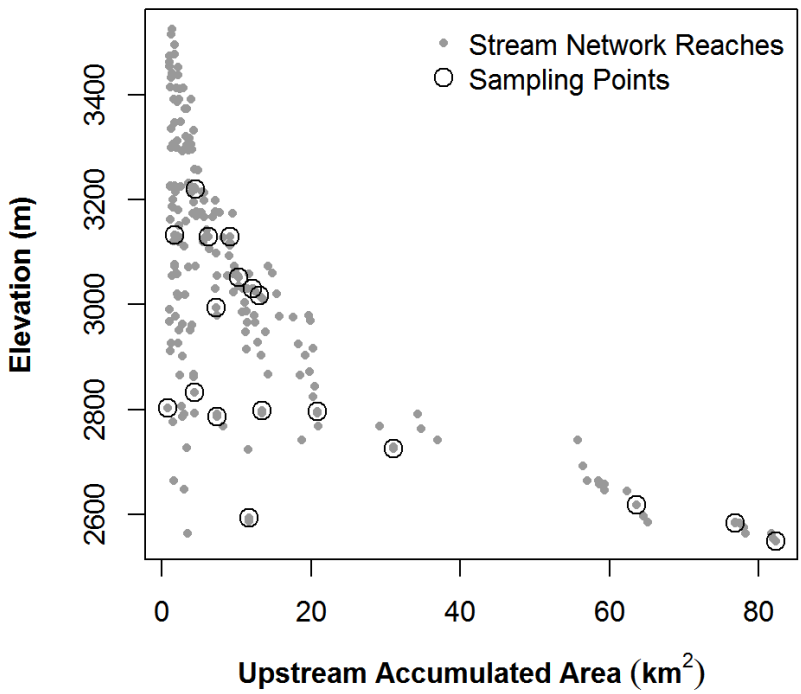

any upstream LoIs, combined with water that is sourced from lateral groundwater inputs without passing through an LoI. Therefore, we assume that the stream temperature at a sampling point is proportionally influenced by fraction of stream discharge derived from the LoIs. Using UAA as a surrogate for discharge, we estimate the fraction of discharge that is sourced from the outflow of one or more LoIs (j) before arriving at a sampling point (i) as the "lake fraction" (LF_i):

$$LF_i = \begin{cases} 0 & \text{for } nLoIs_i = 0 \\ \frac{\sum_{j=1}^{nLoIs_i} UAA_j}{UAA_i} & \text{for } nLoIs_i > 0, \end{cases} \tag{2.2}$$

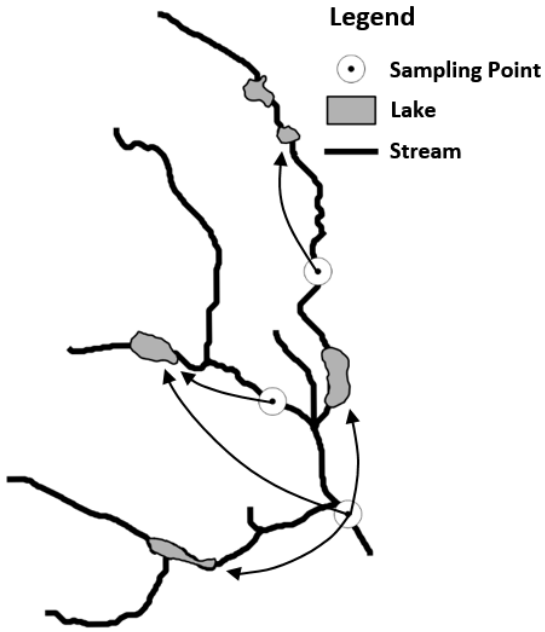

Figure 2.3: Identification of Lakes of Influence (LoIs) for three temperature sampling points on an illustrative, hypothetical stream network. Arrows point upstream and indicate LoIs for each sampling point.

where $nLoIs_i$ is the number of LoIs associated with sampling point i, UAA_i is the upstream accumulated area for sampling point i, and UAA_j is the upstream accumulated area for each LoI j associated with sampling point i.

Lacking data on lake temperature, we used lake elevation as a surrogate for temperature, assuming that higher lakes would be cooler. We calculated the UAA-weighted mean elevation ($\bar{E_{li}}$) of the LoIs for each sampling point i with one or more LoIs:

$$\bar{E_{li}} = \frac{\sum_{j=1}^{nLoIs_i} \left(E_{lj} UAA_j \right)}{\sum_{j=1}^{nLoIs_i} UAA_j}, \tag{2.3}$$

where E_{lj} is the elevation of LoI j. In contrast to LF, $\bar{E}_{li}$ is undefined when $nLoIs_i$ = 0.

Alternative Statistical Models

We developed a collection of alternative models representing specific combinations of mechanisms by which stream and lake characteristics might influence stream temperature across a stream-lake network. The alternative models include conventional forms of simple linear regression (SLR) and multiple linear regression (MLR) models, as well as models representing the weighted influence of lake and stream water inputs at different temperatures. Some independent variables in the models, (e.g. E, UAA) apply to both stream sampling points and LoIs. The subscript "s" is used to refer to values measured at stream sampling points, while the subscript "l" denote a measurement describing LoIs. As $\bar{E}_l$ is not defined for sampling points with no LoIs, we exclude $\bar{E}_l$ from all unweighted SLR and MLR models.

Simple Linear Regression We pose three Simple Linear Regression (SLR) models to assess the independent effects of local elevation, contributing area, and fraction of lake influence on stream temperature:

$$T = a_{es}E_s + b, \tag{2.4}$$

$$T = a_{us}UAA_s + b, \tag{2.5}$$

and

$$T = a_{fl}LF + b \tag{2.6}$$

where T is the stream temperature at a sampling point, a_{es}, a_{us}, and a_{fl} are the slope

coefficients for sampling point elevation (E_s), upstream accumulated area (UAA_s), UAA-weighted mean LoI elevation ($\bar{E}_l$), and lake fraction (LF) respectively, and b is the regression intercept.

Multiple Linear Regression To explore the linear combinations of the effects of E_s, UAA_s, and LF on stream temperature, we derived a collection of four Multiple Linear Regression (MLR) models:

$$T = a_{fl}LF + a_{us}UAA_s + a_{es}E_s + b, \tag{2.7}$$

$$T = a_{fl}LF + a_{us}UAA_s + b, \tag{2.8}$$

$$T = a_{fl}LF + a_{es}E_s + b, \tag{2.9}$$

and

$$T = a_{us}UAA_s + a_{es}E_s + b. \tag{2.10}$$

Weighted Effects Models When lake and stream dynamics both influence stream temperature, the influence of lakes at a sampling point may be proportional to the fraction of stream discharge derived from LoIs. Therefore, we formed a set of three weighted effects models that use LF and its complement to take a flow-weighted average of two linear models, one predicting lake temperature from $\bar{E}_l$ and another predicting stream temperature from E_s and/or UAA_s:

$$T = LF(a'_{el}\bar{E}_l + b_l) + (1 - LF)(a'_{es}E_s + b_s), \tag{2.11}$$

$$T = LF(a'_{el}\bar{E}_l + b_l) + (1 - LF)(a'_{us}UAA_s + b_s), \tag{2.12}$$

and

$$T = LF(a'_{el}\bar{E}_l + b_l) + (1 - LF)(a'_{es}E_s + a_{us}UAA_s + b_s), \tag{2.13}$$

where b_l and b_s are lake and stream temperature intercepts, a'_{el} and a'_{es} are the slope coefficients lake and stream elevation, and all other terms are consistent with those in equations 2.4-2.16. The weighted effects models (equations 2.11-2.13) explicitly represent the mixing of lake-sourced water and non-lake-sourced water, in contrast to the SLR and MLR models (equations 2.4-2.10), which are comprised of linear combinations of terms representing stream and lake characteristics. Therefore, we refer to equations 2.11-2.13 as "stream and lake mixing" models, and characterize equations 2.4-2.10 as "conventional" regression models. LF is equal to zero at sampling points with no LoIs, so the lack of a meaningful $\bar{E}_l$ value for sampling locations with no LoI has no effect on analyses with the stream and lake mixing models.

Model Comparison

In order to assess model performance at different times of the year, we identified four five-day periods with high numbers of active loggers while also distributing the five-day time periods across the duration of the dataset (figure 2.4). For each five-day period, we calculated the average temperature for each sampling point, and fitted all hypothesized model alternatives (equations 2.4 - 2.13) to the data for each time period. Model parsimony was assessed using the sample size corrected Akaike Information Criterion (AICc), which identifies efficient models that minimize information loss by weighing goodness of fit against the number of fitted parameters, and is applicable to

small sample sizes [Akaike, 1998, Hurvich and Tsai, 1993]. Comparative AICc scores were calculated with the *dredge* function from the R [R Core Team, 2016] package *MuMIn* ('Multi Model Inference') version 1.15.6 [Barton, 2016]. To facilitate these comparisons, we expanded equation 2.13 to a linear form:

$$T = a_{el}(LF\bar{E}_l) + b^*LF + a_{es}((1 - LF)E_s) + a_{us}((1 - LF)UAA_s) + b_s, \qquad (2.14)$$

where $b^* = b_l - b_s$, and all other terms are equivalent to those in equation 2.13. We then combined the terms from equation (2.14) with those from equation 2.7, forming an inclusive equation from which hypothesized models can be extracted during AICc analysis:

$$\begin{aligned} T =& a'_{el}(LF\bar{E}_l) + ab^*_{fl}LF + a'_{es}((1 - LF)E_s) + a'_{us}((1 - LF)UAA_s) \\ &+ a_{es}E_s + a_{us}UAA_s + I. \end{aligned} \qquad (2.15)$$

In this form, I represents the overall intercept, equivalent to b in equations 2.4-2.7, and b_s in equations 2.11-2.14. Additionally, the $a_{fl}LF$ term in equations 2.6 and 2.7 - 2.9 is equivalent to the b^*LF term in equation 2.14. We therefore represent this term as $ab^*_{fl}LF$ in the combined form (equation 2.15), but maintain the original notatiol when extracting individual models for AIC comparison. Equation 2.15 includes two forms of the coefficients a_{es}, and a_{us}: a form applied to unweighted independent variables (e.g. $a_{es}E_s$ as used in equation 2.4), and a form applied to independent variables weighted by lake influence (e.g. $(1 - LF)(a'_{es}E_s)$ as used in equation 2.11). Coefficients applied to weighted terms are denoted as a'_{es} and a'_{us}, and potential multicollinearity is avoided by excluding from the analysis any models that contain both weighted and unweighted forms of the same explanatory variables. Although this AICc analysis provides a valid

comparison between the performance of the hypothesized models within each time period, differences between the availability of data from all sampling sites for each time period precludes the use of this AICc analysis for forming comparisons of model performance among time periods [Burnham and Anderson, 2003].

Temporal Analysis

To explore temporal variation in the influence of stream elevation and lake elevation on stream temperature, we analyzed the coefficient of determination (R^2) of stream elevation (equation 2.4) and lake elevation on daily average stream temperature for each day of the complete study period. To facilitate this comparison, we formed a SLR describing the relationship between LoI elevation and stream temperature:

$$T = a_{el}\bar{E}_l + b. \tag{2.16}$$

Because equations 2.4 and 2.16 each have only one independent variable, the R^2 statistic provides a simple and direct comparison of explanatory power between E_s and $\bar{E}_l$. Equation 2.16 can only be applied to data from sampling points with LoIs ($n = 17$ of 18 total sampling points); therefore, we removed the single sampling point without LoIs from this analysis.

Direct comparison of R^2 calculated for each day of the study period requires a consistent sample size over time, but the number of active sampling points varies substantially across the study period (figure 2.4). Therefore, using all available data for each day would have injected problematic variation in the explanatory power of each equation over time. On the other hand, limiting our analysis to only those sampling points with complete records would have limited the range of E_s and $\bar{E}_l$ included in the analysis (figure 2.4. To circumvent these limitations, we resampled

our data, creating 10 sets of 8 randomly selected sampling points (with replacement) from the active sampling points on each day of the study period where at least n=10 sampling point were active. We fitted equations 2.4 and 2.16 to each of the 10 resampled data sets on each day, yielding 10 estimates of r^2 for each equation, for each day of the study period. We plotted the results, along with the daily mean r^2 for each equation, across the study period.

Results

Seasonal Changes in Stream Temperature and Data Availability

Stream temperatures follow a seasonal pattern similar to that of air temperature, with notable warm periods occurring in mid August, 2014, and late June 2015 (figure 2.4). In contrast with the high variability of wintertime air temperatures, winter stream temperatures remain near 0°C from late November 2014 until mid March 2015. The number of sampling points with valid data declined during the study period due to logger malfunctions, and battery depletion. Decreased stream stage during times of low streamflow also resulted in some loggers being exposed to air temperature rather than water temperatures, causing a decrease in the number of sampling points in the winter months. However, increased streamflow and stage during the spring produced a rebound in the number of active sampling points.

Among the four, 5-day analysis periods (table 2.1), the late summer and fall periods had similar streamflows, although air and stream temperatures were lower during the fall period. Total precipitation inputs were similar for the late summer and fall period. Precipitation occurred as numerous small events during the late summer, and most of the fall precipitation occurred as a single 16mm event on 9 October 2014. The early spring period occurred during a time with minimal precipitation inputs and low streamflow, during which air temperatures increased from wintertime levels, and

Figure 2.4: Timeseries of precipitation [Losleben, 2007b], streamflow [U.S. Geological Survey, 2016], and air temperature [Losleben, 2007a] from nearby sensors, along with stream temperature data from all active sampling points, and the number of active sampling points, with the dotted line indicating the threshold (10) for inclusion into the temporal analysis. Daily mean air temperature is indicated by the black line, while grey areas represent the range between daily minima and maxima. Stream temperatures are represented as individual lines for each active point. Five-day time periods selected for statistical analyses are indicated by gray bands extending vertically across the figure.

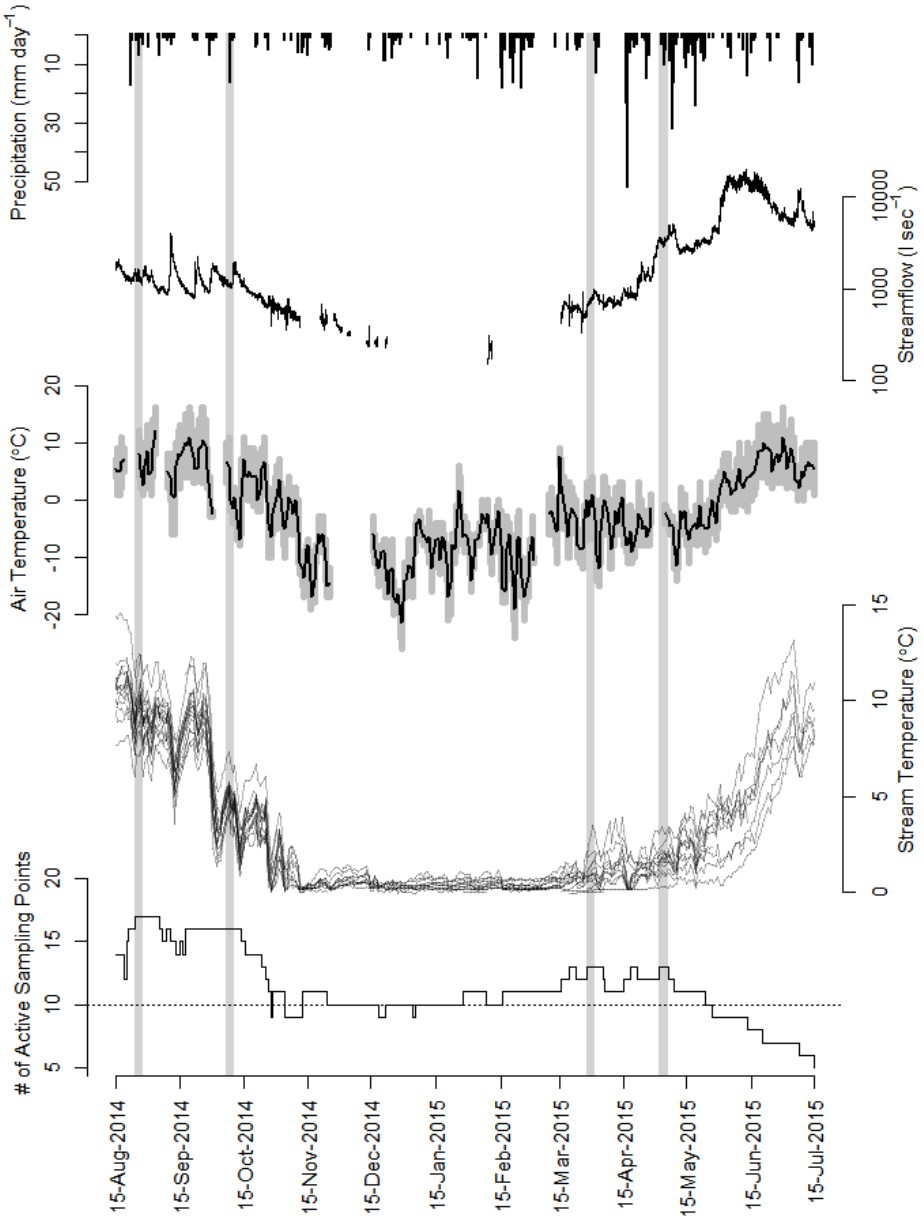

some streams began to warm above their wintertime minimum. This period was identified as a springtime period due to its date range. However, this period may more appropriately be considered to represent late wintertime conditions because snowmelt-driven spring runoff had not yet begun. In contrast, the late spring period had higher streamflow and substantial precipitation inputs. The range of stream temperatures were similar during the early and late spring periods. However, the mean stream temperature was higher during the late spring period.

Table 2.1: Summary of five-day time periods for analysis

Period	Dates	Total Precip.	Mean Streamflow	Mean Air Temperature	Stream Temperature Min	Mean	Max
		mm	$l\ sec^{-1}$	$^{\circ}C$	$^{\circ}C$	$^{\circ}C$	$^{\circ}C$
Late summer	8/24/2014 to 8/28/2014	13	1387	5.3	6.02	9.25	12.47
Fall	10/7/2014 to 10/11/2014	19	1256	2.3	2.93	4.73	7.29
Early spring	3/28/2015 to 4/1/2015	2	761	-1.1	0.1	0.97	3.45
Late spring	5/2/2015 to 5/6/2015	18	13380	-2.8	0.21	1.68	3.38

Identification of Optimal Models

During the late summer period, stream temperature models that exclude the influence of lakes explain at most 10% of the observed variation in stream temperature (table 2.2). In contrast, the stream and lake mixing model incorporating E_s and $\bar{E}_l$ (equation 2.11) is identified by AICc as the optimal model, and explains 60% of the

Table 2.2: Performance of models fitted to 17 active sampling points during the late summer analysis period (24 August, 2014 through 28 August 2014). * Equation 2.4 is identified by AICc as the optimal equation during the early and late spring periods.

	Equation	R^2	$\Delta AICc$
(2.11)	$T = LF(a_{el}\bar{E}_l + b_l) + (1 - LF)(a_{es}E_s + b_s)$	0.60	0.00
(2.12)	$T = LF(a_{el}\bar{E}_l + b_l) + (1 - LF)(a_{us}UAA_s + b_s)$	0.55	1.85
(2.13)	$T = LF(a_{el}\bar{E}_l + b_l) + (1 - LF)(a_{es}E_s + a_{us}UAA_s + b_s)$	0.61	4.50
(2.4)*	$T = a_{es}E_s + b$	0.06	6.73
(2.9)	$T = a_{fl}LF + a_{es}E_s + b$	0.21	7.23
(2.6)	$T = a_{fl}LF + b$	0.03	7.26
(2.5)	$T = a_{us}UAA_s + b$	0.00	7.78
(2.10)	$T = a_{us}UAA_s + a_{es}E_s + b$	0.10	9.48
(2.7)	$T = a_{fl}LF + a_{us}UAA_s + a_{es}E_s + b$	0.28	9.91
(2.8)	$T = a_{fl}LF + a_{us}UAA_s + b$	0.04	10.60

observed variation in stream temperature. This mixing model also performs far better than all SLR and MLR models, which explain at most 28% of the observed variation in stream temperature. For points with one or more LoIs, $\bar{E}_l$ alone was generally found to be a strong predictor of stream temperature during this late summer period (figure 2.5).

The explanatory power of models relying on E_s and/or UAA_s is substantially higher during the fall period than during the late summer period (table 2.3). Furthermore, stream temperature at points with LoIs shows increased influence of E_s and decreased influence of $\bar{E}_l$ compared to the late summer period (figure 2.5). However, the reduction in lake influence does not reduce the explanatory power of the stream and lake mixing models, which instead benefit from the increased coherence

Table 2.3: Performance of models fitted to 16 active sampling points during the fall analysis period (7 October 2014 through 11 October 2014). * Equation 2.4 is identified by AICc as the optimal equation during the early and late spring periods.

	Equation	R^2	$\Delta AICc$
(2.11)	$T = LF(a_{el}\bar{E}_l + b_l) + (1 - LF)(a_{es}E_s + b_s)$	0.67	0.00
(2.13)	$T = LF(a_{el}\bar{E}_l + b_l) + (1 - LF)(a_{es}E_s + a_{us}UAA_s + b_s)$	0.69	4.46
(2.12)	$T = LF(a_{el}\bar{E}_l + b_l) + (1 - LF)(a_{us}UAA_s + b_s)$	0.56	4.58
(2.4)*	$T = a_{es}E_s + b$	0.26	4.74
(2.10)	$T = a_{us}UAA_s + a_{es}E_s + b$	0.33	6.89
(2.9)	$T = a_{fl}LF + a_{es}E_s + b$	0.32	7.18
(2.5)	$T = a_{us}UAA_s + b$	0.02	9.37
(2.7)	$T = a_{fl}LF + a_{us}UAA_s + a_{es}E_s + b$	0.40	9.43
(2.6)	$T = a_{fl}LF + b$	0.01	9.49
(2.8)	$T = a_{fl}LF + a_{us}UAA_s + b$	0.02	12.94

of stream elevation as an explanatory variable. Under these circumstances, equation 2.11 is again identified as the optimal model, with higher explanatory power (67%) than during the late summer period.

In contrast to the late summer and fall periods, all tested models have reduced explanatory power during the early spring (table 2.4), with the optimal model identified by AICc (equation 2.4) explaining only 14% of the observed variation in stream temperature. Similarly, stream temperature at points with LoIs during this period shows little relationship with either E_s or $\bar{E}_l$ (figure 2.5).

Equation 2.4 is again identified as the optimal model in the late spring (table 2.5), and is the best performing SLR model across all of the analyzed periods. Additionally, E_s is a better explanatory variable than $\bar{E}_l$ during this period when the analysis is

Table 2.4: Performance of models fitted to 13 active sampling points during the early spring analysis period (28 March 2015 through 1 April 2015). * Equation 2.11 is identified by AICc as the optimal equation during the late summer and fall periods.

	Equation	R^2	$\Delta AICc$
(2.4)	$T = a_{es}E_s + b$	0.14	0.00
(2.5)	$T = a_{us}UAA_s + b$	0.00	1.83
(2.6)	$T = a_{fl}LF + b$	0.00	1.89
(2.9)	$T = a_{fl}LF + a_{es}E_s + b$	0.20	3.40
(2.10)	$T = a_{us}UAA_s + a_{es}E_s + b$	0.14	4.33
(2.8)	$T = a_{fl}LF + a_{us}UAA_s + b$	0.00	6.16
(2.11)*	$T = LF(a_{el}\bar{E}_l + b_l) + (1 - LF)(a_{es}E_s + b_s)$	0.32	6.73
(2.12)	$T = LF(a_{el}\bar{E}_l + b_l) + (1 - LF)(a_{us}UAA_s + b_s)$	0.26	7.80
(2.7)	$T = a_{fl}LF + a_{us}UAA_s + a_{es}E_s + b$	0.20	8.95
(2.13)	$T = LF(a_{el}\bar{E}_l + b_l) + (1 - LF)(a_{es}E_s + a_{us}UAA_s + b_s)$	0.33	13.96

limited to points with LoIs (figure 2.5). Thus, while much of the observed variance in stream temperature remains unexplained, stream elevation has a clear and substantial influence on stream temperature during this time period.

Across all analyzed periods, stream elevation (E_s) performs consistently better than stream UAA (UAA_S) in mixing and conventional model forms. Additionally, models combining E_s and UAA_s have only marginally higher explanatory power than models using E_s alone. Therefore, UAA_s has little utility for explaining variation in stream temperature in this system.

Temporal Variation in Lake Influence

Comparison of the explanatory power of equations 2.4 and 2.16 when fitted to data from all sites with LoIs across the entire study period suggests that stream

Table 2.5: Performance of models fitted to 13 active sampling points during the late spring analysis period (2 May 2015 through 6 May 2015). * Equation 2.11 is identified by AICc as the optimal equation during the late summer and fall periods.

	Equation	R^2	$\Delta AICc$
(2.4)	$T = a_{es}E_s + b$	0.41	0.00
(2.10)	$T = a_{us}UAA_s + a_{es}E_s + b$	0.49	2.45
(2.9)	$T = a_{fl}LF + a_{es}E_s + b$	0.41	4.29
(2.6)	$T = a_{fl}LF + b$	0.07	5.82
(2.5)	$T = a_{us}UAA_s + b$	0.00	6.75
(2.7)	$T = a_{fl}LF + a_{us}UAA_s + a_{es}E_s + b$	0.49	7.87
(2.11)*	$T = LF(a_{el}\bar{E}_l + b_l) + (1 - LF)(a_{es}E_s + b_s)$	0.46	8.76
(2.8)	$T = a_{fl}LF + a_{us}UAA_s + b$	0.07	10.15
(2.12)	$T = LF(a_{el}\bar{E}_l + b_l) + (1 - LF)(a_{us}UAA_s + b_s)$	0.28	12.35
(2.13)	$T = LF(a_{el}\bar{E}_l + b_l) + (1 - LF)(a_{es}E_s + a_{us}UAA_s + b_s)$	0.47	15.92

temperatures are strongly related to $\bar{E}_l$ in the late summer and fall (figure 2.5). However, stream temperatures show little relationship to $\bar{E}_l$ during the winter. Although the explanatory power does not approach that observed during the late summer and fall, stream temperature again shows some relationship to $\bar{E}_l$ during brief periods in February, April, and May, which appears to correspond to periods where the explanatory power of E_s is lower than other times during the winter and spring.

During August, September, and November 2014, stream temperature shows a remarkable lack of a relationship with E_s. In contrast, stream temperature shows some relationship with E_s during October 2014, and a stronger relationship with E_s during the winter months. Thereafter, the explanatory power of E_s exhibits a general

decline from late winter into spring.

Overall, the temporal analysis suggests that stream temperature is generally more closely related to $\bar{E}_l$ than to E_s during the late summer and early fall, and that stream temperature is more closely related to E_s than $\bar{E}_l$ during the winter and spring (figure 2.5). These results are generally consistent with the results of the AICc analyses of the late summer, fall, early spring, and late spring periods.

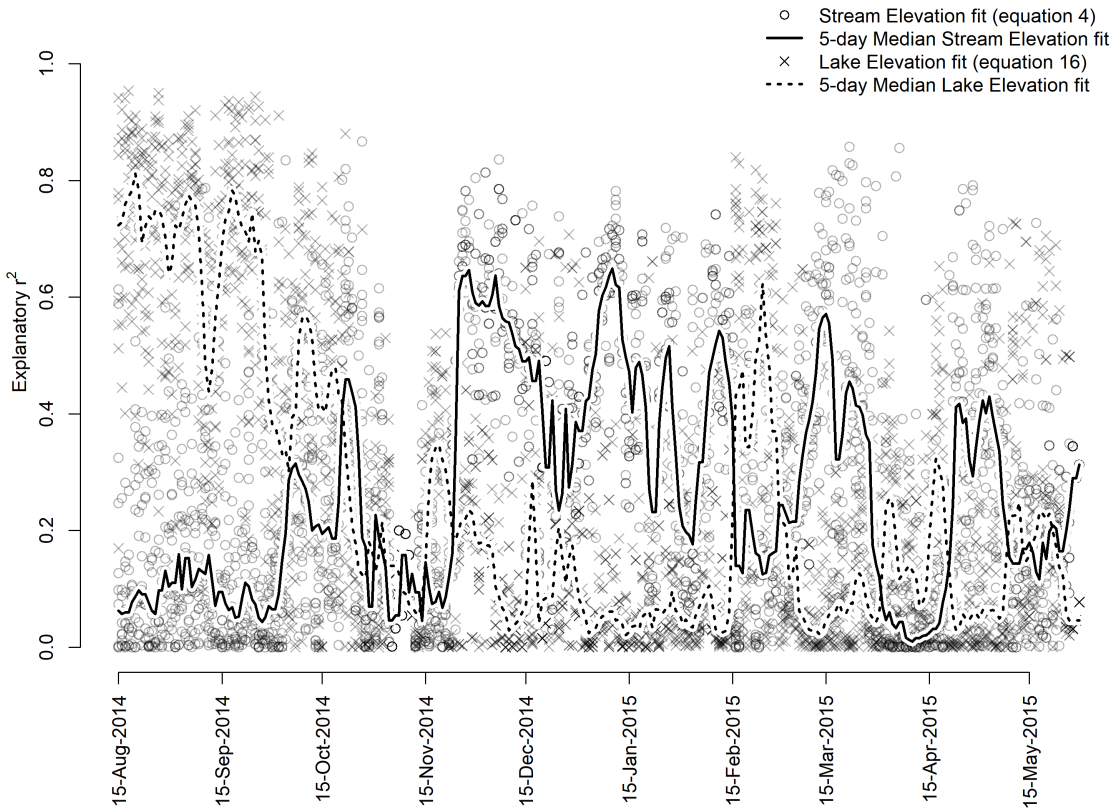

Figure 2.5: Explanatory power of stream elevation (E_s, equation 2.4) and upstream lake elevation ($\bar{E}_l$, equation 2.16) models fitted to randomly sampled sets of 8 sampling sites for each day of the study period. Data is limited to that from sites with LoIs.

Discussion

Stream temperatures of the NSV and GC networks during the late summer and fall follow a complex longitudinal profile that is not directly related to E_s or UAA_s. The absence of these relationships is especially striking given the wide range of elevation and UAA across the sampling points (figure 2.2). Thus, using conventional regression models, we might conclude that stream elevation has little effect on stream temperature, defying the common pattern of longitudinal increase or asymptotic temperature profiles along elevational gradients in stream networks [eg., Crisp and Howson, 1982, Bogan et al., 2003, Caissie, 2006, Vannote et al., 1980], and perhaps also defying logic.

The temporal variation in lake influence on stream temperature observed here suggests that the factors influencing the longitudinal stream temperature profile may also vary seasonally. As indicated by the performance of equation 2.11, substantial influence of upstream lake elevation during the summer and fall cause a discontinuous and non-monotonic temperature profile. During the springtime, decreased influence of upstream lake elevation may reduce the complexity of the stream temperature profile, possibly resulting in simpler profiles driven by atmospheric heat exchange (i.e., the strong performance of equations 2.4 and 2.10 during the late spring (table 2.5). Additionally, stream temperatures become homogeneous during the winter, when temperatures at all active sampling points are near 0°C (figure 2.4). During this time, noise arising from error in temperature measurements or other minor effects may overwhelm the signal associated with any potential network-scale temperature pattern. Overall, the stream temperature profile of our study area can not be described by a single categorical description (as defined by Fullerton et al. [2015]). Instead, the temperature profile of this system may be best categorized as complex

for some parts of the year, and linear, asymptotic, or invariant for other parts of the year.

Multiple factors could contribute to this seasonal shift in longitudinal temperature profile. As lakes can only alter stream network temperature profiles when lake temperatures differ from stream temperatures, lake effects are immaterial during seasons when lake temperatures do not differ systematically from adjacent stream temperatures. For the summer and fall seasons when we observed substantial lake influence on stream temperatures, radiative forcing comprises a substantial component of stream and lake heat budgets [Webb and Zhang, 1997, Wotton, 1995], and may therefore contribute to a large difference between lake and stream temperatures during this time. In contrast, water-atmosphere heat exchange represents a smaller portion of stream and lake heat budgets in the springtime, and is further limited by the formation of ice on lake surfaces during the winter months. Additionally, the seasonal establishment or breakdown of lake stratification influence the magnitude of differences between lake and stream temperatures. Nearby observations of small, high-elevation lakes suggest that thermal stratification does not occur during the ice-free period [Baron and Caine, 2000], although lower elevation or deeper lakes may undergo summer stratification, and shallow lakes may experience substantial atmospherically driven warming even while remaining well mixed. Wintertime stratification may also contribute to a lack of lake effects on stream temperature if stream water inflows and outflows are confined to a thermally distinct epilimnion which may be isolated from atmospheric heat influences by the presence of surface ice.

A prior synoptic study of stream temperature profiles across many streams [Fullerton et al., 2015] showed that complex stream temperature profiles do exist; i.e., streams do not always warm monotonically in a downstream direction. Fullerton

et al. [2015] speculate about the causes of complex patterns, but given their synoptic approach, do not provide in-depth analysis of temperature patterns in individual stream networks. Further, Mellina et al. [2002] identify lake temperature as a driver of complex stream profiles, yet offer regression models that predict temperature change from an initial, stream-specific headwater temperature, rather than equations to predict temperatures across stream networks with variable water sources. The analysis of Fullerton et al. [2015] is also unable to consider the temporal establishment and senescence of complex temperature profiles. While they characterize stream temperature profiles across a broad spatial extent, their data do not have the ability to discern if and under what circumstances complex patterns are seasonal or transient. Our results show that complex temperature patterns can be explained by accounting for the weighted influence of water sources with different initial temperatures, which vary across space and time. Specifically, the performance of the flow-weighted mixing model presented here indicates that the complex late summer and fall stream temperature profiles in the NSV and GC networks arise from interactions among: 1) the spatially variable hydrologic influence of lakes; 2) the effect of elevation on lake temperature; and 3) expected along-stream patterns of temperature change with loss of elevation.

The optimality of the flow-weighted mixing model (equation 2.11) during the late summer and fall periods may result from this model's ability to accommodate sampling points with different levels of lake influence within the same dataset. For points with low LF, the form of equation 2.11 limits the influence of $\bar{E}_l$, effectively simplifying equation 2.11 to equation 2.4. Conversely, for sampling points where lake influence is large (i.e., where $LF \approx 1$ across a network), equation 2.11 effectively simplifies to equation 2.3. Therefore, when fitted to a dataset containing high variability of LF, equation 2.11 attributes lake derived temperature effects to lakes,

and stream derived temperature effects to streams. As high elevation lakes are frequent features in our study area (figure 2.1), our sampling points include only a single point with no LoIs. Nonetheless, equation 2.11 can be applied to all points, and could additionally be used to extrapolate temperatures across the entire network, while an equation using an $\bar{E}_l$ term unweighted by LF would be limited in both explanatory and predictive extent.

Our results demonstrate the utility of a flow-weighted mixing model for explaining complex stream temperature profiles across stream networks with a high density of lakes. When applied in other geographic contexts where elevation may be a less important factor (e.g., prairie streams, coastal streams, desert streams), the lake ($a_{el}\bar{E}_l + b_l$) and stream ($a_{es}E_s + b_s$) components of equation 2.11 could be replaced with more locally appropriate predictive terms for lake and stream temperature, respectively. Additionally, we posit that the application of this mixing model approach is not limited to stream-lake networks, and may instead be broadly applicable to other stream networks that receive water from different origins. For example, this approach may be useful for explaining the effects of any two or more spatially variable water sources with different temperature regimes, such as lakes, groundwater, glacial melt, and geothermal influence.

While the topographically derived water routing used in our mixing model provides a simple and reasonable estimate of the fractional contributions of water sources (equation 2.2), such an approach does not account for spatial or temporal variations in areal water yield. Ephemeral or persistent differences in the distributions of precipitation, evapotranspiration, or snowmelt across elevation or aspect gradients could cause our simple approach to overestimate water sourcing from some areas, and underestimate from others. More detailed studies have identified spatio-temporal variability in water yield caused by watershed response to precipitation events [Leach

et al., 2017] and hillslope aspect [Hinckley et al., 2012]. Thus, our estimation of the fraction of stream water derived form lakes (equation 2.2) may differ seasonally or consistently from the true fraction. Incorporating such detail into the calculation of LF has the potential to improve predictions derived from our mixing model approach.

Conclusion

Complex temperature profiles that are observed using longitudinal snapshots of stream temperature may emerge and dissipate over time in response to the changing temperature dynamics and hydrologic contributions of various sources of stream flow witin watersheds. In our study system, for instance, temperatures in stream networks with abundant lakes are influenced by spatially discontinuous lake effects as well as longitudinally continuous factors such as atmospheric heat exchange and groundwater temperatures. In such cases, mathematically weighting the contribution of discontinuous factors according to their hydrologic contributions can provide parsimonious regression models for describing temperature variation across stream networks. Although simpler models that do not account for distinct water sources can provide a more parsimonious explanation of stream temperatures when water sources have more synchronized temperature regimes, the additional complexity associated with a mixing model approach may be superior during seasons with distinct differences thermal characteristics among different water sources.

A SIMULATION MODELING APPROACH TO QUANTIFYING RESPIRATION EFFECTS ON STREAM NETWORK DENITRIFICATION

Introduction

Anthropogenic alterations to nitrogen cycles have elevated nitrate concentrations in freshwater systems, impairing water quality and contributing to human health, economic, and ecological issues [Dodds, 2006, Vitousek et al., 1997, Tilman et al., 2001, Jickells, 2005]. Effective management of nitrate pollution requires a reduction of nitrate sources as well as an enhanced understanding of the transformation, retention, and removal of nitrate as it moves through terrestrial systems, stream and river networks, estuaries, and oceans [Mitsch et al., 2001, Ribaudo et al., 2001]. In-stream processes have the potential to substantially alter both the magnitude and timing of watershed nitrate export [Peterson et al., 2001, Bernhardt et al., 2003, Boyer et al., 2002]. Stream characteristics including channel geometry, network topology, water velocity, water temperature, nitrate concentration, aerobic respiration rate, and sediment organic content, have been identified as controls on the magnitude of nitrate removed due to denitrification, and the distribution of removal rates across a stream network [Christensen et al., 1990, Alexander et al., 2000, Bernhardt et al., 2005, Wollheim et al., 2006, Mulholland et al., 2008, Alexander et al., 2009, Mulholland et al., 2009, Böhlke et al., 2009, Helton et al., 2018].

In stream ecosystems, denitrification is difficult to differentiate from the multitude of other processes that potentially affect stream nitrate concentrations. In addition to removal through the process of denitrification, stream nitrogen may be converted between nitrate and other inorganic forms, assimilated into or released from biomass. Additionally, despite the substantial contribution of streams to continental denitrification, the diminutive scale of denitrification relative to the

magnitude of other nitrate fluxes [Böhlke et al., 2004] and the inability to quantify small changes in relatively large dissolved dinitrogen background concentrations further complicates in-situ measurements of denitrification rates. Thus, logistical challenges complicate the measurement of stream denitrification rates, with most reach-scale approaches requiring the release and collection of isotopically labeled nitrate to better constrain the magnitude of denitrification [Groffman et al., 2006]. However, these approaches become prohibitively expensive and impractical at network scales. Further, extrapolation from reach to network scales is complicated by the spatial variability of physical, biological and chemical drivers of denitrification rates, and the compounding effects of upstream nitrate removal on downstream nitrate concentrations.

In lieu of a viable observational approach, multiple models have been developed to represent stream denitrification rates at network and larger scales. Recognizing the influence of streamflow, channel geometry, and hydrologic residence time on the exposure of nitrate to the benthic environment, Seitzinger et al. [2002] developed a regional-scale model wherein the fraction of stream nitrate removed across a given reach is determined from an empirically determined function of the ratio of the depth to the residence time of that reach. This approach is attractive due to its simplicity; however, it cannot account for any variation in the biotic demand for denitrification, and thus cannot represent biological controls on denitrification rates. A subsequent model developed by Mulholland et al. [2008] incorporated a mechanistic representation of hydrologic controls on solute uptake, along with an empirically-determined relationship between stream nitrate concentration and denitrification uptake velocity, a measure of biological uptake relative to nitrate concentration. By accounting for hydrologic as well as biological controls, this model is capable of representing supply and demand limitation of denitrification rates. Application

of this model demonstrates a decrease in nitrate removal efficiency at higher levels of nitrate loading, along with a disproportionate contribution of small streams to whole-network nitrate removal. Alexander et al. [2009] use a similar approach to investigate the seasonal changes in whole-network denitrification, finding that nitrate removal efficiency is greatest during months with low discharge and low levels of nitrate loading. Additionally, after explicitly designing the model structure to account for seasonal effects of discharge on nitrate removal, this approach suggests stream temperature as a further control on seasonal variations of denitrification rates.

To improve our understanding of controls on the overall magnitude of network-scale nitrate removal, along with the distribution of denitrification rates across stream networks, we have developed a model linking nitrogen and carbon dynamics across a simulated stream network. Our model builds on the previous model developed by Mulholland et al. [2008], adding an empirically derived relationship between whole-stream aerobic respiration rate and denitrification uptake rate. In addition to reducing the uncertainty surrounding the prediction of denitrification uptake velocity, this addition enables the model to represent linkages between factors which affect aerobic respiration rates and denitrification rates. We demonstrate the behavior of this model using stream temperature as a driver of stream respiration rates, thus enabling us to develop model scenarios incorporating reasonable ranges of variation in respiration rates across a simulated network. We then conduct numerical experiments based on these scenarios that illustrate the interactive effects of variation in nitrate supply and biological demand on the overall magnitude and spatial distribution of denitrification from stream networks.

Methods

We modified the existing Mulholland et al. [2008] ("LINX-II") stream network denitrification model to incorporate the effect of whole-stream respiration rate on simulated removal of nitrate due to denitrification. To understand how the addition of whole-stream respiration as a driver of denitrification influenced model behavior, we compared model output between the LINX-II model, and the modified form. We refer to the LINX-II model formulation as the "C" model, due to its prediction of denitrification uptake velocity from stream nitrate concentration alone, and we term the modified model the "C&R" model, as it uses both stream respiration and nitrate concentration to predict denitrification uptake velocity. In our simulation experiments, the two models use identical values for all shared parameters, therefore, all differences between the two models stem from the addition of respiration to the C&R model. We also investigated the response of the C&R model to variation in stream network scale respiration rates by creating model scenarios representing low respiration rates associated with cool stream temperature profiles typical of Rocky Mountain streams, and high respiration rates associated with warm stream temperature profiles typical of Appalachian Mountain streams.

Model Development

We re-implemented the Mulholland et al. [2008] model by treating water and nitrate as ecosystem 'currencies' in a structured network within the latest version (v2.0) of the Network Exchange Objects (NEO) modeling framework [Izurieta et al., 2012]. The network is a segmented representation of a stream network, with each segment connected to one downstream 'receiving' segment, any upstream 'contributing' segments, and one 'contributing' hillslope area. Consistent units are used for

all fundamental dimensions described by the model (length=m, time=s, mass=mg, temperature=°C), and equations reported below use these units exclusively. Stream flow is represented across the model using a steady state, flow accumulation approach. In the model, each segment i integrates the flow from its n_c upstream contributing segments and its contributing hillslope area. The discharge associated with any segment is thus:

$$Q_i = Q_{h_i} + \sum_{c_i=1}^{n_{c_i}} Q_{c_i} \tag{3.1}$$

where Q_i is the discharge of segment i, Q_{c_i} is the discharge in any contributing segment(s) (c) to segment i, and Q_{h_i} is the inflow of water from the contributing hillslope area h adjacent to segment i.

The concentration of nitrate is assumed to be equal in all hillslope contributed waters (Q_h) across the stream network. The nitrate concentration of each segment i is calculated as the flow-weighted average concentration of all contributing hillslope areas and upstream segments, modified by nitrate removal within segment i:

$$[NO_3^- - N]_i = \frac{\sum_{ci_j=1}^{n_{ci_j}} \left([NO_3^- - N]_{ci_j} \cdot Q_{ci_j}\right) + \left([NO_3^- - N]_{h_i} \cdot Q_{h_i}\right)}{Q_i} \cdot (1 - FR_i) \tag{3.2}$$

where $[NO_3^- - N]$ is the nitrate concentration, with subscript ci_j denoting all contributing segments j to segment i, and subscript h_i denoting the contributing hillslope area to segment i. FR_i is the fractional removal of nitrate from stream segment i removed via denitrification, calculated as:

$$FR_i = 1 - e^{-\frac{V_{f_{den_i}} \cdot A_i}{Q_i}} \tag{3.3}$$

where $V_{f_{den_i}}$ is the denitrification uptake velocity of segment i, Q_i is the discharge of segment i, and A_i is the surface area of segment i.

The model developed by Mulholland et al. [2008] uses a simple linear regression (SLR) approach to fit a power law relationship estimating denitrification uptake velocity from nitrate concentration within a stream segment, based on observations across 48 streams in the continental U.S. and Puerto Rico:

$$log_{10}(V_{f_{den_i}}) = -4.975 - 0.493 \cdot log_{10}([NO_3 - N]_i). \tag{3.4}$$

Here, the intercept differs from that reported by Mulholland et al. [2008] (-2.975), as they calculated $V_{f_{den}}$ in units of cm s^{-1}.

We verified that our implementation of the C model re-creates the Mulholland et al. [2008] model by comparing model outputs from identical scenarios (original model parameters and output provided by A. Helton). We then modified equation 3.4, forming a multiple linear regression (MLR) in which nitrate removal velocity is calculated from both nitrate concentration and whole-stream respiration rate, rather than from nitrate concentration alone. Data from one of the 48 streams Mulholland et al. [2008] used to fit equation 3.4 did not have an estimate of stream respiration. Therefore, we used data from the remaining 47 streams to recalculate equation 3.4, and to fit the new MLR:

$$log_{10}(V_{f_{den_i}}) = -4.978 - 0.493 \cdot log_{10}([NO_3 - N]_i), \tag{3.5}$$

$$log_{10}(V_{f_{den_i}}) = -3.930 - 0.438 \cdot log_{10}([NO_3 - N]_i) + 0.91748 \cdot log_{10}(R_i), \tag{3.6}$$

where R_i is the whole-stream respiration rate of segment i (mg O_2 m^{-2} sec^{-1}).

To visualize differences between estimates of nitrate removal velocity derived from the SLR (equation 3.5) and MLR (equation 3.6), we plotted observations of nitrate removal velocity against observed nitrate concentration along with a line representing the SLR relationship and a family of lines representing the MLR relationship across the observed range of respiration rates.

Model Scenarios

We developed nine different model scenarios to discern the effects of adding respiration as a predictor of nitrate removal velocity on model results (table 3.1). We compared results from the C model (using the SLR, equation 3.5) to the revised C&R model (using the MLR, equation 3.6) at three different hillslope nitrate concentrations. We selected hillslope nitrate concentrations of 0.1, 10, and 1000 mg NO_3^--N m^{-3} (equivalent to ug NO_3^--N l^{-1}), a range which encompasses much of the range of nitrate concentrations observed by Mulholland et al. [2008]. This range represents systems varying from those where nitrate availability is likely to limit productivity, to those where nitrate availability is unlikely to limit productivity. The C&R model scenarios were further extended by using respiration rates associated with cool and warm stream network temperatures. We identify these scenarios by their model formulation (i.e uptake derived from concentration (LINX-II); "Cool" = uptake derived from concentration and respiration using Colorado stream temperatures; "Warm" = uptake derived from concentration and respiration using North Carolina stream temperatures), with a subscript indicating the hillslope concentration (table 3.1).

Table 3.1: Summary of scenarios representing a range of temperature conditions and nitrate loading concentrations for concentration only and concentration & respiration simulation models

Model formulation	Concentration			Concentration and respiration					
Abbreviation	C			C&R					
Scenario Name	$C_{0.1}$	C_{10}	C_{1000}	$Cool_{0.1}$	$Cool_{10}$	$Cool_{1000}$	$Warm_{0.1}$	$Warm_{10}$	$Warm_{1000}$
Hillslope $[NO_3^- - N]$	0.1	10	1000	0.1	10	1000	0.1	10	1000
Water Temperature	–			Cool (Colorado)			Warm (North Carolina)		
Respiration Rate	–			$R = f(temperature)$					
Removal Velocity	$V_{f-den} = f([NO_3^- - N])$			$V_{f-den} = f([NO_3^- - N], Respiration)$					
Network Topology	North Saint Vrain, Colorado								

Model Parameterization

Topology The structure of the simulation model was built to represent the network topology of the North Saint Vrain (NSV), a small, steep stream network draining an area of 81.9 km^2 with elevations ranging from 2553 to 4347 m, located in Rocky Mountain National Park, Colorado. A simplified representation of the NSV network was derived from a 1/3 arc-second (˜10 meter) resolution DEM dataset provided by the United States Geologic Survey using a combination of GDAL, GRASS, and QGIS tools [USGS, 2015, GDAL/OGR contributors, 2019, GRASS Development Team, 2018, QGIS Development Team, 2018]. The watershed boundary and stream network were identified using the GRASS r.watershed module, with an outflow location of (W 105.55297, N 40.21082), and a minimum exterior basin size (i.e. the minimum drainage area to form a headwater stream) of 0.5 km^2. The resulting stream features were vectorized and smoothed, in order to to remove the unrealistic stair-step pattern (and associated exaggerated lengths) of diagonally oriented reaches which results from their raster origin, producing a stream network containing 69.8 km of streams. Stream vectors were then initially segmented at each stream confluence, and then further segmented using the GRASS tool v.split.length, producing segments up to but not exceeding 600 m long. For each segment, adjacent segments and contributing areas (i.e. areas of the watershed that drain directly to the segment) were identified. This GIS based workflow was validated by recreating the network structure and topology used in the original Mulholland et al. [2008] model.

Stream Flow, Stream Width, and Hillslope Nitrate Concentration All scenarios assume a constant water yield from all hillslope areas, calculated as:

$$Q_h = 2.6610^{-8} \cdot A_h \tag{3.7}$$

where Q_h is the volumetric flow of water yielded from hillslope h with area A_h. This relationship approximates midsummer stream flow in the NSV, consistent with measurements taken within the NSV by Day and Hall [2017], and data from the nearby U.S Geological Survey Big Thomson Moraine Park streamflow gage.

Stream width is defined in relation to stream flow as:

$$W_i = 7.17 \cdot Q_i^{0.0348} \tag{3.8}$$

where W_i is the width of segment i (m), and Q_i is the discharge of segment i. This relationship is retained from the previous LINX-II model implementations [Mulholland et al., 2008, Helton et al., 2011]. For each segment, we calculate surface area (A_i) as the product of the segment's length and width.

Nitrate is introduced into the stream network as a constant concentration in all hillslope contributions, with model scenarios representing low, moderate, and high hillslope concentrations (table 3.1).

Respiration and Temperature In addition to the parameter needs of the C model, the C&R model requires a description of aerobic respiration rates across the stream network. Due to the difficulty in measuring respiration rates, along with the large number of factors which may augment or constrain respiration rates, we do not attempt to meet this additional parameterization requirement by forming a locally representative model of respiration rates. However, assuming a constant respiration rate would be highly unrealistic, and would preclude any examination of the effects of variable respiration rates on network scale denitrification. Therefore, we derive a reasonable range of respiration rates from stream temperatures that provide a foothold for exploring the network-scale implications of variation in biological demand for nitrate by assuming an Arrhenius-type relationship between stream respiration rates

and temperature [Arrhenius, 1889]. We used a local respiration rate estimate of 0.0439 mg O_2 m^{-2} s^{-1} at a stream temperature of 8°C [Madinger and Hall, 2019] , along with an activation energy of 0.65 joules observed by Perkins et al. [2012] to form the stream temperature - respiration relationship:

$$R_i = 1.95 \cdot 10^{10} \cdot e^{\frac{-0.65}{(T_i+273.5)\cdot 8.62\cdot 10^{-5}}} \tag{3.9}$$

where R_i is the respiration rate of segment i, and T_i is the temperature of segment i.

We parameterized cool and warm stream temperature conditions based on relationships between stream temperature and elevation, where cool conditions represent high elevation Rocky Mountain streams, and warm conditions represent lower elevation Appalachian streams.

Cool Temperature We use temperature data collected for chapter 2 to develop a generalized temperature regime representative of a Rocky Mountain stream network. A statistical model describing the contribution of both lake and stream elevation to stream temperature was fitted to observations of average stream temperature for the period of August 17, 2014 to August 23, 2014 collected with 11 Onset HOBO pendant logging thermometers deployed in streams across the NSV network. To make the cool temperature scenario generally representative of Rocky Mountain stream networks, we discounted the influence of lake elevation on stream temperature, thereby producing a simple temperature-elevation relationship:

$$T_i = 24.2 - 0.00488 \cdot E_i, \tag{3.10}$$

where T_i is the temperature and E_i is the elevation of stream segment i.

Warm Temperature Daily means of late summer stream temperature measured at the Coweeta Hydrologic Laboratory, located in the Appalachian mountains of North Carolina [Webster, 2014], were regressed against stream elevation. To apply this relationship to the simulation model while retaining the range of temperatures characteristic of this warmer region, we re-scaled the elevation values within the Coweeta dataset to match the range of values found within the NSV stream network. When applied to the NSV network, the resulting relationship produces a distribution of temperatures which are representative of late summer conditions in the southern Appalachian Mountains:

$$T_i = 35.9 - 0.00579 \cdot E_i, \tag{3.11}$$

where T_i is the temperature and E_i is the elevation of stream segment i.

Analysis and Visualization

We calculated the cumulative fractional removal (CFR) for each stream segment as the removal of nitrate from the stream network up to and including that segment. Because hillslope nitrate concentration is held constant within each simulation, the CFR of each segment i can be calculated from the nitrate concentration of segment i, and the hillslope nitrate concentration of the simulation:

$$CFR_i = 1 - \frac{[NO_3^- - N]_i}{[NO_3^- - N]_h}. \tag{3.12}$$

The CFR at the outflow represents the "whole network" fractional removal, i.e., the ratio of mass removal of nitrate across the network to the mass of nitrate delivered to the stream network from the hillslopes.

We explored the simulation results by examining the spatial distribution of

denitrification across the NSV network. Additionally, we used the R statistical computing environment [R Core Team, 2014] to analyze and plot relationships among simulated stream segment $[NO_3 - N]$, $V_{f_{den}}$, R, and areal denitrification rate. Although different from the units of the model equations (presented above), results are presented in the familiar units of μg N l^{-1} for concentration, cm sec^{-1} for denitrification uptake velocity, l sec^{-1} for stream discharge, g O_2 m^{-2} day^{-1} for respiration, and μg N m^{-2} sec^{-1} for areal denitrification rate.

Results and Discussion

Prediction of Nitrate Removal Velocity

Our model reproduced results from the published LINX-II model [Mulholland et al., 2008] when using equation 3.4 to predict $V_{f_{den}}$, thereby demonstrating the equivalence between our model implementation and that of the LINX-II model. Throughout the rest of this paper, reported results from the C model formulation use equation 3.5 to predict $V_{f_{den}}$, which produces nearly identical results as equation 3.4, due to the strong similarity between the slopes and intercepts in the two equations. Thus, the C model formulation used here is directly comparable to the LINX-II model.

The addition of a respiration term to the prediction of $V_{f_{den}}$ in the C&R model (equation 3.6) substantially improves upon the explanatory power of the simpler C model (equation 3.5) (table 3.2). In fact, much of the unexplained variance in $V_{f_{den}}$ relative to the original C regression line is explained by variation in whole-stream respiration rates across sites (figure 3.1). Specifically, sites with low respiration rates tend to plot below the C regression line, while sites with high respiration tend to plot above the line. Thus, the family of regression lines plotted in figure (3.1) for the C&R model (equation 3.6) largely captures the effect of respiration rate on $V_{f_{den}}$. As the effect of R appears to be independent from the effect of $[NO_3^- - N]$, the

combined explanatory power (R^2) of nitrate concentration and respiration is nearly the sum of the explanatory power of each term separately (table 3.2). However, the C&R model does show slightly decreased sensitivity of $V_{f_{den}}$ to stream nitrate concentration relative to the C model, as indicated by the small reduction in slope of C&R regression lines relative to C regression line (figure 3.1). As a result, the single C regression line from equation 3.5 predicts $V_{f_{den}}$ values associated with somewhat higher R^2 in equation 3.6 as $[NO_3^- - N]$ decreases.

Table 3.2: Intercepts, coefficients, and explanatory power of three linear regression models predicting observed $V_{f_{den}}$ (log(m sec^{-1})) across 47 streams. Units for [NO_3^-] are log(mg m^{-3}) and units for respiration rate are log(mg O_2 m^{-2} sec^{-1}).

Model form	Independent variable	Intercept	[NO_3^-] coeff.	Respiration coeff.	R^2
C	[NO_3^-]	-4.978	-0.493	-	0.37
-	Respiration Rate	-0.472	-	1.051	0.33
C&R	[NO_3^-], Respiration Rate	-3.93	-0.438	0.918	0.62

Network Simulation Results

Our simulations illustrate the effects of nitrate loading and respiration rates on reach- and network-scale nitrate removal. Comparison of CFR between model scenarios reveals the interactive effects of hillslope nitrate concentrations and respiration rates under warm and cool conditions on the spatial distribution of nitrate removal and the magnitude of whole-network cumulative fractional removal. The differences between scenarios are modulated by the effects of serial processing of nitrate across the simulations, which leads to substantial variability in nitrate removal velocity within simulations with large whole-network CFR. Examination of spatial patterns of predicted areal denitrification rates suggests conditions under which nitrate removal is primarily limited by nitrate scarcity, or by biological denitrification

Figure 3.1: Relationships among $V_{f_{den}}$, $[NO_3^- - N]$, and R in the LINX-II dataset [Mulholland et al., 2008]. Black dashed line indicates the SLR model relating $V_{f_{den}}$ and $[NO_3^- - N]$ (equation 3.5) used in the C formulation, while the greyscale solid lines represent the additional influence of R used in the C&R formulation (equation 3.6).

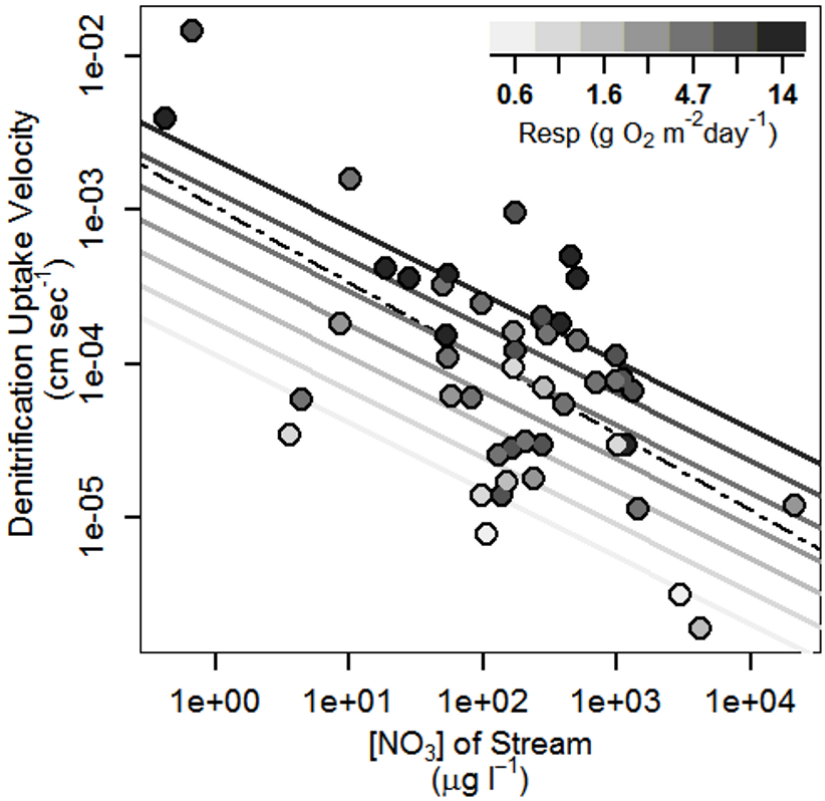

Figure 3.2: Cumulative fractional removal (CFR) of nitrate for each modeled segment across all 9 scenarios, with whole-network CFR indicated by call-outs on each terminal segment. Substantial differences in whole-network CFR driven by hillslope concentrations necessitate different colormaps; thus, each row has an independent colormap.

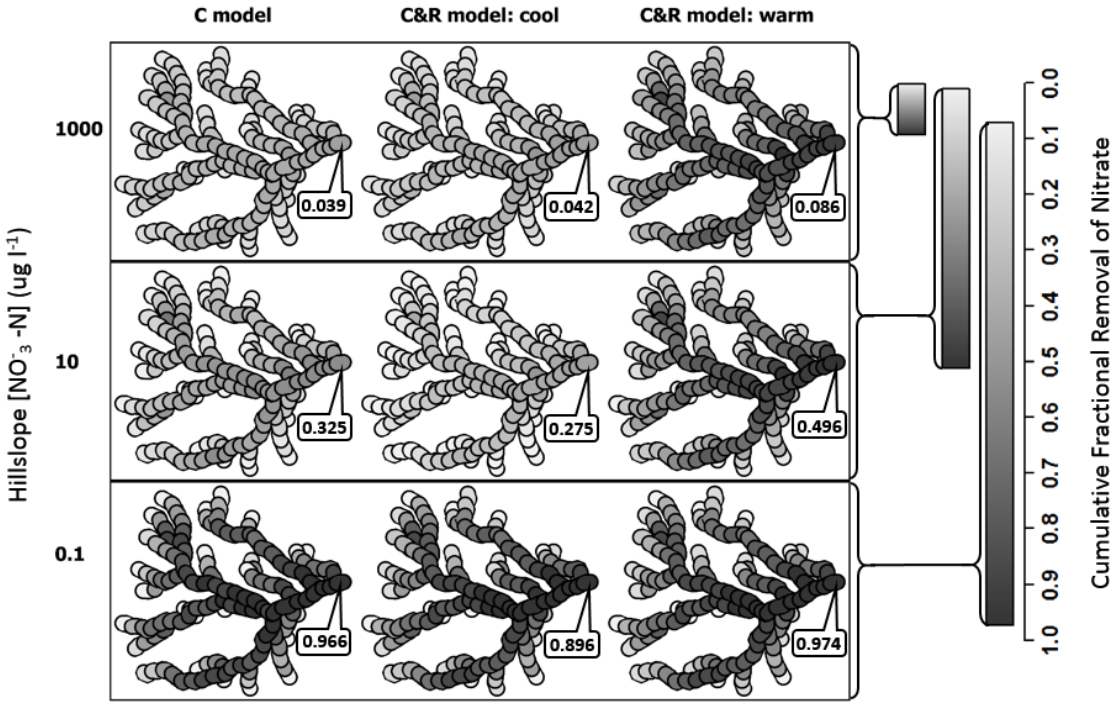

demand, which is regulated in our model by both stream nitrate concentrations and respiration rates.

Cumulative Fractional Removal of Nitrate (CFR) Patterns of CFR predicted by our simulations reveal the spatial distribution of nitrate removal, and are similar to those reported by Mulholland et al. [2008] in several ways. Across all model scenarios, CFR increases from a value near 0 in headwater reaches, where little nitrate removal has occurred, to a maximum value at the stream network outflow (figure 3.2). In

all scenarios, this increase in CFR happens more rapidly along headwater reaches than along mainstem reaches, a pattern that is strongest in the low concentration scenarios. Additionally, our results show an inverse relationship between the hillslope nitrate concentration and the whole-network CFR (note different scales of grey-scale bars for each hillslope concentration in figure 3.2).

These patterns, which are common to the scenarios evaluated here as well as the scenarios considered by Mulholland et al. [2008], arise from a downstream increase in the ratio of stream flow to channel area (hydraulic load) of the simulated reaches, along with the increasing dilution of laterally-sourced water by upstream-sourced water. The downstream increase in hydraulic load arises from the proportionally greater increase in stream discharge than stream bed area (equation 3.8), and is consistent with patterns of hydraulic geometry generally observed in streams and rivers [Leopold and Maddock Jr., 1953]. As the fractional removal of nitrate from a reach determined from $V_{f_{den}}$, bed area, and discharge (equation 3.3), larger segments with increased hydraulic loads remove a smaller fraction of nitrate than an upstream segment with equivalent biological demand (i.e., equal $V_{f_{den}}$). Further, the dilution of direct hillslope contributions of water and nitrate to a segment by the influx of water and nitrate from upstream reaches increases in a downstream direction. As this upstream-sourced water has already been subjected to denitrification in upstream reaches, the nitrate concentration is lower than that of hillslope-sourced water, leading to a lower nitrate concentration for the overall inputs to downstream reaches (equation 3.2). The resulting decreased nitrate concentration of downstream segments leads to a reduction in the mass of nitrate removed, thus leading toward a reduction in the rate of depletion of nitrate concentration, and a corresponding stabilization of CFR. The overall pattern of a rapid increase in CFR in headwater reaches and a stabilization of CFR in mainstem reaches is thus broadly applicable to stream networks, although

heterogeneity in stream width, hillslope nitrate concentrations, or respiration rates may disrupt this pattern.

Due to the simulated effect of temperature on respiration rates (equation 3.9), and therefore denitrification uptake rates (equation 3.6), predicted whole-network CFR values are generally higher for the C&R Warm scenarios than the C scenarios, and lower for the C&R Cool scenarios than for the C scenarios. The Warm scenario predicts nearly equivalent (101% as much) whole-network CFR as the C scenario at low hillslope concentrations (0.1 mg NO_3^--N m^{-3}), substantially more (152% as much) whole-network CFR as the C scenario at moderate hillslope concentrations (10 mg NO_3^--N m^{-3}), and more than double (221% as much) whole-network CFR than the C scenarios at high hillslope concentrations (1000 mg NO_3^--N m^{-3}). The pattern of whole-network CFR for Cool scenarios is less consistent, with the Cool scenario predicting slightly lower (93% as much) whole-network CFR than the C scenario at low hillslope concentrations, substantially lower (85% as much) whole-network CFR as the C scenario at moderate hillslope concentrations, and slightly greater (108%) as much) whole-network CFR that the C scenario at high hillslope concentrations.

Nitrate Removal Velocity ($V_{f_{den}}$) Solutes like nitrate are processed serially in stream networks; nitrate that is not removed from a given reach flows to the next reach, where it may be removed, or may continue to flow downstream. In our simulations, serial processing of nitrate results in reduced concentration and an associated increase in $V_{f_{den}}$ as water flows downstream. The effect of variation in concentration on $V_{f_{den}}$ is most visible for low hillslope concentrations (i.e., $[NO_3^- - N]_h$=0.1 in figure 3.3A), where high values of $V_{f_{den}}$ cause high fractional removal of nitrate in stream reaches. In contrast, the effects of serial processing are less pronounced at high hillslope concentrations (i.e., $[NO_3^- - N]_h$=1000 in figure

Figure 3.3: Relationship between $V_{f_{den}}$ and $[NO_3^- - N]$ for each model scenario. Color hues distinguish between C&R Warm, C&R Cool, and C scenarios, while color shades indicate segment discharge. Grey background lines are from figure 3.1, with dashed lines indicating the $V_{f_{den}}$-[NO_3^--N] relationship for the C model formulation, and solid lines indicating the slope of the $V_{f_{den}}$-[NO_3^--N] relationship for the C&R model formulation at respiration rates ranging from 0.6 to 14 g O_2 m^{-2} day^{-1}.

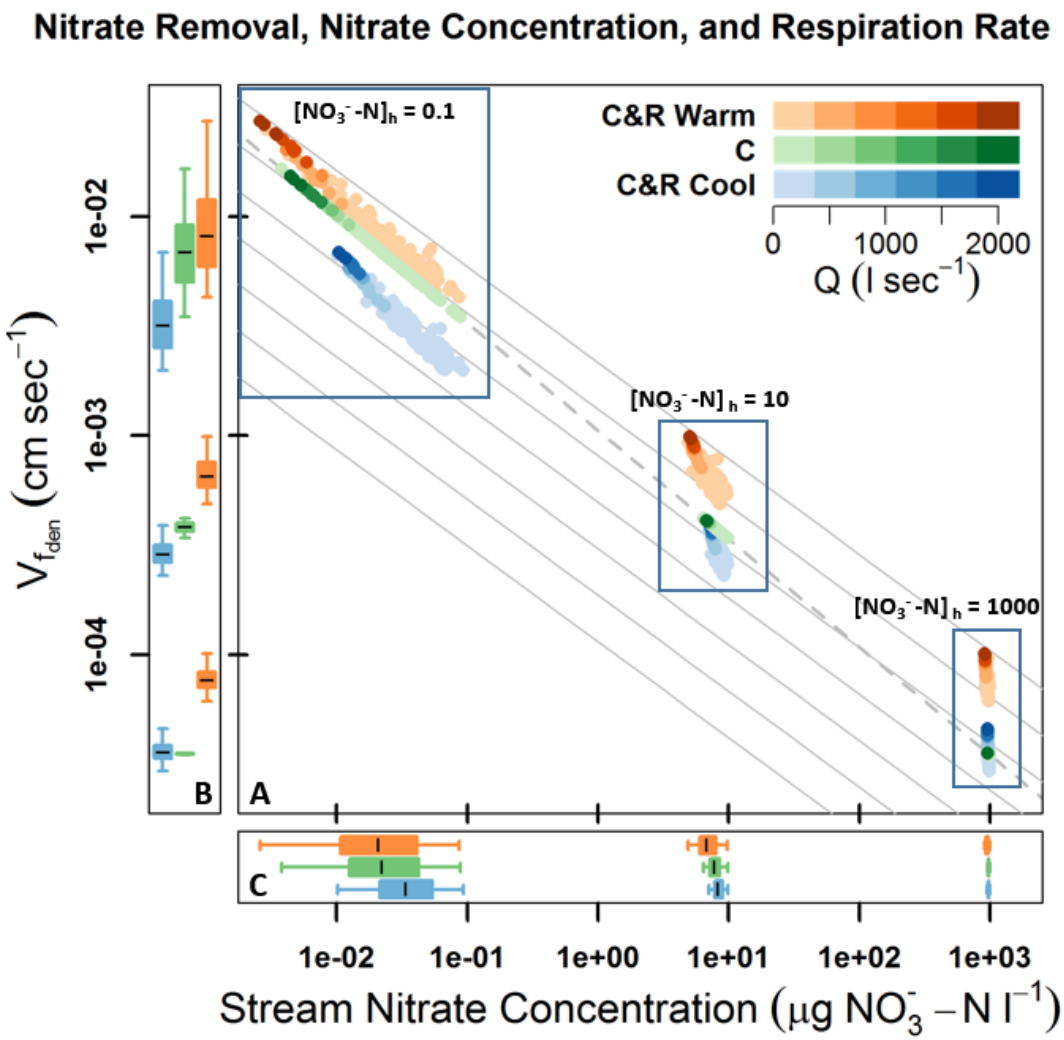

3.3A), where values of $V_{f_{den}}$ are low, fractional removal of nitrate in each steam reach is low, and therefore, the fractional decline in concentration is small. Although different network extents and topologies alter the expression of this serial processing, these results are broadly consistent with the findings of [Mulholland et al., 2008] due to the similar $V_{f_{den}}$-[NO_3^--N] relationships used.

While $V_{f_{den}}$ is influenced by nitrate concentration in all simulations, the slope of this relationship differs between the C and C&R models (table 3.2). Due to the decreased slope of the $V_{f_{den}}$-[NO_3^--N] relationship used in the C&R model as compared to the C model, the two model formulations can produce equivalent predictions of $V_{f_{den}}$ either when nitrate concentration is high and respiration rate is low, or when nitrate concentration is low and respiration rate is high (figure 3.1). This effect is illustrated by the similarities between the whole-network CFR of the $Cool_{1000}$ and C_{1000} scenarios, and in the similarities between the $Warm_{0.1}$ and $C_{0.1}$ scenarios (figure 3.2).

In addition to the effect of [NO_3^--N] on $V_{f_{den}}$, the C&R model formulations considered here incorporate the effect of R on $V_{f_{den}}$, which provides an additional mechanism for variation in $V_{f_{den}}$ that can not be represented by the C configuration or the approach used by Mulholland et al. [2008]. Simulation results from C&R scenarios plotted in figure 3.3A reveal the vertical shift associated with the additive effect of R, however the slope of the $V_{f_{den}}$ - nitrate concentration relationship does not consistently follow the slope described by equation 3.6. Instead, the increase in respiration rates across the simulated networks, which is driven by warming stream temperatures in a downstream direction, causes $V_{f_{den}}$ to increase in lower, warmer reaches (equation 3.6), thereby increasing the slope of the network-wide $V_{f_{den}}$-[NO_3^--N] relationship.

While the slope of network-wide $V_{f_{den}}$-[NO_3^--N] relationship differs between the

C and C&R model formulations regardless of hillslope nitrate concentration, this difference is more pronounced in the moderate and high concentration scenarios, and less evident in the low concentration scenarios. At moderate and high concentrations, serial processing alone produces only a slight increase in $V_{f_{den}}$ due to the minimal depletion of nitrate concentration across the simulations, as illustrated by the minimal variation in both $V_{f_{den}}$ (figure 3.3B) and nitrate concentration (figure 3.3C) for the C_{10} and C_{1000} scenarios. However, the increased respiration rates of lower, warmer streams contribute to variation in $V_{f_{den}}$ in the C&R scenarios, regardless of the magnitude of the serial processing effect. Therefore, the slope of the network-wide $V_{f_{den}}$-[NO_3^--N] relationship is largely driven by serial processing of nitrate for all low concentration scenarios, and is therefore similar between the scenarios. In contrast, the slope of the network-wide $V_{f_{den}}$-[NO_3^--N] relationship differs strongly between the C and C&R models at high concentrations, where varied respiration rates make a more substantial contribution to the variation in $V_{f_{den}}$.

Areal Denitrification Rate In contrast to information provided by the fractional removal of nitrate and the denitrification uptake velocity, the rate of nitrate removal per stream bed area (areal denitrification rate; U) reveals the absolute rate of denitrification relative to the stream-bed surface area, and can therefore reveal supply limitations of denitrification rates that are not apparent from examination of $V_{f_{den}}$ alone. However, inferences derived from comparisons of U in field studies are confounded by uncontrolled variation in stream morphology. Stream morphology is held constant between all of our simulations, therefore allowing for straightforward comparisons across modeled scenarios.

While simulated $V_{f_{den}}$, fractional removal, and whole-network CFR are inversely correlated with hillslope nitrate concentration across all scenarios, U is positively

Figure 3.4: Relationships between areal denitrification rate and stream segment discharge for all model scenarios. Areal denitrification rates vary strongly between scenarios of different hillslope concentrations, naturally forming upper, middle, and lower groups (high, moderate, and low hillslope concentrations respectively). Each plotted point represents a simulated segment, with the hue distinguishing between C&R Warm, C&R Cool, and C scenarios, and the shade representing that segment's respiration rate.

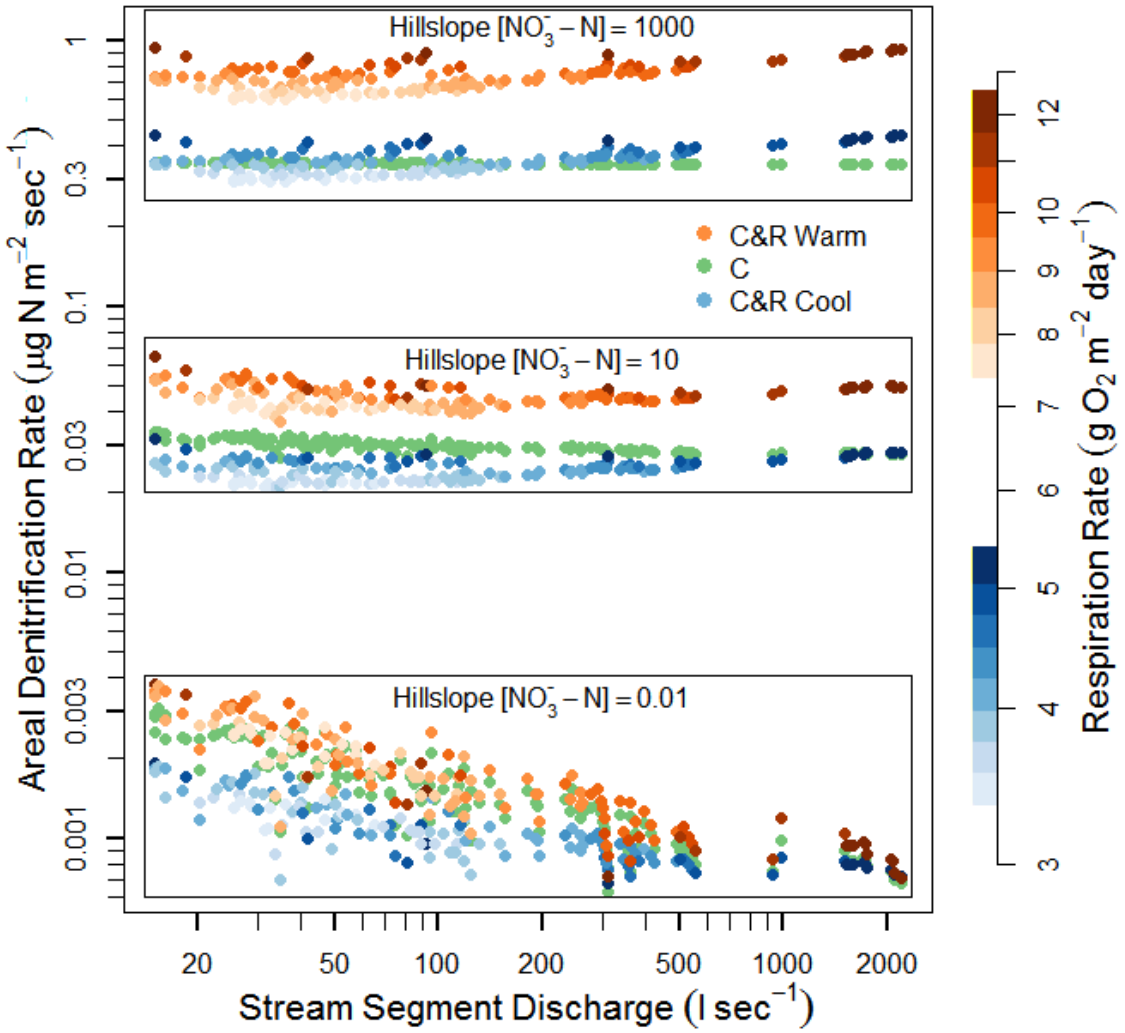

correlated with with hillslope nitrate concentration (figure 3.4). Thus, while the fraction of available N removed from the system decreases, U nevertheless increases at higher concentrations. These results are consistent with saturating uptake kinetic models (e.g., Michaelis-Menten), where uptake rate is limited by the availability of a solute at low concentrations, but some other factor limits uptake rates at high concentrations.

As serial processing causes a substantial downstream decline in nitrate concentrations across some scenarios, U exhibits a corresponding trend. In the $C_{0.1}$ scenario, high fractional removal causes a steep downstream decline in U (figure 3.4), which is driven by the substantial reduction in nitrate concentration across the simulation. The C_{10} scenario, which predicts a smaller overall N removal fraction, shows less of a decline in U, and the C_{1000} scenario, which predicts a very small overall N removal fraction, shows an almost constant U across the simulated network.

In addition to the effect of nitrate concentration on the distribution of U across a stream network, stream respiration rate (R) influences network-scale patterns of U in the C&R scenarios. In the high concentration scenarios, the longitudinal decline in nitrate concentrations is proportionally small; therefore, U is nearly constant for the C_{1000} scenario, and variation in U in the $Warm_{1000}$ and $Cool_{1000}$ scenarios is largely driven by variation in R (figure 3.4). As R is driven by temperature, which increases in a downstream direction with elevation loss, U tends to be higher in larger, warmer streams. This same effect in visible, though less pronounced, in the $Warm_{10}$ and $Cool_{10}$ scenarios, where variation in U is influenced both by the downstream depletion of nitrate concentration, and variation in R. At low concentrations, the large magnitude of the depletion of nitrate concentration is the dominant control on variation in U, with variation in R making only a minor contribution.

In combination, results from all nine scenarios reveal two distinct mechanisms

which can contribute to systematic longitudinal variation in U. First, where high fractional removal of nitrate causes substantial depletion of nitrate concentration through serial processing, the decreasing availability of nitrate in a downstream direction causes a decrease in U. Second, where the depletion of nitrate concentration across the simulated network is proportionally small and the effects of respiration are considered, the temperature-driven increase in R in a downstream direction causes a downstream increase in U. Thus, agreement between the longitudinal trends of the C and C&R scenarios indicates the dominance of the first mechanism, while disagreement between the longitudinal trends of the C and C&R scenarios indicates the relevance of the second mechanism.

Therefore, our results suggest that variation in U across stream networks is controlled by the available supply of nitrate in stream networks at low and moderate hillslope concentrations, when the magnitude of denitrification is large enough relative to the stream nitrate concentration to cause a substantial depletion of nitrate concentration across the simulated network. Alternately, at high hillslope concentrations, we find that variation in U across stream networks is controlled by biological demand, represented by network-wide patterns of R. These different mechanisms are also apparent values of whole-network CFR predicted by our scenarios (figure 3.2). At low concentrations, when nitrate removal is limited by the availability of nitrate, the spread between the scenarios is minimal, with the $Warm_{0.1}$ scenario predicting 109% as much nitrate removal as the $Cool_{0.1}$. This spread increases substantially to 205% at high concentrations, when nitrate removal is responsive to biological demand not limited by nitrate availability.

Additional variability in U not associated with Q or R is apparent in the $Warm_{0.1}$, $Cool_{0.1}$, and $C_{0.1}$ scenarios, where high nitrate removal rates deplete stream nitrate to concentrations well below hillslope nitrate concentrations. Segments which

receive most of their water and nitrate input from upstream segments (i.e., those with a small lateral contributing area relative to the total contributing area to that segment) therefore receive water with a lower nitrate concentration (equation 3.2), which decreases U in those segments. In contrast, segments which receive more water directly from their lateral contributing area (i.e., those with a large lateral contributing area relative to the total contributing area) receive water with a higher nitrate concentration, and predict higher U. These effects are minimal in segments with higher Q, where lateral contributing areas represent a small portion of the total contributing area, and at higher hillslope concentrations, where the nitrate concentration of water from upstream segments is more similar to the hillslope concentration.

Implications for anthropogenic alterations to patterns of N removal

Results of the nine model scenarios suggest variable controls of stream nitrate concentration and biological denitrification capacity on nitrate removal. In systems with low nitrate concentrations, we suggest that nitrate removal rates are primarily limited by nitrate availability, and not by whole-stream metabolic activity. Thus, spatial variability of nitrate sources in such systems may influence the spatial patterns of nitrate removal, while spatial variability of whole-stream metabolic capacity will have little effect on the distribution or overall magnitude of nitrate removal. In contrast, where supplies of nitrate are substantially in excess of denitrification demand, we suggest that the magnitude and spatial distribution of nitrate removal is controlled by the biological demand for nitrate by denitrification, and is thus susceptible to factors such as stream temperature and aerobic respiration rate.

The results presented here represent only the influence of temperature on variation in respiration, and do not consider other factors which may also influence

respiration. While the relationship between temperature and respiration rate used here is consistent with theory and empirical evidence [Arrhenius, 1889, Perkins et al., 2012], local variation in other factors, such as stream channel geometry or sediment organic carbon content, are also likely to influence respiration rates. However, our use of temperature to drive network-wide patterns of respiration rate enables us demonstrate the influence of variation in respiration rate, whether driven by temperature or other factors, on the magnitude and spatial distribution of nitrate removal in stream networks where nitrogen is not limiting. Building on this foundation, a more detailed understanding of spatial controls on respiration rates is critical to moving this work forward, and will potentially reveal numerous reach- to landscape-scale controls on stream denitrification rates.

Conclusion

Our model simulations reveal that whole-stream respiration rates may indicate a substantial influence of biological demand on variation in rates of nitrate removal from stream networks. Additionally, we find that rates of N removal may be less sensitive to stream nitrate concentration than previously suggested. In combination, these results suggest that patterns of N removal from high-concentration systems may be closely related to patterns of respiration rates, and that N removal from warmer, higher concentration streams may be more significant than would be predicted from nitrate concentrations alone. Further examination of mechanisms which drive spatial variability in stream respiration rates may yield more detailed understanding of the spatial patterns of stream denitrification and their relationship to upland characteristics.

LOSS OF CHANNEL COMPLEXITY DUE TO HISTORICAL LOGGING LIMITS STREAM NETWORK DENITRIFICATION CAPACITY

Introduction

The removal of nitrate from streams and rivers through the process of denitrification is an important component of terrestrial nitrogen cycling [Seitzinger et al., 2006, Ranalli and Macalady, 2010], however, the biological and geomorphic controls on rates of nitrate removal by denitrification are only partially understood. Anthropogenic alterations to the global nitrogen cycle have vastly increased nitrate delivery to streams and rivers, though this increase has been partially offset by increased rates of nitrate removal from streams and rivers [Galloway et al., 2004]. While nitrate removal from streams by denitrification has not maintained nitrate concentrations at pre-industrial levels, stream denitrification does have the potential to substantially alter stream nitrate concentrations and downstream nitrate transport, with consequences for water quality and ecosystem function at local and regional scales. Empirically-informed models and mass-balance approaches suggest a wide range of likely network-scale nitrate removal fractions [Howarth et al., 1996, Alexander et al., 2000, Seitzinger et al., 2002, Mulholland et al., 2008], with estimates for different stream networks varying from less than 20% to 50% or more. However, these approaches have limited ability to identify network-scale relationships between denitrification rates and biological and hydrogeomorphic factors.

Previous work has suggested that whole-network denitrification rates may be influenced by network topology, stream nitrate concentration, channel width, depth, and discharge [Alexander et al., 2000, Wollheim et al., 2006, Mulholland et al., 2008, Alexander et al., 2009, Helton et al., 2018]. Additional factors are known to correlate with variation in denitrification rates at finer scales, including dissolved oxygen con-

centration, aerobic respiration rate, stream temperature, sediment size, and organic carbon content, [Arango et al., 2007, Arango and Tank, 2008, Martin et al., 2001, Mulholland et al., 2009, Piña-Ochoa and Álvarez Cobelas, 2006, Reisinger et al., 2016, Stelzer and Bartsch, 2012, Taylor and Townsend, 2012]. Many of these factors may be highly variable across stream networks, potentially creating localized areas with conditions favorable to denitrification that contribute substantially to whole-network denitrification [McClain et al., 2003, Seitzinger et al., 2006]. While investigating the network-scale implications of these factors may improve our understanding of natural and anthropogenic constraints on denitrification, observational approaches remain elusive [Groffman et al., 2006]. Denitrification can be accurately measured in incubation chambers containing samples of benthic substrate and streamwater [Arango et al., 2007, Madinger and Hall, 2019], but the use of such measurements to calculate reach- or network-scale processes becomes more problematic with increases in the physical, chemical, and hydrologic heterogeneity of the system. The use of isotopic tracers to measure whole-stream denitrification rates is promising [Böhlke et al., 2004, Mulholland et al., 2009], although such methods are expensive, and limited to reach-scale measurements. Watershed scale N budget approaches may provide estimates of whole-network denitrification rates [Schaefer and Alber, 2007, van Breemen et al., 2002], but direct comparisons of altered and unaltered watersheds are subject to confounding factors including differences in upland ecosystems, soils, stream hydrology, and network topology. Therefore, we suggest that the development of spatially explicit network-scale denitrification models that selectively incorporate these potential controls allows for the exploration of reasonable scenarios of stream network heterogeneity that will broaden our understanding of the natural and anthropogenic constraints on network-scale denitrification [Boyer et al., 2006, Helton et al., 2011].

Anthropogenic alterations to upland and fluvial systems have substantially affected the physical and chemical characteristics of streams, with potentially widespread consequences for reach- and network-scale denitrification. For example, agriculturally-driven channelization and loss of riparian vegetation have been suggested to reduce denitrification rates [Kemp and Dodds, 2002], while the restoration of lateral connectivity and sediment retention have been suggested to enhance reach-scale denitrification [Craig et al., 2008, Kaushal et al., 2008, Newcomer Johnson et al., 2016]. Similarly, numerous studies have documented extensive and persistent simplifying effects of historical logging practices on channel morphology, commonly including reductions in side channels, pools, and channel-spanning logjams, as well as the resulting reduction in the retention of sediment and organic carbon [Wohl, 2014, Valett et al., 2002, Mellina and Hinch, 2009, Francis et al., 2008, Collins et al., 2012, Gurnell et al., 2005, Livers and Wohl, 2016, Sear et al., 2010, Entrekin et al., 2008, Warren et al., 2007].

To investigate the consequences of logging-induced stream channel simplification on network-scale denitrification, we consider the northern Front Range region of Colorado, USA, as a tractable case study with broader implications for understanding the role of channel simplification in altering nitrogen uptake dynamics. Comparisons between unlogged and logged sections of this region suggest that historical logging has pushed streams into a simplified alternate stable state, characterized by a reduction in the occurrence of both side channels and channel spanning jams [Wohl, 2011, Livers et al., 2017]. Based on this logging effect, we hypothesize that network-scale denitrification rates are reduced under logged conditions due to the reduced wetted area and reduced aerobic respiration rate, which arise in turn from the logging-driven loss of multi-channel reaches and channel-spanning jams. We address this hypothesis using a spatially-explicit stream network denitrification model capable of simulating

the effects of hydrology, channel morphology, stream nitrate concentration, and whole-stream aerobic respiration rate on reach- and network-scale nitrate removal.

Methods

We used a simulation model of stream denitrification to quantify stream channel geomorphic response to logging, and simulate resulting changes in biotic removal of nitrate (via denitrification) from a sub-alpine stream network. We parameterized channel morphology in two ways: an unlogged scenario based on the current channel morphology in an a watershed within Rocky Mountain National Park, and a logged scenario based on the expected changes to channel morphology in the watershed if it were logged, derived from analysis of nearby logged watersheds. In addition to the default parameterization of unlogged and logged conditions, we used a Monte Carlo propagation of uncertainty surrounding the effect of logging on whole-network denitrification by re-fitting regression models used to represent the logging effect to resampled datasets.

Study Area

Model development and parameterization was based on extensive field work [Livers and Wohl, 2016, Madinger and Hall, 2019, Wohl and Beckman, 2014, Venarsky et al., 2018] that has occurred across three stream networks located on the eastern slope of the northern Colorado Front Range, as well as multiple sites located in the neaby Snowy Mountains of southern Wyoming (figure 4.1). Study watersheds include the North St Vrain (NSV), Glacier Creek (GC), and Cache la Poudre (ClP). The majority of the study area is characterized by sub-alpine coniferous forest, while alpine vegetation is dominant at elevations above the tree line at ca. 3500 meters [Veblen and Lorenz, 1986]. Portions of this study area were logged during the late

19th and early 20th centuries, with persistent effects on upland and riparian forest, and fluvial geomorphology [Veblen and Lorenz, 1986, Livers et al., 2017]. As with many forested areas [Muotka and Laasonen, 2002, Tornlund and Ostlund, 2002, Wohl, 2014], logging in this region involved the construction of splash dams and the removal of channel obstructions in order to facilitate the downstream transportation of timber, with well documented effects on channel complexity, the longitudinal density of in-stream wood and logjams, and sediment retention [Wohl and Beckman, 2011, Livers and Wohl, 2016].

Data Sources

We compiled data from reach- and point-scale field surveys of channel morphology, sediment volume, carbon content, stream temperature, and aerobic respiration rates (table 4.1). Measurements of whole-stream aerobic respiration rate performed by Madinger and Hall [2019] were conducted at locations corresponding to morphologic surveys performed by Livers and Wohl [2016], facilitating comparison of respiration rates with morphologic variables. Relationships between reach- and point-scale measurements were determined by calculating the mean values of point measurements located within each sampling reach.

Simulation Model Description

We used a previously developed stream network denitrification simulation model to estimate whole-network nitrate removal from unlogged and logged scenarios. The model is described in detail in chapter 3, and we provide a brief summary of its features and assumptions most relevant to this effort. The model builds on the approach of Mulholland et al. [2008], which uses the mathematics of nutrient spiralling theory [Stream Solute Workshop, 1990] to estimate the fractional removal of nitrate from each of a collection of networked stream segments. By tracking nitrate flow

Figure 4.1: Location of study area within the western United States, along with the extent of stream morphology surveys, and the location of respiration sites. From north to south, streams depicted are: 1) sections of the Rock Creek, South French Creek, and Mullen Creek networks, located in the Snowy mountains (all in green), 2) sections of the Cache La Poudre network (in orange), 3) the Glacier Creek network (in red), and 4) the North Saint Vrain network (in blue).

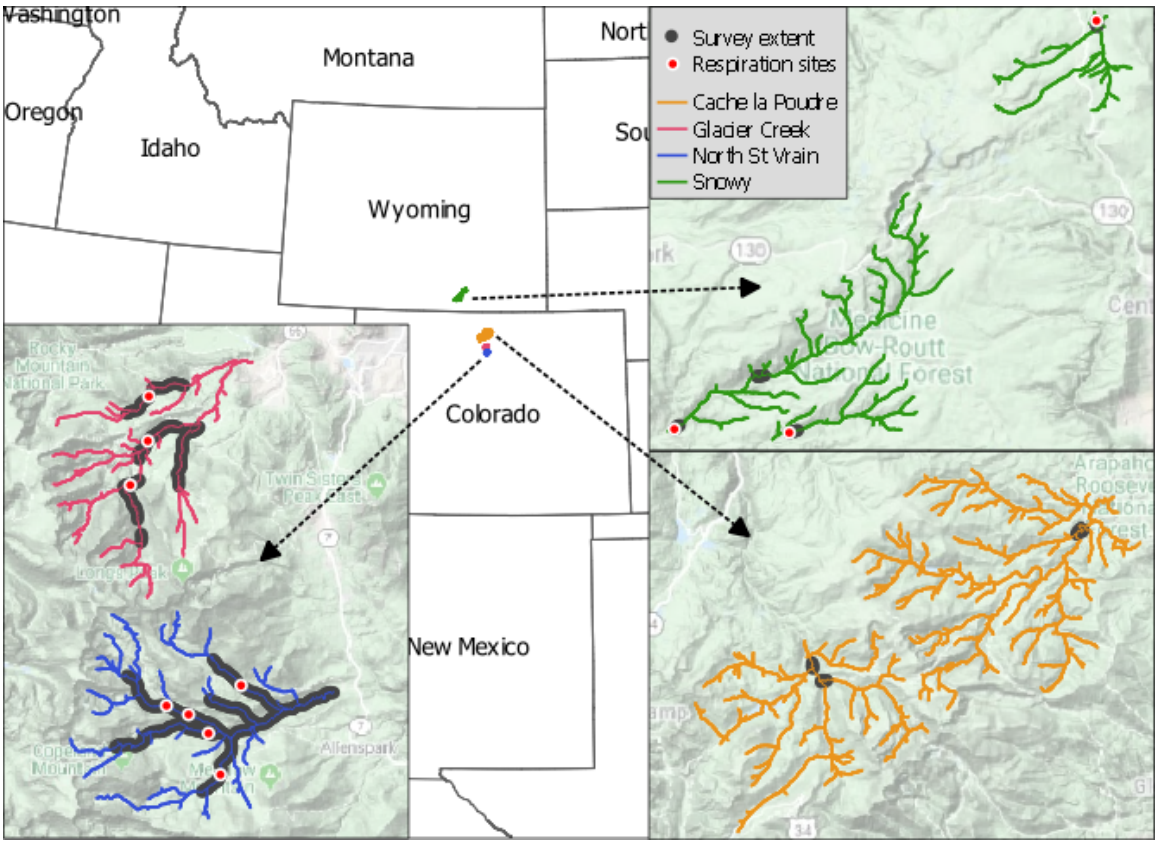

Table 4.1: Summary of data sources used in the development and parameterization of the simulation models.

Source	Variable	Extent
[Madinger and Hall, 2019]	Aerobic Respiration Rate (r), Stream Temperature (t)	11 sites across NSV, GC, and Snowy
[Livers and Wohl, 2016]	Jam Count (C_j), Survey reach length (L), Bankfull width (W_b), Mean channel count (C_c), Total sediment organic carbon, (OC_s), Wood volume per area (V_w), Presence of historical logging ($isLogged$)	25 reaches across NSV, GC, ClP and Snowy
[Wohl and Beckman, 2014]	Jam Count (C_j), Survey reach length (L), Bankfull width (W_b), Presence of historical logging ($isLogged$)	67 reaches across NSV and GC
[Venarsky et al., 2018]	Wetted width (W_w), Bankfull width (W_b), Mean channel count (C_c)	115 100m reaches across NSV, GC, and ClP
USGS DEM	Stream elevation (E), Upstream accumulated area (UAA), Lateral elevation range within 10m (LR_{10})	calculated at points spaced every 100m along all streams within the study area

into and through the segments of the modeled stream network, along with nitrate removal from each segment, the model simulates denitrification within the stream network. Whole-network denitrification can then be calculated as the fraction of the total nitrate delivered to the stream network from the watershed that is removed via denitrification, which we report as the 'network removal fraction' of a simulation.

For each individual segment, fractional nitrate removal due to denitrification is calculated as:

$$FR = 1 - e^{-\frac{V_{f_{den}}(L \cdot W_w)}{Q}}, \tag{4.1}$$

where FR is the fraction of segment nitrate removed of a given segment, $V_{f_{den}}$ is nitrate removal velocity (due to denitrification) that segment (m s^{-1}), L and W_w are the length (m) and wetted width (m) of that segment, and Q_i is the discharge from that segment (m^3 s^{-1}). Building upon data collected by Mulholland et al. [2008], we define a relationship between nitrate removal velocity, stream nitrate concentration, and aerobic respiration rate as:

$$log_{10}(V_{f_{den_i}}) = \beta_0 + \beta_N \cdot log_{10}([NO_3 - N]_i) + \beta_R \cdot log_{10}(R_i), \tag{4.2}$$

where $[NO_3 - N]_i$ and R_i are the nitrate concentration (μg NO_3-N l^{-1}) and aerobic respiration rate (mg O_2 m^{-2} sec^{-1}) of segment i. This relationship between R and $V_{f_{den}}$ has been previously identified by Mulholland et al. [2009], but not incorporated into a network-scale simulation model until recently (chapter 3). For the default paramaterization, we used fitted values of -3.93002 for β_0, -0.4382 for β_N, and 0.9175 for β_R, consistent with those used in chapter 3. Realizations of β values for the Monte Carlo analysis were determined by repeated linear regressions of this equation to resampled permutations of the Mulholland et al. [2008] dataset.

Equations (4.1)-(4.2) enable the calculation of nitrate removal from a given

stream reach, dependant upon that reach's outflow, nitrate concentration, length, wetted width, and respiration rate. The discharge from each reach is determined from the sum of water contributions from upstream reaches and adjacent hillslope areas. Nitrate concentrations of a reach are similarly determined from upstream sources, however, nitrate removal reduces the nitrate concentration of each reach in accordance with equation 4.1. Thus, the nitrate concentration in water exported from a given reach is determined from the initial concentration of nitrate in hillslope water contributions, nitrate removal from upstream reaches, and nitrate removal of that reach.

Model Parameterization

The topologic and hydrologic structure of our simulation model was parameterized to represent the NSV network and was identical for all model runs ("C"s in table 4.2). Consistent with the approach used in chapter 3, the simulation model consisted of 149 networked stream segments, each ∼500 m in length, with a total length of 70 km. Each segment receives water inputs from adjacent hillslope areas at a constant water yield of of $2.55 \cdot 10^{-8} \frac{m^3}{m^2 s}$, leading to a discharge of 2.19 $\frac{m^3}{sec}$ at the watershed outlet.

Model Scenarios Unlogged scenarios were parameterized to represent the NSV in its current state that has not been affected by logging, while logged scenarios were parameterized to represent the expected geomorphic effects of logging on the NSV. Logging effects were estimated based on previous surveys of the NSV and nearby stream networks in unlogged and logged areas performed by Livers and Wohl [2016], Wohl and Beckman [2014], and Venarsky et al. [2018]. Unlogged and logged simulations were differentiated by their parameterizations of the number of parallel channels (channel count, C_c) and the longitudinal density of channel-spanning jams

Table 4.2: Model variables and associated role in defining scenarios, and Monte Carlo simulation runs.

Variable Description	variable	Role
Stream Discharge	Q	C
Reach Length	L	C
Channel count	C_c	S,M
Jam density	D_j	S,M
Wetted Width	W_w	M
Respiration Rate	R	M
Uptake Velocity	$V_{f_{den}}$	M

C - Constant: held constant across both scenarios and Monte Carlo simulation runs.

S - Scenario: used to differentiate logged scenario from unlogged scenario.

M - Monte Carlo: varied among each of the 10,000 parameter sets used in Monte Carlo simulation.

(jam density, D_j) ("S"s in table 4.2), consistent with observations of decreased C_c and D_j in logged areas [Livers and Wohl, 2016, Wohl, 2014, Venarsky et al., 2018]. We found C_c and D_j to be associated with stream reach width and respiration rate, which we assume to be primary components of the influence of logging on stream denitrification rate.

We developed a regression model relating total stream reach wetted width to the upstream accumulated area (UAA), and the number of parallel channels (channel count, C_c) of a reach:

$$W_w = (\beta_0 \cdot UAA^{\beta_U}) \cdot (1 + \beta_C \cdot (C_c - 1)), \tag{4.3}$$

where W_w is the wetted width (m), UAA is the upslope accumulated area (km^2), and C_c is the number of parallel channels of a stream reach. For the default parameterization, we used fitted values of 2.445 for β_0, 0.304 for β_U, and 0.673 for β_C. While additional factors are likely to effect W_w, we find this relationship to clearly and reasonably represent the effect of logging on W_w, while explaining the majority of the observed variation in wetted width (detailed in appendix A). Wetted widths for each simulated channel were then determined using GIS-derived estimates of the UAA of each segment, and C_c values corresponding to either unlogged or logged conditions, dependant on the scenario. As UAA values were constant among all model runs, variation in C_c is the sole source of differing widths between the unlogged and logged scenarios.

For the unlogged model scenario, we used survey data of the NSV to determine the C_c for each segment. Unsurveyed segments were assumed to have a single channel, because the median value for C_c across all unlogged reaches was 1. Surveys of C_c represent stream reaches with lengths and placements that differed from the stream segments simulated by the model. The C_c value for a given model segment was calculated as the mean C_c value from all surveyed reaches that overlap that model segment, weighted by the length of overlap. For the logged scenario, we determined the C_c of each simulated segment by first calculating the percentile rank of C_c for each reach in the unlogged scenario, and then finding the C_c value associated with that percentile in the cumulative distribution of C_c from logged channel surveys. This approach, detailed in appendix A, produces a reasonable estimate of the values of C_c expected for the NSV under logged conditions. Further, this approach preserves the previously recognized influence of larce scale geomorphic factors such as valley confinement on the spatial pattern of C_c across the NSV [Livers and Wohl, 2016], without requiring an explicit quantification of this effect.

Incorporating respiration rate into the calculation of $V_{f_{den}}$ (equation 4.2) requires a scheme for determining respiration rates of model segments for unlogged and logged scenarios. We considered stream sediment carbon content, longitudinal channel-spanning logjam density, total wood volume, and stream temperature as potential correlates of respiration rate. Of these four variables, only jam density was significantly associated with respiration rate (appendix A), with the data suggesting that higher jam densities are associated with higher respiration rates. Whole-stream respiration rates are likely to be constrained by a number of physical, chemical, and biological factors across the spectrum of water-column, benthic, and hyporheic habitats where measured whole-stream respiration occurs. Further, maximal respiration rates of any specific habitat within a stream may be limited not only by the size of that habitat, but also by the delivery of oxygen or organic carbon to that habitat. Therefore, we would expect the relationship between jam density and respiration rate to saturate at high jam densities, when respiration rates become increasingly constrained by factors that are not directly related to jam density. As this expectation is consistent with the apparent pattern in our dataset (appendix A), we formed a hyperbolic saturation relationship between respiration rate and jam density:

$$R = \beta_0 + \frac{\beta_{Rmax} \cdot D_j}{\beta_{D_{j,half}} + D_j}, \tag{4.4}$$

where R_i is the respiration rate (g O_2 m^{-2} day^{-1}) of segment i, and D_j is the jam density of the surveyed reach (count km^{-1}). For the default model simulations, this relationship was used with fitted values of 1.1559 for β_0, 9.263 for β_{Rmax}, and 21.057 for $\beta_{D_{j,half}}$, producing a saturating relationship used to predict respiration rates from unlogged or logged jam densities.

Jam density for the unlogged scenarios was parameterized with survey data from the NSV, which was translated from surveyed reaches to each model segment by calculating the mean D_j value from all surveyed reaches that overlap that model segment, weighted by the length of overlap. Unsurveyed segments that were sufficiently below treeline ($E < 3250$) and of sufficient size ($UAA > 4km^2$) were considered suitable for jams and were assigned a jam density of 10.5 jams km^{-1}, the median value for jam density in unlogged areas. To parameterize jam density for logged scenarios, we first formed an estimate of the effect of logging on jam density (detailed in appendix A) and then calculated jam densities for the logged scenarios by applying the estimated logging effect to the unlogged jam density values. Based on this estimated logging effect, we estimated that historical logging reduced jam densities to 47.5% of the unlogged value, and therefore calculated jam densities for the default parameterization of the logged scenarios as 47.5% of the value of unlogged jam densities.

Monte Carlo Analysis We performed a Monte Carlo analysis in order to consider the influence of logging on whole-network denitrification across a range of hillslope nitrate concentrations, and to incorporate uncertainty stemming from residual error in the empirical relationships used to derive model parameters. Our Monte Carlo analysis consisted of 5000 realizations, with each realization consisting of a pair of unlogged and logged model runs. Hillslope nitrate concentrations for each realization were sampled from a uniform distribution spanning the interval [0.1, 100000] μg NO_3-N L^{-1} , with the sampled concentration applied to all contributing water. Uncertainty surrounding the effects of logging was quantified by refitting equations (4.2), (4.3), and (4.4), described above, and equations (A.1) and (A.6), described in appendix A, to resampled datasets, producing an ensemble of fitted parameter value estimates for

each equation. Resampled datasets were bootstrapped by drawing random samples from the original dataset, with replacement, until the size of the resampled dataset was equal to the size of the original dataset. Additionally, because the assignment of logged C_c values to the simulated NSV is a major source of uncertainty associated with the logging effect, we determined variant C_c values for the logged scenario by randomly sampling logged C_c values from the entire set of logged C_c values in our dataset. For each paired realization in the Monte Carlo analysis, we used a given realization of the parameter values the variant forms of equations (4.2), (4.3), (4.4), and (A.1), in conjunction with logged D_j values calculated from a realization for parameter values of equation (A.6), and the resampled values of logged C_c, to generate a realization of the unlogged and logged scenarios.

Due to the small number of observations (n=11) used to fit the relationship between respiration rate and jam density (equation (4.4)), realizations of parameter values of this equation have the potential to produce unreasonable values when used to predict R across the simulations. We allowed all realizations of equation 4.4. However, we forced predicted values of R that were less than the minimum value observed across the combined datasets of Madinger and Hall [2019] and Mulholland et al. [2008] (0.42 $g\ O_2\ m^{-2}\ day^{-1}$) to take on that minimum value, and forced predicted values of R that were greater than the maximum value in the combined datasets (23.1 $g\ O_2\ m^{-2}\ day^{-1}$) to take on that maximum value. Therefore, Monte Carlo realizations can represent substantially different relationships between respiration rate and jam density in accordance with the residual error from equation (4.4), but cannot produce unreasonable values for R.

Tolerance intervals surrounding the effect of logging on nitrate removal were determined as quantiles of the ensemble of pairwise differences between the unlogged and logged predictions for a given model realization. By comparing results unlogged

and logged scenarios for each realization, we quantified the uncertainty associated with both the form of the logging effect (e.g., the magnitude by which jam density is reduced under logged conditions) and the uncertainty arising from the expression of the logging effect on denitrification rates (e.g., the relationship between respiration rate and jam density). This approach avoided irrelevant comparisons between unlogged and logged scenarios that differ in their behaviors (e.g., a comparison between unlogged and logged scenarios that use different relationships between respiration rate and jam density). Thus, the difference in nitrate removal within each paired realization of unlogged and logged simulations arises from the variably parameterized effects of logging on jam density and channel count, as compounded by the behavior of that particular model realization.

Results

Simplification of Stream Morphology

Our method of estimating the effects of historical logging on the NSV resulted in a reduction in the density of channel-spanning logjams, and a near-complete loss of stream reaches with multi-channel planforms (figure (4.2)). Jam densities varied from 0 - 30 (count km^{-}1) across the unlogged scenario, and from 0 to 14 across the logged scenario, corresponding with respiration rates ranging from 0.02 - 0.08 mg O_2 m^{-2} sec^{-1} in the unlogged scenario and 0.02 - 0.06 mg O_2 m^{-2} sec^{-1} in the logged scenario. Channel counts varied from 1 to 4.3 for the unlogged scenario and 1 to 1.2 for the logged scenario, and total wetted widths varying from 2 to 19.5 m for the unlogged scenario and 2 to 9.3 m for the logged scenario. Jam density, respiration rate, channel count, and wetted width all vary around the default values summarized here for the Monte Carlo simulations. We use that variation for the propagation of uncertainty through the denitrification simulations, but, for brevity, we do not present it here.

Figure 4.2: Jam densities (count km^{-}1) and channel counts for the simulated NSV under unlogged and logged conditions depict the projected simplifying effects of logging.

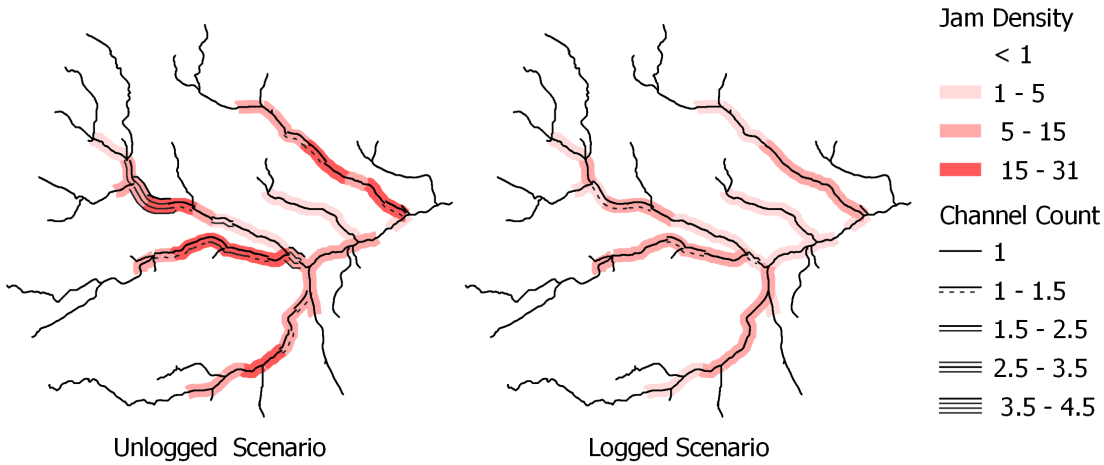

Whole Network Nitrate Removal

For both unlogged and logged scenarios, our results show that total nitrate removal is positively correlated with hillslope nitrate concentration, but nitrate removal as a fraction of the total nitrate load across the simulated network ('network removal fraction') is inversely related to hillslope nitrate concentrations (figure 4.3a). This pattern is evident across all model runs, with individual Monte Carlo realizations simulating network removal fractions ranging from near 1 at low hillslope N concentrations, to near 0 at high hillslope concentrations.

Comparison of the unlogged and logged scenarios reveals a reduction in the simulated network removal fraction in the logged scenarios, which we term the 'logging effect'. This logging effect is most substantial at moderate and high hillslope concentrations, with model runs indicating a nearly constant 30% reduction in network removal fraction at hillslope concentrations of 10 μg N l^{-1} or greater (figure

Figure 4.3: Linear (a) and log (b) scaled whole network removal fractions predicted by unlogged and logged scenarios across a range of hillslope concentrations, along with the ratio of unlogged to logged removal fractions (c), and the distribution of stream nitrate concentrations observed by Mulholland et al. [2008] in 72 small North American streams (d).

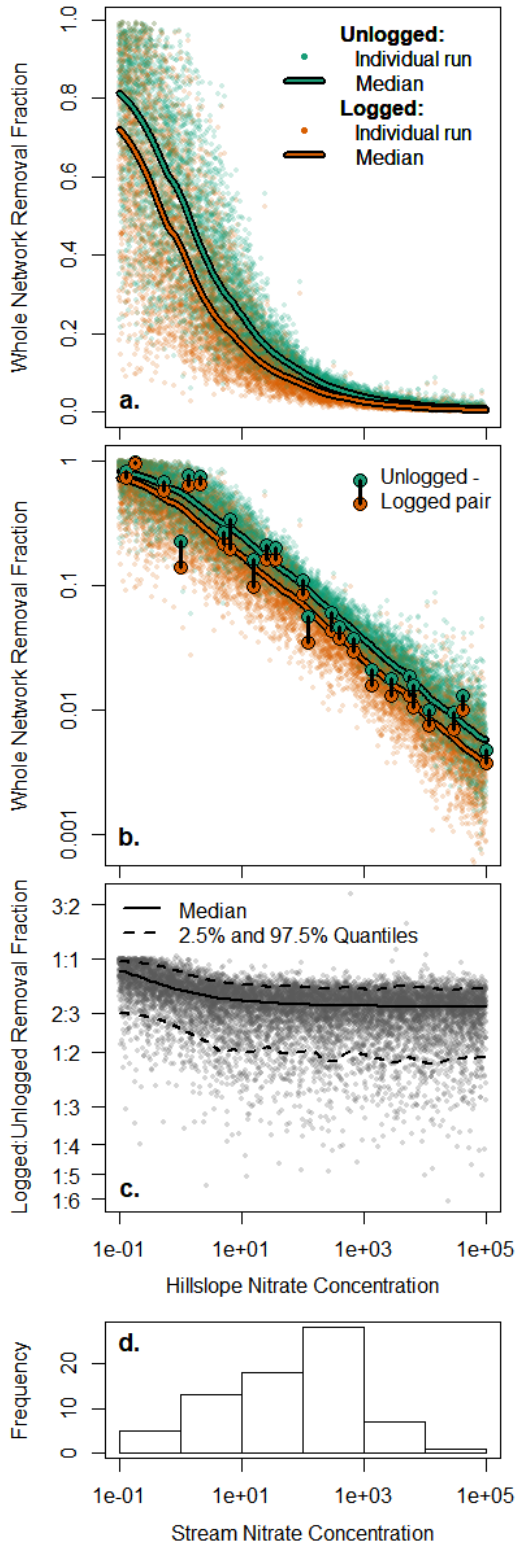

4.3c). At lower hillslope concentrations, the magnitude of the logging effect becomes increasingly sensitive to changes in hillslope nitrate concentration, with the logging effect decreasing from 20% to 8% as hillslope nitrate concentrations were decreased from 1 to 0.1 μg N l^{-1}.

Understanding the extent to which this finding of insensitivity of the logging effect to hillslope concentration is applicable requires a comparison between hillslope concentrations and stream concentrations. However, hillslope nitrate concentrations can be substantially different from stream nitrate concentrations in situations where fractional removal is large due to the depletion of nitrate concentration. At low hillslope concentrations, high network removal fractions reduce stream nitrate concentrations to as little as 20% of the value of hillslope concentrations, while stream nitrate concentrations comprise greater than 80% of hillslope concentrations when hillslope concentrations are high. Therefore, stream nitrate concentrations higher than 10 μ g N l^{-1} correspond with the range of hillslope concentrations for which logging effect is insensitive to hillslope concentrations, while stream nitrate concentrations higher than 10 μ g N l^{-1} correspond with the range of hillslope concentrations for which the magnitude of the logging effect is strongly influenced by hillslope concentration.

While substantial uncertainty surrounds the simulated logging effect, the Monte Carlo analysis demonstrates an unambiguous logging effect at moderate and high hillslope nitrate concentrations, with the magnitude of this effect decreasing to the point of irrelevance at low hillslope concentrations. Of the paired realizations with hillslope concentrations of 10 μg N l^{-1} or greater, 95% simulate a logging effect of between 16% and 63%, while less than 0.1% simulate a logging effect of 5% or less. At lower concentrations, many of the realizations simulate insubstantial logging effects, with 15% of the realizations with hillslope concentrations of 1 μg N l^{-1} or less

predicting a $< 5\%$ decrease in whole network removal due to logging. Additionally, across the entire range of hillslope concentrations, only 8 of the 5,000 pairs of unlogged and logged model realizations (0.16%) simulate greater removal under logged conditions than unlogged conditions.

Discussion

By controlling for all other sources of variation, our simulations allow for an unconfounded exploration of the consequences of logging-driven channel simplification on whole-network nitrate removal. Unlogged and logged simulations have identical hydrology, network topology, and nitrate loading, and differ only in their parameterization of jam density and the occurrence of multi-thread channel planforms. Thus, while our parameterization of unlogged and logged scenarios does not necessarily capture all of the effects of logging, differences in whole-network nitrate removal between the unlogged and logged simulations can be attributed directly to the simulated effects of logging. Further, we suggest that the simplified representation of logging effects presented here captures the dominant linkages between logging-induced channel simplification and whole network denitrification rate, and thus provides a reasonable characterization of the effect of logging on network-scale denitrification. While incorporating a more detailed representation of the effect of logging on channel width and respiration rate could add precision to our simulations, adding more detail to our parameterization scheme could also make our simulation results more specific to the studied system, and less representative of logging effects generally. Our approach therefore provides a clear interpretation of logging effects while avoiding the difficulty associated with observational comparisons between unlogged and logged networks, which can be confounded by uncontrollable differences in network size, topology, hydrology, nutrient loading, and other factors may obscure controls on whole-network

denitrification capacity.

The relationship between jam density and aerobic respiration rate is reasonable, although we were expecting a stronger relationship between organic carbon availability and respiration. Because sediment organic carbon is a primary substrate used in aerobic respiration, we anticipated a relationship between the amount of sediment carbon stored in a reach and the respiration rate of that reach. However, due to the high gradients and velocities of many streams in our study area, opportunities for the deposition of fine sediments and organic matter are rare in the absence of jams. Therefore, while the quantity of benthic carbon is representative of the amount of substrate present to fuel aerobic respiration, the longitudinal density of jams may be indicative of the rate of accumulation of that substrate. Given the potential variability in both the biological availability of stored sediment carbon, we find it reasonable that estimated respiration rates are correlated with jam densities but not with sediment carbon. This finding is similar to findings from previous surveys of stream respiration rates that identified large wood and channel geometry, but not benthic organic matter, as correlates of respiration rate [Houser et al., 2005, Bott et al., 1985].

The effects of logging on denitrification simulated here arise from the decreased jam density and channel count of a subset of the modeled reaches in the logged scenario. Reaches with multiple channels are often associated with high jam densities in our study area, therefore simulated reaches that are wider in the unlogged scenario also tend to have increased jam density and respiration rates (figure 4.2)). The increased respiration rates associated with these complex reaches leads to increased denitrification uptake velocity ($V_{f_{den}}$), which is scaled by the increased width of these complex reaches in the calculation of fractional nitrate removal (equation (4.1)). Thus, the denitrification rates of these complex reaches, and the magnitude of the

simulated logging effect, are enhanced by the multiplicative interaction between jam density and channel count.

The lower magnitude of the logging effect at low hillslope concentrations seen in our results suggests a decrease in the sensitivity of nitrate removal to respiration rate and wetted width under these conditions. At low nitrate concentrations, $V_{f_{den}}$ of any given simulated segment is elevated due to the inverse relationship between $V_{f_{den}}$ and nitrate concentration described in equation (4.2). Under these conditions, the fraction of nitrate removed from the given segment becomes less sensitive to further variation in $V_{f_{den}}$, or variation in segment width, due to the non-linear form of equation (4.1). However, the total amount of N removed from the given segment is still sensitive to changes in nitrate concentration because the amount of nitrate removed is calculated as the product of the amount of nitrate present in that segment and the removal fraction. The effect of the reduced respiration rates and wetted widths of the logged scenarios on whole-network nitrate removal is therefore minimized at low nitrate concentrations, consistent with the findings of chapter 3 that nitrate removal rates of whole networks and individual stream segments are controlled by nitrate supply under such conditions.

At higher nitrate concentrations, the fractional removal of nitrate is small, and nitrate removal becomes controlled by the denitrification capacity of the stream network, rather than by nitrate supply. In our simulations, the full magnitude of the logging effect is expressed at hillslope concentrations around 10 μg l^{-1}, and is not affected by further increases in nitrate concentration. The specific nitrate concentration at which this transition away from supply limitation occurs in our simulations is controlled by the magnitude of the logging-induced alteration of denitrification capacity. However, both the decreased magnitude of the logging effect at low hillslope concentrations, and the insensitivity of the logging effect to changes

in nitrate concentration when hillslope concentration are high arise from the non-linearity of equation 4.1, a commonly accepted relationship that is not specific to our study area or modeling scheme [Stream Solute Workshop, 1990, Wollheim et al., 2006]. Therefore, we expect this mechanism to be broadly relevant, although different representations of the logging effect, or different realizations of equation 4.2 could change the concentration at which this transition occurs in other systems.

Through the explicit inclusion of complexity in reach structure, our simulations incorporate greater heterogeneity in denitrification rates than has been previously considered. Previous approaches have considered variations in stream size and channel geometry, with resulting implications for the relationship between stream size and denitrification capacity [Mulholland et al., 2008, Alexander et al., 2000]. While these approaches are insightful, they are incapable of representing variation in denitrification associated with physical or biological heterogeneity. Incorporating reach-scale heterogeneity into simulation model enables the evaluation potentially important of mechanisms that influence large-scale denitrification rates by alteration of the heterogeneous template upon which denitrification occurs [McClain et al., 2003, Groffman et al., 2009]. By incorporating a more explicit description of reach-scale heterogeneity in channel planform and biological activity, in conjunction with recognition of specific mechanisms affecting reach-scale denitrification, the approach presented here advances our understanding of the effects of land use and management strategies on channel complexity, and whole-network denitrification.

The effects of logging observed here provide an example of the cascading and persistent effects of land use on network-scale denitrification capacity. The mechanisms connecting logging to reduced denitrification capacity are likely to be broadly applicable, although the specific magnitude of the logging effect simulated here is specific to the size, topology, hydrology, and channel morphology of the

simulated network, as well as the representation of logging effects on wetted width and respiration rate. Links between logging, a reduction in in-stream wood, and a subsequent a reduction in channel complexity, are widespread, and have been observed in many forested systems [Scott and Wohl, 2018, Wohl, 2017, Mellina and Hinch, 2009, Francis et al., 2008, Valett et al., 2002, Muotka and Syrjänen, 2007]. Thus, we expect that many logged streams have undergone a reduction in wetted width due to a loss of multi-thread reaches. Similarly, respiration rates have likely been reduced in streams that have experienced a logging-induced loss of jam density, especially in high gradient systems where channel-spanning structures such as jams comprise a substantial component of the system's ability to capture and retain organic sediments.

Channel simplification is not exclusively caused by logging, and is common to a broad range of streams in urban, agricultural, and undeveloped areas. Management actions intended to reduce flooding, provide transportation corridors, protect property, and enhance recreational opportunities often result in a reduction of multi-channel planforms and channel spanning structures, and may have widespread consequences for stream network denitrification capacity. Restoration approaches are increasingly considering the importance of in-stream wood and channel complexity [Kail et al., 2007, Jones et al., 2014], with intentions of enhancing reach-scale sediment retention, carbon retention, and nutrient removal [Entrekin et al., 2008, Muotka and Laasonen, 2002, Craig et al., 2008]. Given the large extent of channel simplification, and the increasing awareness of a relationship between channel complexity and biogeochemical cycles, our findings provide important insight into the potential network-scale effects of channel simplification on denitrification.

The magnitude of the logging effect simulated here suggests that connections between channel simplification and denitrification have implications for the management of nitrate pollution at regional to continental scales. As nitrate loads to streams and

rivers come from numerous sources that are deeply ingrained into modern society, management of the negative consequences of elevated nitrate concentrations can benefit from a consideration of nitrate removal pathways such as stream denitrification [Mitsch et al., 2001]. While the effects of channel simplification on network-scale nitrate removal capacity are neither the sole cause of elevated nitrate concentrations, nor a complete solution to nitrate pollution, our findings do suggest that strategies to promote channel complexity could be one component of an effective, holistic approach to mitigating the widespread impacts of nitrate pollution issues.

Conclusion

We demonstrate the potential for a substantial network-scale reduction in nitrate removal capacity as a consequence of the persistent, simplifying effect of historical logging on denitrification rates in a montaine stream network. This consequence arises from the links between historic land use, contemporary stream channel structure, and biological productivity, which lead to alterations of both the wetted area across which denitrification occurs, as well as the biological demand for denitrification. In our simulations, the logging-induced reduction in whole-network nitrate removal is minimal when stream nitrate concentrations are very low, however, it increases to a stable value of approximately 30% at stream concentrations of around 10 μ g l^{-1} or higher. The simulated magnitude by which the capacity to remove N is reduced under logged conditions suggests that large-scale efforts to manage nitrate pollution would benefit from an increased consideration of connections between land use, channel simplification, and in-stream processes.

The methods applied here suggest an approach to understanding the cascading effects of channel simplification on stream morphology, hydrology, productivity, and ultimately reach and network scale denitrification rates. Further, channel

simplification is not solely a consequence of logging. It is instead a widespread consequence of agricultural, urban, and extractive land uses. Where channel simplification is similar to that observed in our study site, a similar loss in network-scale denitrification capacity might be expected. More broadly, the links among channel geometry, respiration rate, and denitrification rate demonstrated here suggest extensive natural and anthropogenic controls on in-stream nitrate removal from reach to regional scales.

CONCLUSION

The work presented here documents the development and application of a spatially explicit stream network simulation model that represents connections between stream hydrogeomorphology, aerobic respiration rate, and denitrification rate. This model is applied to a small, subalpine stream network under scenarios designed to explore: 1) the implications of temperature-controlled, network scale patterns of respiration rates on the distribution and overall magnitude of stream network denitrification, and 2) the effect of logging-induced channel simplification on whole network denitrification rates. The first analysis is complimented by an analysis of patterns of stream temperature across this network, revealing the spatially and temporally variable influence of in-network lakes on stream temperatures. In sum, this work emphasizes the diverse set of factors that influence reach and watershed scale biogeochemical characteristics and processes.

Lake temperatures can differ from stream temperatures due to the high residence time and increased influence of atmospheric heat exchange on lake water. When lakes are located within stream networks, the distinct temperatures of lakes causes discontinuities in stream temperature profiles, with effects that persist in downstream reaches. The work presented here applies a hydrologic mixing model integrating the spatially discontinuous influences of lake effects with the longitudinally continuous influences of atmospheric heat exchange and groundwater contributions. The application of this mixing model reveals that lake effects dominate stream temperature patterns in the late summer, while lakes have a lesser influence on stream temperatures during winter and spring. This source-water mixing model approach may be broadly applicable to systems where stream temperature profiles are influenced by multiple water sources with distinct thermal regimes, and suggests that complex patterns in

stream temperature profiles may emerge and and dissipate across seasons in response to the diversity of water temperatures from different sources.

Previous work has incorporated an inverse relationship between nitrate concentration and denitrification rates, along with effects of hydrology and channel geometry, into simulations of stream network denitrification [Mulholland et al., 2008, Alexander et al., 2009]. The denitrification simulation model presented here updates these previous approaches with the addition of an empirical relationship between whole-stream aerobic respiration rate and denitrification efficiency. Due to this addition, the work presented here suggests decreased sensitivity of N removal to nitrate concentrations, along with additional heterogeneity in nitrate removal due to variation in respiration rates. A theoretically-derived relationship between aerobic respiration rate and stream temperature is used to determine network-scale patterns of respiration rates across model scenarios representing different stream temperatures and nitrate loading rates. This first set of model simulations reveal that whole-stream aerobic respiration rates may have a substantial influence on rates of nitrate removal from stream networks, that rates of N removal may be less sensitive to stream nitrate concentration than previously suggested, and that denitrification rates may be primarily controlled by the supply of nitrate at lower nitrate concentrations, and by biological denitrification capacity at higher nitrate concentrations. While the use of respiration rates to indicate variation in biological demand for denitrification is simplistic, our model demonstrates the potential network-scale significance of the linkage between carbon and nitrogen cycling, and represents a step towards interpreting the potential network-scale implications of a wide variety of stream characteristics that may alter both respiration rates and denitrification rates.

Stream temperatures used to drive respiration rates across this first application of the model represent expected temperatures across a lake free stream network.

Incorporating lake driven complexity of stream temperature profiles would add an additional source of heterogeneity in the biotic demand for denitrification to the simulations. However, doing so would incorporate only a single mechanism (temperature) linking lakes to downstream denitrification rates without considering the potential effects of other mechanisms. In addition to altering downstream temperatures, lakes exhibit different bigeochemical cycling dynamics than streams, thus altering the concentrations of oxygen, carbon, and nitrate to downstream reaches. Incorporating the effect of lake-driven temperature patterns on network denitrification would therefore provide an incomplete and potentially misleading depiction of the effect of lakes on downstream denitrification rates, and was avoided in this work. Nonetheless incorporating the effects of respiration rate on denitrification enables the model to represent linkages between denitrification rates and stream temperature, carbon, and oxygen dynamics, and therefore provides a foundation for incorporating lakes into stream network denitrification models.

The second application of the model involved scenarios representing unlogged and logged states of the stream network, with logged states exhibiting a reduction in the occurrence of multi-channel reaches and channel-spanning logjams. While the physical effects of these alterations are apparent, the consequences of this loss of complexity on network-scale stream denitrification rates have not been previously examined. Model results suggest that channel simplification associated with historical logging substantially reduces stream network denitrification capacity under common nitrate concentrations, although this difference decreases at low rates of N loading when denitrification rates are primarily controlled by nitrate supply.

The mechanisms driving the logging effect explored here suggest that the greater denitrification capacity of unlogged stream networks arises from both the greater stream width and a greater number of channel-spanning structures. Further, the

spatial co-occurence of wide stream reaches, and stream reaches with a large number of channel-spanning structures increases the denitrification capacity of the unlogged simulations beyond the additive combination of the two. Therefore, model results suggest that network-scale denitrification capacity may be sensitive not only to stream width and channel-spanning structures, but also to the spatial arrangement of wide reaches and reaches with channel-spanning structures.

Stream denitrification rates may be maximized at boundaries between aerobic and anaerobic conditions, which may in turn be associated with stream complexity at multiple scales. Maximal denitrification rates require the delivery of sufficient supplies of nitrate and labile organic carbon, but also require an absence (or very low concentration) of dissolved oxygen. These conditions can be created by a variety of structures in stream systems, ranging from deep, stagnant pools that are isolated enough from atmospheric gas exchange to facilitate the depletion of dissolved oxygen, to water downwelling into hyporheic zones. However, conditions favorable to high denitrification rates may not occur in simplified, homogeneous stream systems where all water is oxygenated, or in stream systems where hyporheic flowpaths are not present. While the work presented here explores the effects of specific forms of channel simplification on denitrification rates, many different forms of physical, chemical, and hydrologic complexity may enhance stream denitrification rates. The significance of logging-induced channel simplification for whole-network denitrification rates described here suggests that other forms of channel simplification may also have substantial and widespread consequences for stream nitrogen cycling.

REFERENCES CITED

Tim B Abbe and David R Montgomery. Patterns and processes of wood debris accumulation in the Queets river basin, Washington. *Geomorphology*, 51(1-3):81–107, March 2003. ISSN 0169555X. doi: 10.1016/S0169-555X(02)00326-4. URL http://linkinghub.elsevier.com/retrieve/pii/S0169555X02003264.

John D. Aber, Knute J. Nadelhoffer, Paul Steudler, and Jerry M. Melillo. Nitrogen Saturation in Northern Forest Ecosystems. *BioScience*, 39(6):378–386, June 1989. ISSN 0006-3568. doi: 10.2307/1311067. URL http://www.jstor.org/stable/1311067.

V. Acuña, A. Wolf, U. Uehlinger, and K. Tockner. Temperature dependence of stream benthic respiration in an Alpine river network under global warming. *Freshwater Biology*, 53(10):2076–2088, October 2008. ISSN 1365-2427. doi: 10.1111/j.1365-2427.2008.02028.x. URL http://onlinelibrary.wiley.com/doi/10.1111/j.1365-2427.2008.02028.x/abstract.

Hirotogu Akaike. Information Theory and an Extension of the Maximum Likelihood Principle. In *Selected Papers of Hirotugu Akaike*, Springer Series in Statistics, pages 199–213. Springer, New York, NY, 1998. ISBN 978-1-4612-7248-9 978-1-4612-1694-0. doi: 10.1007/978-1-4612-1694-0_15. URL https://link.springer.com/chapter/10.1007/978-1-4612-1694-0_15.

Richard B. Alexander, Richard A. Smith, and Gregory E. Schwarz. Effect of stream channel size on the delivery of nitrogen to the Gulf of Mexico. *Nature*, 403(6771):758–761, February 2000. ISSN 0028-0836. doi: 10.1038/35001562. URL http://www.nature.com/nature/journal/v403/n6771/full/403758a0.html.

Richard B. Alexander, John Karl Böhlke, Elizabeth W. Boyer, Mark B. David, Judson W. Harvey, Patrick J. Mulholland, Sybil P. Seitzinger, Craig R. Tobias, Christina Tonitto, and Wilfred M. Wollheim. Dynamic modeling of nitrogen losses in river networks unravels the coupled effects of hydrological and biogeochemical processes. *Biogeochemistry*, 93(1-2):91–116, January 2009. ISSN 0168-2563, 1573-515X. doi: 10.1007/s10533-008-9274-8. URL http://link.springer.com/article/10.1007/s10533-008-9274-8.

Christopher B. Anderson and Amy D. Rosemond. Ecosystem engineering by invasive exotic beavers reduces in-stream diversity and enhances ecosystem function in Cape Horn, Chile. *Oecologia*, 154(1):141–153, November 2007. ISSN 1432-1939. doi: 10.1007/s00442-007-0757-4. URL https://doi.org/10.1007/s00442-007-0757-4.

Donald M. Anderson, Patricia M. Glibert, and Joann M. Burkholder. Harmful algal blooms and eutrophication: Nutrient sources, composition, and consequences. *Estuaries*, 25(4):704–726, August 2002. ISSN 0160-8347. doi: 10.1007/BF02804901. URL https://doi.org/10.1007/BF02804901.

C. W. Andrus, B. A. Long, and H. A. Froehlich. Woody Debris and Its Contribution to Pool Formation in a Coastal Stream 50 Years after Logging. *Canadian Journal of Fisheries and Aquatic Sciences*, 45(12):2080–2086, December 1988. ISSN 0706-652X. doi: 10.1139/f88-242. URL `https://www.nrcresearchpress.com/doi/abs/10.1139/f88-242`.

Alison P. Appling, Robert O. Hall, Charles B. Yackulic, and Maite Arroita. Overcoming Equifinality: Leveraging Long Time Series for Stream Metabolism Estimation. *Journal of Geophysical Research: Biogeosciences*, 123(2):624–645, February 2018. ISSN 21698953. doi: 10.1002/2017JG004140. URL `http://doi.wiley.com/10.1002/2017JG004140`.

C. P. Arango and J. L. Tank. Land use influences the spatiotemporal controls on nitrification and denitrification in headwater streams. *Journal of the North American Benthological Society*, 27(1):90–107, March 2008. ISSN 0887-3593. doi: 10.1899/07-024.1. URL `http://www.bioone.org/doi/abs/10.1899/07-024.1`.

Clay P. Arango, Jennifer L. Tank, Jamie L. Schaller, Todd V. Royer, Melody J. Bernot, and Mark B. David. Benthic organic carbon influences denitrification in streams with high nitrate concentration. *Freshwater Biology*, 52(7):1210–1222, July 2007. ISSN 1365-2427. doi: 10.1111/j.1365-2427.2007.01758.x. URL `https://onlinelibrary.wiley.com/doi/abs/10.1111/j.1365-2427.2007.01758.x`.

Ivan Arismendi, Mohammad Safeeq, Sherri L. Johnson, Jason B. Dunham, and Roy Haggerty. Increasing synchrony of high temperature and low flow in western North American streams: double trouble for coldwater biota? *Hydrobiologia*, September 2012. ISSN 0018-8158, 1573-5117. doi: 10.1007/s10750-012-1327-2. URL `http://www.springerlink.com/index/10.1007/s10750-012-1327-2`.

Svante Arrhenius. Über die Dissociationswärme und den Einfluss der Temperatur auf den Dissociationsgrad der Elektrolyte. *Zeitschrift für Physikalische Chemie*, 4U(1), January 1889. ISSN 2196-7156, 0942-9352. doi: 10.1515/zpch-1889-0408. URL `http://www.degruyter.com/view/j/zpch.1889.4.issue-1/zpch-1889-0408/zpch-1889-0408.xml`.

Svante Arrhenius. *Quantitative laws in biological chemistry*. London : G. Bell, 1915. URL `http://archive.org/details/quantitativelaws00arrhrich`.

J. I. L. L. S. Baron and N. E. L. Caine. Temporal coherence of two alpine lake basins of the Colorado Front Range, U.S.A. *Freshwater Biology*, 43(3):463–476, March 2000. ISSN 1365-2427. doi: 10.1046/j.1365-2427.2000.00517.x. URL `https://onlinelibrary.wiley.com/doi/abs/10.1046/j.1365-2427.2000.00517.x`.

Kamil Barton. *MuMIn: Multi-Model Inference*, 2016. URL `https://CRAN.R-project.org/package=MuMIn`. R package version 1.15.6.

Jake J. Beaulieu, Jennifer L. Tank, Stephen K. Hamilton, Wilfred M. Wollheim, Robert O. Hall, Patrick J. Mulholland, Bruce J. Peterson, Linda R. Ashkenas, Lee W. Cooper, Clifford N. Dahm, Walter K. Dodds, Nancy B. Grimm, Sherri L. Johnson, William H. McDowell, Geoffrey C. Poole, H. Maurice Valett, Clay P. Arango, Melody J. Bernot, Amy J. Burgin, Chelsea L. Crenshaw, Ashley M. Helton, Laura T. Johnson, Jonathan M. O'Brien, Jody D. Potter, Richard W. Sheibley, Daniel J. Sobota, and Suzanne M. Thomas. Nitrous oxide emission from denitrification in stream and river networks. *Proceedings of the National Academy of Sciences*, page 201011464, December 2010. ISSN 0027-8424, 1091-6490. doi: 10.1073/pnas.1011464108. URL `http://www.pnas.org/content/early/2010/12/14/1011464108`.

Jake J. Beaulieu, Clay P. Arango, David A. Balz, and William D. Shuster. Continuous monitoring reveals multiple controls on ecosystem metabolism in a suburban stream: *Ecosystem metabolism in a suburban stream*. *Freshwater Biology*, 58 (5):918–937, May 2013. ISSN 00465070. doi: 10.1111/fwb.12097. URL `http://doi.wiley.com/10.1111/fwb.12097`.

Natalie D. Beckman and Ellen Wohl. Carbon storage in mountainous headwater streams: The role of old-growth forest and logjams. *Water Resources Research*, 50 (3):2376–2393, March 2014a. ISSN 1944-7973. doi: 10.1002/2013WR014167. URL `http://onlinelibrary.wiley.com/doi/10.1002/2013WR014167/abstract`.

Natalie D. Beckman and Ellen Wohl. Effects of forest stand age on the characteristics of logjams in mountainous forest streams: FOREST STAND AGE AND LOGJAMS. *Earth Surface Processes and Landforms*, pages n/a–n/a, February 2014b. ISSN 01979337. doi: 10.1002/esp.3531. URL `http://doi.wiley.com/10.1002/esp.3531`.

E. S. Bernhardt, G. E. Likens, D. C. Buso, and C. T. Driscoll. In-stream uptake dampens effects of major forest disturbance on watershed nitrogen export. *Proceedings of the National Academy of Sciences*, 100(18):10304–10308, September 2003. ISSN 0027-8424, 1091-6490. doi: 10.1073/pnas.1233676100. URL `http://www.pnas.org/cgi/doi/10.1073/pnas.1233676100`.

E. S. Bernhardt, J. B. Heffernan, N. B. Grimm, E. H. Stanley, J. W. Harvey, M. Arroita, A. P. Appling, M. J. Cohen, W. H. McDowell, R. O. Hall, J. S. Read, B. J. Roberts, E. G. Stets, and C. B. Yackulic. The metabolic regimes of flowing waters. *Limnology and Oceanography*, 63(S1):S99–S118, March 2018. ISSN 1939-5590. doi: 10.1002/lno.10726. URL `https://aslopubs.onlinelibrary.wiley.com/doi/abs/10.1002/lno.10726`.

Emily S. Bernhardt, Gene E. Likens, Robert O. Hall, Don C. Buso, Stuart G. Fisher, Thomas M. Burton, Judy L. Meyer, William H. Mcdowell, Marilyn S. Mayer, W. Breck Bowden, Stuart E. G. Findlay, Kate H. Macneale, Robert S.

Stelzer, and Winsor H. Lowe. Can't See the Forest for the Stream? In-stream Processing and Terrestrial Nitrogen Exports. *BioScience*, 55(3):219–230, March 2005. ISSN 0006-3568. doi: 10.1641/0006-3568(2005)055[0219:ACSTFF]2.0.CO;2. URL http://www.bioone.org/doi/abs/10.1641/0006-3568%282005%29055[0219:ACSTFF]2.0.CO;2.

Melody J. Bernot and Walter K. Dodds. Nitrogen Retention, Removal, and Saturation in Lotic. *Ecosystems*, 8(4):442–453, June 2005. ISSN 1432-9840, 1435-0629. doi: 10.1007/s10021-003-0143-y. URL http://link.springer.com/article/10.1007/s10021-003-0143-y.

Melody J. Bernot, Daniel J. Sobota, Robert O. Hall, Patrick J. Mulholland, Walter K. Dodds, Jackson R. Webster, Jennifer L. Tank, Linda R. Ashkenas, Lee W. Cooper, Clifford N. Dahm, Stanley V. Gregory, Nancy B. Grimm, Stephen K. Hamilton, Sherri L. Johnson, William H. Mcdowell, Judith L. Meyer, Bruce Peterson, Geoffrey C. Poole, H. Maurice Valett, Clay Arango, Jake J. Beaulieu, Amy J. Burgin, Chelsea Crenshaw, Ashley M. Helton, Laura Johnson, Jeff Merriam, B. R. Niederlehner, Jonathan M. O'brien, Jody D. Potter, Richard W. Sheibley, Suzanne M. Thomas, and Kym Wilson. Inter-regional comparison of land-use effects on stream metabolism. *Freshwater Biology*, 55(9):1874–1890, September 2010. ISSN 1365-2427. doi: 10.1111/j.1365-2427.2010.02422.x. URL http://onlinelibrary.wiley.com/doi/10.1111/j.1365-2427.2010.02422.x/abstract.

Travis Bogan, Omid Mohseni, and Heinz G. Stefan. Stream temperature-equilibrium temperature relationship. *Water Resources Research*, 39(9), September 2003. ISSN 00431397. doi: 10.1029/2003WR002034. URL http://doi.wiley.com/10.1029/2003WR002034.

F. H. Bormann and G. E. Likens. Nutrient Cycling. *Science*, 155(3761):424–429, January 1967. ISSN 0036-8075, 1095-9203. doi: 10.1126/science.155.3761.424. URL https://www.sciencemag.org/lookup/doi/10.1126/science.155.3761.424.

T. L. Bott, J. T. Brock, C. S. Dunn, R. J. Naiman, R. W. Ovink, and R. C. Petersen. Benthic community metabolism in four temperate stream systems: An inter-biome comparison and evaluation of the river continuum concept. *Hydrobiologia*, 123(1):3–45, April 1985. ISSN 0018-8158, 1573-5117. doi: 10.1007/BF00006613. URL http://link.springer.com/10.1007/BF00006613.

Elizabeth W. Boyer, Christine L. Goodale, Norbert A. Jaworski, and Robert W. Howarth. Anthropogenic Nitrogen Sources and Relationships to Riverine Nitrogen Export in the Northeastern U.S.A. *Biogeochemistry*, 57/58:137–169, 2002. ISSN 0168-2563. URL https://www.jstor.org/stable/1469687.

Elizabeth W. Boyer, Richard B. Alexander, William J. Parton, Changsheng Li, Klaus Butterbach-Bahl, Simon D. Donner, R. Wayne Skaggs, and

Stephen J. Del Grosso. Modeling Denitrification in Terrestrial and Aquatic Ecosystems at Regional Scales. *Ecological Applications*, 16(6):2123–2142, 2006. ISSN 1939-5582. doi: 10.1890/1051-0761(2006)016[2123:MDITAA]2.0.CO;2. URL https://esajournals.onlinelibrary.wiley.com/doi/abs/10.1890/1051-0761%282006%29016%5B2123%3AMDITAA%5D2.0.CO%3B2.

Martin A. Briggs, Laura K. Lautz, Danielle K. Hare, and Ricardo González-Pinzón. Relating hyporheic fluxes, residence times, and redox-sensitive biogeochemical processes upstream of beaver dams. *Freshwater Science*, 32(2):622–641, April 2013. ISSN 2161-9549. doi: 10.1899/12-110.1. URL http://www.bioone.org/doi/full/10.1899/12-110.1.

Martin A. Briggs, Laura K. Lautz, and Danielle K. Hare. Residence time control on hot moments of net nitrate production and uptake in the hyporheic zone. *Hydrological Processes*, 28(11):3741–3751, May 2014. ISSN 1099-1085. doi: 10.1002/hyp.9921. URL http://onlinelibrary.wiley.com/doi/10.1002/hyp.9921/abstract.

Lee E. Brown and David M. Hannah. Spatial heterogeneity of water temperature across an alpine river basin. *Hydrological Processes*, 22(7):954–967, March 2008. ISSN 1099-1085. doi: 10.1002/hyp.6982. URL http://onlinelibrary.wiley.com/doi/10.1002/hyp.6982/abstract.

Amy J. Burgin and Stephen K. Hamilton. Have we overemphasized the role of denitrification in aquatic ecosystems? A review of nitrate removal pathways. *Frontiers in Ecology and the Environment*, 5(2):89–96, March 2007. ISSN 1540-9309. doi: 10.1890/1540-9295(2007)5[89:HWOTRO]2.0.CO;2. URL http://onlinelibrary.wiley.com/doi/10.1890/1540-9295(2007)5[89:HWOTRO]2.0.CO;2/abstract.

Kenneth P. Burnham and David R. Anderson. *Model Selection and Multimodel Inference: A Practical Information-Theoretic Approach*. Springer Science & Business Media, December 2003. ISBN 978-0-387-95364-9.

Douglas A. Burns. Retention of NO $$_3^ - $$ in an upland streamenvironment: A mass balance approach. *Biogeochemistry*, 40(1):73–96, January 1998. ISSN 0168-2563, 1573-515X. doi: 10.1023/A:1005916102026. URL https://link.springer.com/article/10.1023/A:1005916102026.

John Karl Böhlke, Judson W. Harvey, and Mary A. Voytek. Reach-Scale Isotope Tracer Experiment to Quantify Denitrification and Related Processes in a Nitrate-Rich Stream, Midcontinent United States. *Limnology and Oceanography*, 49(3):821–838, May 2004. ISSN 0024-3590. URL http://www.jstor.org/stable/3597799.

John Karl Böhlke, Ronald C. Antweiler, Judson W. Harvey, Andrew E. Laursen, Lesley K. Smith, Richard L. Smith, and Mary A. Voytek. Multi-scale measurements

and modeling of denitrification in streams with varying flow and nitrate concentration in the upper Mississippi River basin, USA. *Biogeochemistry*, 93(1-2):117–141, January 2009. ISSN 0168-2563, 1573-515X. doi: 10.1007/s10533-008-9282-8. URL http://link.springer.com/article/10.1007/s10533-008-9282-8.

D. Caissie. The thermal regime of rivers: a review. *Freshwater Biology*, 51(8): 1389–1406, August 2006. ISSN 1365-2427. doi: 10.1111/j.1365-2427.2006.01597.x. URL http://onlinelibrary.wiley.com/doi/10.1111/j.1365-2427.2006.01597.x/abstract.

Daniel Caissie, Mysore G. Satish, and Nassir El-Jabi. Predicting water temperatures using a deterministic model: Application on Miramichi River catchments (New Brunswick, Canada). *Journal of Hydrology*, 336(3):303–315, April 2007. ISSN 0022-1694. doi: 10.1016/j.jhydrol.2007.01.008. URL http://www.sciencedirect.com/science/article/pii/S0022169407000169.

John L. Campbell, James W. Hornbeck, Myron J. Mitchell, Mary Beth Adams, Mark S. Castro, Charles T. Driscoll, Jeffrey S. Kahl, James N. Kochenderfer, Gene E. Likens, James A. Lynch, Peter S. Murdoch, Sarah J. Nelson, and James B. Shanley. Input-Output Budgets of Inorganic Nitrogen for 24 Forest Watersheds in the Northeastern United States: A Review. *Water, Air & Soil Pollution*, 151(1-4): 373–396, January 2004. ISSN 00496979. URL http://search.ebscohost.com/login.aspx?direct=true&db=eih&AN=16603977&site=eds-live.

Krista A. Capps, Regina Rancatti, Nathan Tomczyk, Thomas B. Parr, Aram J. K. Calhoun, and Malcolm Hunter. Biogeochemical Hotspots in Forested Landscapes: The Role of Vernal Pools in Denitrification and Organic Matter Processing. *Ecosystems*, 17(8):1455–1468, December 2014. ISSN 1435-0629. doi: 10.1007/s10021-014-9807-z. URL https://doi.org/10.1007/s10021-014-9807-z.

Peter Bondo Christensen, Lars Peter Nielsen, Jan Sorensen, and Niels Peter Revsbech. Denitrification in Nitrate-Rich Streams: Diurnal and Seasonal Variation Related to Benthic Oxygen Metabolism. *Limnology and Oceanography*, 35(3):640–651, May 1990. ISSN 0024-3590. URL http://www.jstor.org/stable/2837615.

Daniel A. Cluis. Relationship Between Stream Water Temperature and Ambient Air Temperature: A Simple Autoregressive Model for Mean Daily Stream Water Temperature Fluctuations. *Hydrology Research*, 3(2):65–71, April 1972. ISSN 0029-1277, 2224-7955. doi: https://doi.org/10.2166/nh.1972.0004. URL http://hr.iwaponline.com/content/3/2/65.

Brian D. Collins, David R. Montgomery, Kevin L. Fetherston, and Tim B. Abbe. The floodplain large-wood cycle hypothesis: A mechanism for the physical and biotic structuring of temperate forested alluvial valleys in the North Pacific coastal ecoregion. *Geomorphology*, 139-140:460–470, February 2012. ISSN 0169-555X.

doi: 10.1016/j.geomorph.2011.11.011. URL http://www.sciencedirect.com/science/article/pii/S0169555X11006088.

Laura S. Craig, Margaret A. Palmer, David C. Richardson, Solange Filoso, Emily S. Bernhardt, Brian P. Bledsoe, Martin W. Doyle, Peter M. Groffman, Brooke A. Hassett, Sujay S. Kaushal, Paul M. Mayer, Sean M. Smith, and Peter R. Wilcock. Stream restoration strategies for reducing river nitrogen loads. *Frontiers in Ecology and the Environment*, 6(10):529–538, 2008. ISSN 1540-9309. doi: 10.1890/070080. URL https://esajournals.onlinelibrary.wiley.com/doi/abs/10.1890/070080.

D.t. Crisp and G. Howson. Effect of air temperature upon mean water temperature in streams in the north Pennines and English Lake District. *Freshwater Biology*, 12(4): 359–367, August 1982. ISSN 1365-2427. doi: 10.1111/j.1365-2427.1982.tb00629.x. URL http://onlinelibrary.wiley.com/doi/10.1111/j.1365-2427.1982.tb00629.x/abstract.

Natalie K. Day and Robert O. Hall. Ammonium uptake kinetics and nitrification in mountain streams. *Freshwater Science*, 36(1):41–54, March 2017. ISSN 2161-9549, 2161-9565. doi: 10.1086/690600. URL http://www.journals.uchicago.edu/doi/10.1086/690600.

B. O.L. Demars, J. R. Manson, J. S. Ólafsson, G. M. Gíslason, and N. Friberg. Stream hydraulics and temperature determine the metabolism of geothermal Icelandic streams. *Knowledge and Management of Aquatic Ecosystems*, 402:05, 2011a. ISSN 1961-9502. doi: 10.1051/kmae/2011046. URL http://www.kmae-journal.org/10.1051/kmae/2011046.

BenoîT O.L. Demars, J. Russell Manson, Jon S. óLafsson, GíSli M. GíSlason, Rakel GudmundsdóTtir, Guy Woodward, Julia Reiss, Doris E. Pichler, Jes J. Rasmussen, and Nikolai Friberg. Temperature and the metabolic balance of streams: Temperature and the metabolic balance of streams. *Freshwater Biology*, 56 (6):1106–1121, June 2011b. ISSN 00465070. doi: 10.1111/j.1365-2427.2010.02554.x. URL http://doi.wiley.com/10.1111/j.1365-2427.2010.02554.x.

Robert J. Diaz and Rutger Rosenberg. Spreading Dead Zones and Consequences for Marine Ecosystems. *Science*, 321(5891):926–929, August 2008. ISSN 0036-8075, 1095-9203. doi: 10.1126/science.1156401. URL https://science.sciencemag.org/content/321/5891/926. Publisher: American Association for the Advancement of Science Section: Review.

Walter K. Dodds. Nutrients and the "dead zone": the link between nutrient ratios and dissolved oxygen in the northern Gulf of Mexico. *Frontiers in Ecology and the Environment*, 4(4):211–217, May 2006. ISSN 1540-9309. doi: 10.1890/1540-9295(2006)004[0211:NATDZT]2.0.CO;2. URL http://onlinelibrary.wiley.com/doi/10.1890/1540-9295(2006)004[0211:NATDZT]2.0.CO;2/abstract.

Charles T. Driscoll, David Whitall, John Aber, Elizabeth Boyer, Mark Castro, Christopher Cronan, Christine L. Goodale, Peter Groffman, Charles Hopkinson, Kathleen Lambert, Gregory Lawrence, and Scott Ollinger. Nitrogen Pollution in the Northeastern United States: Sources, Effects, and Management Options. *BioScience*, 53(4):357–374, April 2003. ISSN 0006-3568, 1525-3244. doi: 10.1641/0006-3568(2003)053[0357:NPITNU]2.0.CO;2. URL `http://bioscience.oxfordjournals.org/content/53/4/357`.

Sally A. Entrekin, Jennifer L. Tank, Emma J. Rosi-Marshall, Timothy J. Hoellein, and Gary A. Lamberti. Responses in organic matter accumulation and processing to an experimental wood addition in three headwater streams. *Freshwater Biology*, 53(8):1642–1657, 2008. ISSN 1365-2427. doi: 10.1111/j.1365-2427.2008.01984.x. URL `https://onlinelibrary.wiley.com/doi/abs/10.1111/j.1365-2427.2008.01984.x`.

Troy R. Erickson and Heinz G. Stefan. Linear air/water temperature correlations for streams during open water periods. *Journal of Hydrologic Engineering*, 5 (3):317–321, 2000. doi: 10.1061/(ASCE)1084-0699(2000)5:3(317). URL `http://ascelibrary.org/doi/abs/10.1061/(ASCE)1084-0699(2000)5:3(317)`.

C. S. Fellows, H. M. Valett, C. N. Dahm, P. J. Mulholland, and S. A. Thomas. Coupling Nutrient Uptake and Energy Flow in Headwater Streams. *Ecosystems*, 9(5):788–804, August 2006. ISSN 1432-9840, 1435-0629. doi: 10.1007/s10021-006-0005-5. URL `http://link.springer.com/article/10.1007/s10021-006-0005-5`.

David Fowler, Mhairi Coyle, Ute Skiba, Mark A. Sutton, J. Neil Cape, Stefan Reis, Lucy J. Sheppard, Alan Jenkins, Bruna Grizzetti, James N. Galloway, Peter Vitousek, Allison Leach, Alexander F. Bouwman, Klaus Butterbach-Bahl, Frank Dentener, David Stevenson, Marcus Amann, and Maren Voss. The global nitrogen cycle in the twenty-first century. *Philosophical Transactions: Biological Sciences*, 368(1621):1–13, 2013. ISSN 0962-8436. URL `https://www.jstor.org/stable/41938084`.

Robert A. Francis, Geoff E. Petts, and Angela M. Gurnell. Wood as a driver of past landscape change along river corridors. *Earth Surface Processes and Landforms*, 33(10):1622–1626, 2008. ISSN 1096-9837. doi: 10.1002/esp.1626. URL `https://onlinelibrary.wiley.com/doi/abs/10.1002/esp.1626`.

Aimee H. Fullerton, Christian E. Torgersen, Joshua J. Lawler, Russell N. Faux, E. Ashley Steel, Timothy J. Beechie, Joseph L. Ebersole, and Scott G. Leibowitz. Rethinking the longitudinal stream temperature paradigm: region-wide comparison of thermal infrared imagery reveals unexpected complexity of river temperatures. *Hydrological Processes*, 29(22):4719–4737, October 2015. ISSN 1099-1085. doi:

10.1002/hyp.10506. URL http://onlinelibrary.wiley.com/doi/10.1002/hyp.10506/abstract.

J. N. Galloway, F. J. Dentener, D. G. Capone, E. W. Boyer, R. W. Howarth, S. P. Seitzinger, G. P. Asner, C. C. Cleveland, P. A. Green, E. A. Holland, D. M. Karl, A. F. Michaels, J. H. Porter, A. R. Townsend, and C. J. Vöosmarty. Nitrogen Cycles: Past, Present, and Future. *Biogeochemistry*, 70(2):153–226, September 2004. ISSN 1573-515X. doi: 10.1007/s10533-004-0370-0. URL https://doi.org/10.1007/s10533-004-0370-0.

James N. Galloway, William H. Schlesinger, Hiram Levy, Anthony Michaels, and Jerald L. Schnoor. Nitrogen fixation: Anthropogenic enhancement-environmental response. *Global Biogeochemical Cycles*, 9(2):235–252, June 1995. ISSN 08866236. doi: 10.1029/95GB00158. URL http://doi.wiley.com/10.1029/95GB00158.

James N. Galloway, John D. Aber, Jan Willem Erisman, Sybil P. Seitzinger, Robert W. Howarth, Ellis B. Cowling, and B. Jack Cosby. The Nitrogen Cascade. *BioScience*, 53(4):341–356, 2003. ISSN 0006-3568. doi: 10.1641/0006-3568(2003)053[0341:tnc]2.0.co;2. URL https://www.jstor.org/stable/10.1641/0006-3568(2003)053[0341:tnc]2.0.co;2.

G. Garner, I. A. Malcolm, J. P. Sadler, and D. M. Hannah. What causes cooling water temperature gradients in a forested stream reach? *Hydrol. Earth Syst. Sci.*, 18(12):5361–5376, December 2014. ISSN 1607-7938. doi: 10.5194/hess-18-5361-2014. URL https://www.hydrol-earth-syst-sci.net/18/5361/2014/.

GDAL/OGR contributors. *GDAL/OGR Geospatial Data Abstraction software Library*. Open Source Geospatial Foundation, 2019. URL https://gdal.org.

GRASS Development Team. *Geographic Resources Analysis Support System (GRASS GIS) Software, Version 7.4*. Open Source Geospatial Foundation, 2018. URL http://grass.osgeo.org.

Nancy B. Grimm and Stuart G. Fisher. Nitrogen Limitation in a Sonoran Desert Stream. *Journal of the North American Benthological Society*, 5(1):2–15, March 1986. ISSN 0887-3593. doi: 10.2307/1467743. URL https://www.journals.uchicago.edu/doi/abs/10.2307/1467743. Publisher: The University of Chicago Press.

Peter M. Groffman, Ann M. Dorsey, and Paul M. Mayer. N processing within geomorphic structures in urban streams. *Journal of the North American Benthological Society*, 24(3):613–625, September 2005. ISSN 0887-3593. doi: 10.1899/04-026.1. URL https://www.journals.uchicago.edu/doi/abs/10.1899/04-026.1.

Peter M. Groffman, Mark A. Altabet, J. K. Böhlke, Klaus Butterbach-Bahl, Mark B. David, Mary K. Firestone, Anne E. Giblin, Todd M. Kana, Lars Peter Nielsen,

and Mary A. Voytek. Methods for Measuring Denitrification: Diverse Approaches to a Difficult Problem. *Ecological Applications*, 16(6):2091–2122, December 2006. ISSN 1939-5582. doi: 10.1890/1051-0761(2006)016[2091:MFMDDA]2.0.CO;2. URL http://onlinelibrary.wiley.com/doi/10.1890/1051-0761(2006)016[2091:MFMDDA]2.0.CO;2/abstract.

Peter M. Groffman, Klaus Butterbach-Bahl, Robinson W. Fulweiler, Arthur J. Gold, Jennifer L. Morse, Emilie K. Stander, Christina Tague, Christina Tonitto, and Philippe Vidon. Challenges to incorporating spatially and temporally explicit phenomena (hotspots and hot moments) in denitrification models. *Biogeochemistry*, 93(1):49–77, March 2009. ISSN 1573-515X. doi: 10.1007/s10533-008-9277-5. URL https://doi.org/10.1007/s10533-008-9277-5.

A. M. Gurnell, H. Piégay, F. J. Swanson, and S. V. Gregory. Large wood and fluvial processes. *Freshwater Biology*, 47(4):601–619, 2002. ISSN 1365-2427. doi: 10.1046/j.1365-2427.2002.00916.x. URL https://onlinelibrary.wiley.com/doi/abs/10.1046/j.1365-2427.2002.00916.x.

Angela Gurnell, Klement Tockner, Peter Edwards, and Geoffrey Petts. Effects of deposited wood on biocomplexity of river corridors. *Frontiers in Ecology and the Environment*, 3(7):377–382, 2005. ISSN 1540-9309. doi: 10.1890/1540-9295(2005)003[0377:EODWOB]2.0.CO;2. URL https://esajournals.onlinelibrary.wiley.com/doi/abs/10.1890/1540-9295%282005%29003%5B0377%3AEODWOB%5D2.0.CO%3B2.

Robert O. Hall. A stream's role in watershed nutrient export. *Proceedings of the National Academy of Sciences of the United States of America*, 100(18):10137–10138, September 2003. ISSN 0027-8424. doi: 10.1073/pnas.1934477100. URL http://www.ncbi.nlm.nih.gov/pmc/articles/PMC193526/.

Robert O. Hall, Michelle A. Baker, Christopher D. Arp, and Benjamin J. Koch. Hydrologic control of nitrogen removal, storage, and export in a mountain stream. *Limnology and Oceanography*, 54(6):2128–2142, 2009. ISSN 00243590. doi: 10.4319/lo.2009.54.6.2128. URL http://www.aslo.org/lo/toc/vol_54/issue_6/2128.html.

David M. Hannah, Iain A. Malcolm, Chris Soulsby, and Alan F. Youngson. A comparison of forest and moorland stream microclimate, heat exchanges and thermal dynamics. *Hydrological Processes*, 22(7):919–940, March 2008. ISSN 1099-1085. doi: 10.1002/hyp.7003. URL http://onlinelibrary.wiley.com/doi/10.1002/hyp.7003/abstract.

K. Harwood and A. G. Brown. Fluvial processes in a forested anastomosing river: Flood partitioning and changing flow patterns. *Earth Surface Processes and Landforms*, 18(8):741–748, 1993. ISSN 1096-9837. doi: 10.1002/esp.3290180808.

URL https://onlinelibrary.wiley.com/doi/abs/10.1002/esp.3290180808. _eprint: https://onlinelibrary.wiley.com/doi/pdf/10.1002/esp.3290180808.

Cindie Hebert, Daniel Caissie, Mysore G. Satish, and Nassir El-Jabi. Study of stream temperature dynamics and corresponding heat fluxes within Miramichi River catchments (New Brunswick, Canada). *Hydrological Processes*, 25(15):2439–2455, 2011. ISSN 08856087. doi: 10.1002/hyp.8021. URL http://doi.wiley.com/10.1002/hyp.8021.

Ashley M Helton, Geoffrey C Poole, Judy L Meyer, Wilfred M Wollheim, Bruce J Peterson, Patrick J Mulholland, Emily S Bernhardt, Jack A Stanford, Clay Arango, Linda R Ashkenas, Lee W Cooper, Walter K Dodds, Stanley V Gregory, Robert O Hall, Stephen K Hamilton, Sherri L Johnson, William H McDowell, Jody D Potter, Jennifer L Tank, Suzanne M Thomas, H Maurice Valett, Jackson R Webster, and Lydia Zeglin. Thinking outside the channel: modeling nitrogen cycling in networked river ecosystems. *Frontiers in Ecology and the Environment*, 9(4):229–238, May 2011. ISSN 1540-9295. doi: 10.1890/080211. URL http://www.esajournals.org/doi/abs/10.1890/080211.

Ashley M. Helton, Robert O. Hall, and Enrico Bertuzzo. How network structure can affect nitrogen removal by streams. *Freshwater Biology*, 63(1):128–140, 2018. ISSN 1365-2427. doi: 10.1111/fwb.12990. URL https://onlinelibrary.wiley.com/doi/abs/10.1111/fwb.12990.

Alan R. Hill, Kevin J. Devito, S. Campagnolo, and K. Sanmugadas. Subsurface denitrification in a forest riparianzone: Interactions between hydrology and supplies ofnitrate and organic carbon. *Biogeochemistry*, 51(2):193–223, November 2000. ISSN 1573-515X. doi: 10.1023/A:1006476514038. URL https://doi.org/10.1023/A:1006476514038.

Eve-Lyn S. Hinckley, Brian A. Ebel, Rebecca T. Barnes, Robert S. Anderson, Mark W. Williams, and Suzanne P. Anderson. Aspect control of water movement on hillslopes near the rain–snow transition of the Colorado Front Range. *Hydrological Processes*, 28(1):74–85, 2012. ISSN 1099-1085. doi: 10.1002/hyp.9549. URL https://onlinelibrary.wiley.com/doi/abs/10.1002/hyp.9549.

Alexander J. Horne. Algal nitrogen fixation in Californian streams: diel cycles and nocturnal fixation. *Freshwater Biology*, 5(5):471–477, 1975. ISSN 1365-2427. doi: 10.1111/j.1365-2427.1975.tb00149.x. URL https://onlinelibrary.wiley.com/doi/abs/10.1111/j.1365-2427.1975.tb00149.x. _eprint: https://onlinelibrary.wiley.com/doi/pdf/10.1111/j.1365-2427.1975.tb00149.x.

Jeffrey N. Houser, Patrick J. Mulholland, and Kelly O. Maloney. Catchment disturbance and stream metabolism: patterns in ecosystem respiration and gross primary production along a gradient of upland soil and vegetation disturbance.

Journal of the North American Benthological Society, 24(3):538–552, September 2005. ISSN 0887-3593, 1937-237X. doi: 10.1899/04-034.1. URL https://www.journals.uchicago.edu/doi/10.1899/04-034.1.

R. W. Howarth, G. Billen, D. Swaney, A. Townsend, N. Jaworski, K. Lajtha, J. A. Downing, R. Elmgren, N. Caraco, T. Jordan, F. Berendse, J. Freney, V. Kudeyarov, P. Murdoch, and Zhu Zhao-Liang. Regional Nitrogen Budgets and Riverine N & P Fluxes for the Drainages to the North Atlantic Ocean: Natural and Human Influences. *Biogeochemistry*, 35(1):75–139, 1996. ISSN 0168-2563. URL https://www.jstor.org.proxybz.lib.montana.edu/stable/1469226.

Robert W. Howarth and Roxanne Marino. Nitrogen as the limiting nutrient for eutrophication in coastal marine ecosystems: Evolving views over three decades. *Limnology and Oceanography*, 51(1part2):364–376, January 2006. ISSN 00243590. doi: 10.4319/lo.2006.51.1_part_2.0364. URL http://doi.wiley.com/10.4319/lo.2006.51.1_part_2.0364.

Clifford M. Hurvich and Chih-Ling Tsai. A corrected Akaike Information Criterion for vector autoregressive model selection. *Journal of Time Series Analysis*, 14 (3):271–279, 1993. ISSN 1467-9892. doi: 10.1111/j.1467-9892.1993.tb00144.x. URL http://onlinelibrary.wiley.com/doi/10.1111/j.1467-9892.1993.tb00144.x/abstract.

Sarah E. Inwood, Jennifer L. Tank, and Melody J. Bernot. Factors Controlling Sediment Denitrification in Midwestern Streams of Varying Land Use. *Microbial Ecology*, 53(2):247–258, February 2007. ISSN 1432-184X. doi: 10.1007/s00248-006-9104-2. URL https://doi.org/10.1007/s00248-006-9104-2.

Clemente Izurieta, Geoffrey Poole, Robert A. Payn, Isaac Griffith, Ryan Nix, Ashley Helton, Emily Bernhardt, and Amy J. Burgin. Development and Application of a Simulation Environment (NEO) for Integrating Empirical and Computational Investigations of System-Level Complexity. pages 1–6. IEEE, May 2012. ISBN 978-1-4673-1401-5 978-1-4673-1402-2 978-1-4673-1400-8. doi: 10.1109/ICISA.2012.6220928. URL http://ieeexplore.ieee.org/lpdocs/epic03/wrapper.htm?arnumber=6220928.

T. Jickells. External inputs as a contributor to eutrophication problems. *Journal of Sea Research*, 54(1):58–69, July 2005. ISSN 1385-1101. doi: 10.1016/j.seares.2005.02.006. URL http://www.sciencedirect.com/science/article/pii/S1385110105000092.

Kim K. Jones, Kara Anlauf-Dunn, Paul S. Jacobsen, Matt Strickland, Lora Tennant, and Sharon E. Tippery. Effectiveness of Instream Wood Treatments to Restore Stream Complexity and Winter Rearing Habitat for Juvenile Coho Salmon.

Transactions of the American Fisheries Society, 143(2):334–345, 2014. ISSN 0002-8487. doi: 10.1080/00028487.2013.852623. URL https://doi.org/10.1080/00028487.2013.852623.

Nicholas E. Jones. Incorporating lakes within the river discontinuum: longitudinal changes in ecological characteristics in stream-lake networks. *Canadian Journal of Fisheries and Aquatic Sciences*, 67(8):1350–1362, 2010. ISSN 0706-652X. doi: 10.1139/F10-069. URL http://www.nrcresearchpress.com/doi/abs/10.1139/f10-069.

Jochem Kail, Daniel Hering, Susanne Muhar, Marc Gerhard, and Sabine Preis. The use of large wood in stream restoration: experiences from 50 projects in Germany and Austria. *Journal of Applied Ecology*, 44(6):1145–1155, 2007. ISSN 1365-2664. doi: 10.1111/j.1365-2664.2007.01401.x. URL https://besjournals.onlinelibrary.wiley.com/doi/abs/10.1111/j.1365-2664.2007.01401.x.

Sujay S. Kaushal, Peter M. Groffman, Paul M. Mayer, Elise Striz, and Arthur J. Gold. Effects of Stream Restoration on Denitrification in an Urbanizing Watershed. *Ecological Applications*, 18(3):789–804, 2008. ISSN 1939-5582. doi: 10.1890/07-1159.1. URL https://esajournals.onlinelibrary.wiley.com/doi/abs/10.1890/07-1159.1.

Melody J. Kemp and Walter K. Dodds. Comparisons of Nitrification and Denitrification in Prairie and Agriculturally Influenced Streams. *Ecological Applications*, 12(4):998–1009, August 2002. ISSN 1939-5582. doi: 10.1890/1051-0761(2002)012[0998:CONADI]2.0.CO;2. URL http://onlinelibrary.wiley.com/doi/10.1890/1051-0761(2002)012[0998:CONADI]2.0.CO;2/abstract.

John S. Kominoski, Amy D. Rosemond, Jonathan P. Benstead, Vlad Gulis, and David W. P. Manning. Experimental nitrogen and phosphorus additions increase rates of stream ecosystem respiration and carbon loss: Nutrients increase whole-stream respiration. *Limnology and Oceanography*, 63(1):22–36, January 2018. ISSN 00243590. doi: 10.1002/lno.10610. URL http://doi.wiley.com/10.1002/lno.10610.

Lisa A. Kunza and Robert O. Hall. Nitrogen fixation can exceed inorganic nitrogen uptake fluxes in oligotrophic streams. *Biogeochemistry*, 121(3):537–549, December 2014. ISSN 1573-515X. doi: 10.1007/s10533-014-0021-z. URL https://doi.org/10.1007/s10533-014-0021-z.

J. A. Leach, W. Lidberg, L. Kuglerová, A. Peralta-Tapia, A. Ågren, and H. Laudon. Evaluating topography-based predictions of shallow lateral groundwater discharge zones for a boreal lake-stream system. *Water Resources Research*, 53(7):5420–5437, April 2017. ISSN 1944-7973. doi: 10.1002/2016WR019804. URL https://agupubs.onlinelibrary.wiley.com/doi/abs/10.1002/2016WR019804.

L.B. Leopold and Thomas Maddock Jr. The hydraulic geometry of stream channels and some physiographic implications. USGS Numbered Series 252, 1953. URL http://pubs.er.usgs.gov/publication/pp252.

Bridget Livers and Ellen Wohl. Sources and interpretation of channel complexity in forested subalpine streams of the Southern Rocky Mountains: CHANNEL COMPLEXITY IN FORESTED STREAMS. *Water Resources Research*, 52(5): 3910–3929, May 2016. ISSN 00431397. doi: 10.1002/2015WR018306. URL http://doi.wiley.com/10.1002/2015WR018306.

Bridget Livers, Ellen Wohl, Karen J. Jackson, and Nicholas A. Sutfin. Historical land use as a driver of alternative states for stream form and function in forested mountain watersheds of the Southern Rocky Mountains: Alternative states of forested Southern Rocky Mountain streams. *Earth Surface Processes and Landforms*, November 2017. ISSN 01979337. doi: 10.1002/esp.4275. URL http://doi.wiley.com/10.1002/esp.4275.

Mark Losleben. Air temperature data for Saddle chart recorder from 1981 - ongoing. *Environmental Data Initiative*, 2007a. doi: 10.6073/pasta/898ace0c0a391f3679f9da8ef138ad26. URL http://niwot.colorado.edu/index.php/data/data/air-temperature-data-for-saddle-chart-recorder-1981-ongoing.

Mark Losleben. Precipitation data for C1 chart recorder from 1952 - ongoing. *Environmental Data Initiative*, 2007b. doi: 10.6073/pasta/ed56d9c8a354382238f145039105c964. URL http://niwot.colorado.edu/index.php/data/data/precipitation-data-for-c1-chart-recorder-1952-ongoing.

Hilary L. Madinger and Robert O. Hall. Linking denitrification with ecosystem respiration in mountain streams. *Limnology and Oceanography Letters*, 4(5):145–154, 2019. ISSN 2378-2242. doi: 10.1002/lol2.10111. URL https://aslopubs.onlinelibrary.wiley.com/doi/abs/10.1002/lol2.10111.

Hannah K. Marchant, Soeren Ahmerkamp, Gaute Lavik, Halina E. Tegetmeyer, Jon Graf, Judith M. Klatt, Moritz Holtappels, Eva Walpersdorf, and Marcel M. M. Kuypers. Denitrifying community in coastal sediments performs aerobic and anaerobic respiration simultaneously. *The ISME Journal*, 11(8):1799–1812, August 2017. ISSN 1751-7370. doi: 10.1038/ismej.2017.51. URL https://www.nature.com/articles/ismej201751. Number: 8 Publisher: Nature Publishing Group.

Lara A. Martin, Patrick J. Mulholland, Jackson R. Webster, and H. Maurice Valett. Denitrification potential in sediments of headwater streams in the southern Appalachian Mountains, USA. *Journal of the North American Benthological Society*, 20(4):505–519, December 2001. ISSN 0887-3593. doi: 10.2307/1468084. URL http://www.jstor.org/stable/1468084.

Michael E. McClain, Elizabeth W. Boyer, C. Lisa Dent, Sarah E. Gergel, Nancy B. Grimm, Peter M. Groffman, Stephen C. Hart, Judson W. Harvey, Carol A. Johnston, Emilio Mayorga, William H. McDowell, and Gilles Pinay. Biogeochemical Hot Spots and Hot Moments at the Interface of Terrestrial and Aquatic Ecosystems. *Ecosystems*, 6(4):301–312, June 2003. ISSN 1432-9840. doi: 10.1007/s10021-003-0161-9. URL `https://doi.org/10.1007/s10021-003-0161-9`.

Eric Mellina and Scott G. Hinch. Influences of riparian logging and in-stream large wood removal on pool habitat and salmonid density and biomass: a meta-analysis. *Canadian Journal of Forest Research*, 39(7):1280–1301, July 2009. ISSN 0045-5067. doi: 10.1139/X09-037. URL `https://www.nrcresearchpress.com/doi/10.1139/X09-037`.

Eric Mellina, R Dan Moore, Scott G Hinch, J Stevenson Macdonald, and Greg Pearson. Stream temperature responses to clearcut logging in British Columbia: the moderating influences of groundwater and headwater lakes. *Canadian Journal of Fisheries and Aquatic Sciences*, 59(12):1886–1900, 2002. ISSN 0706-652X. doi: 10.1139/f02-158. URL `http://www.nrcresearchpress.com/doi/abs/10.1139/f02-158`.

William J. Mitsch, John W. Day, J. Wendell Gilliam, Peter M. Groffman, Donald L. Hey, Gyles W. Randall, and Naiming Wang. Reducing Nitrogen Loading to the Gulf of Mexico from the Mississippi River Basin: Strategies to Counter a Persistent Ecological Problem Ecotechnology—the use of natural ecosystems to solve environmental problems—should be a part of efforts to shrink the zone of hypoxia in the Gulf of Mexico. *BioScience*, 51(5):373–388, May 2001. ISSN 0006-3568, 1525-3244. doi: 10.1641/0006-3568(2001)051[0373:RNLTTG]2.0.CO;2. URL `http://bioscience.oxfordjournals.org/content/51/5/373`.

Wendy A. Monk, Nathan M. Wilbur, R. Allen Curry, Rolland Gagnon, and Russell N. Faux. Linking landscape variables to cold water refugia in rivers. *Journal of Environmental Management*, 118:170–176, March 2013. ISSN 0301-4797. doi: 10.1016/j.jenvman.2012.12.024. URL `http://www.sciencedirect.com/science/article/pii/S0301479712006627`.

Patrick J. Mulholland, Ashley M. Helton, Geoffrey C. Poole, Robert O. Hall, Stephen K. Hamilton, Bruce J. Peterson, Jennifer L. Tank, Linda R. Ashkenas, Lee W. Cooper, Clifford N. Dahm, Walter K. Dodds, Stuart E. G. Findlay, Stanley V. Gregory, Nancy B. Grimm, Sherri L. Johnson, William H. McDowell, Judy L. Meyer, H. Maurice Valett, Jackson R. Webster, Clay P. Arango, Jake J. Beaulieu, Melody J. Bernot, Amy J. Burgin, Chelsea L. Crenshaw, Laura T. Johnson, B. R. Niederlehner, Jonathan M. O'Brien, Jody D. Potter, Richard W. Sheibley, Daniel J. Sobota, and Suzanne M. Thomas. Stream denitrification across biomes and its response to anthropogenic nitrate loading. *Nature*, 452(7184):

202–205, March 2008. ISSN 0028-0836. doi: 10.1038/nature06686. URL http://www.nature.com/nature/journal/v452/n7184/full/nature06686.html.

Patrick J. Mulholland, Robert Hall, Daniel Sobota, Walter Dodds, Stuart Findlay, Nancy Grimm, Stephen Hamilton, William McDowell, Jon O'Brien, Jennifer Tank, Linda Ashkenas, Lee W. Cooper, Cliff Dahm, Stanley Gregory, Sherri Johnson, Judy Meyer, Bruce Peterson, Geoff Poole, H. Maurice Valett, Jackson Webster, Clay Arango, Jake Beaulieu, Melody Bernot, Amy Burgin, Chelsea Crenshaw, Ashley Helton, Laura Johnson, Bobbie Niederlehner, Jody Potter, Rich Sheibley, and Suzanne Thomas. Nitrate Removal in Stream Ecosystems Measured by 15n Addition Experiments: 2. Denitrification. *Limnology and Oceanography*, 54 (3), May 2009. doi: 10.4319/lo.2009.54.3.0666. URL http://www.osti.gov/energycitations/product.biblio.jsp?osti_id=951921.

Timo Muotka and Pekka Laasonen. Ecosystem recovery in restored headwater streams: the role of enhanced leaf retention. *Journal of Applied Ecology*, 39(1):145–156, 2002. ISSN 1365-2664. doi: 10.1046/j.1365-2664.2002.00698.x. URL https://besjournals.onlinelibrary.wiley.com/doi/abs/10.1046/j.1365-2664.2002.00698.x.

Timo Muotka and Jukka Syrjänen. Changes in habitat structure, benthic invertebrate diversity, trout populations and ecosystem processes in restored forest streams: a boreal perspective. *Freshwater Biology*, 52(4):724–737, 2007. ISSN 1365-2427. doi: 10.1111/j.1365-2427.2007.01727.x. URL https://onlinelibrary.wiley.com/doi/abs/10.1111/j.1365-2427.2007.01727.x.

J. Denis Newbold, Jerry W. Elwood, Robert V. O'Neill, and Webster Van Winkle. Measuring Nutrient Spiralling in Streams. *Canadian Journal of Fisheries and Aquatic Sciences*, 38(7):860–863, July 1981. ISSN 0706-652X, 1205-7533. doi: 10.1139/f81-114. URL http://www.nrcresearchpress.com/doi/abs/10.1139/f81-114.

Tamara A. Newcomer Johnson, Sujay S. Kaushal, Paul M. Mayer, Rose M. Smith, and Gwen M. Sivirichi. Nutrient Retention in Restored Streams and Rivers: A Global Review and Synthesis. *Water*, 8(4):116, April 2016. doi: 10.3390/w8040116. URL https://www.mdpi.com/2073-4441/8/4/116.

Daniel M. Perkins, Gabriel Yvon-Durocher, Benoît O.L. Demars, Julia Reiss, Doris E. Pichler, Nikolai Friberg, Mark Trimmer, and Guy Woodward. Consistent temperature dependence of respiration across ecosystems contrasting in thermal history. *Global Change Biology*, 18(4):1300–1311, 2012. ISSN 1365-2486. doi: 10.1111/j.1365-2486.2011.02597.x. URL http://onlinelibrary.wiley.com/doi/10.1111/j.1365-2486.2011.02597.x/abstract.

B. J. Peterson, J. E. Hobbie, A. E. Hershey, M. A. Lock, T. E. Ford, J. R. Vestal, V. L. Mckinley, M. A. J. Hullar, M. C. Miller, R. M. Ventullo, and G. S. Volk. Transformation of a Tundra River from Heterotrophy to Autotrophy by Addition of Phosphorus. *Science*, 229(4720):1383–1386, September 1985. ISSN 0036-8075, 1095-9203. doi: 10.1126/science.229.4720.1383. URL `http://www.sciencemag.org/cgi/doi/10.1126/science.229.4720.1383`.

Bruce J. Peterson, Wilfred M. Wollheim, Patrick J. Mulholland, Jackson R. Webster, Judy L. Meyer, Jennifer L. Tank, Eugènia Martí, William B. Bowden, H. Maurice Valett, Anne E. Hershey, William H. McDowell, Walter K. Dodds, Stephen K. Hamilton, Stanley Gregory, and Donna D. Morrall. Control of Nitrogen Export from Watersheds by Headwater Streams. *Science*, 292(5514):86–90, April 2001. ISSN 0036-8075, 1095-9203. doi: 10.1126/science.1056874. URL `http://www.sciencemag.org/content/292/5514/86`.

E. Piña-Ochoa and M. Álvarez Cobelas. Denitrification in Aquatic Environments: A Cross-system Analysis. *Biogeochemistry*, 81(1):111–130, October 2006. ISSN 0168-2563, 1573-515X. doi: 10.1007/s10533-006-9033-7. URL `https://link.springer.com/article/10.1007/s10533-006-9033-7`.

Geoffrey C. Poole. Fluvial landscape ecology: addressing uniqueness within the river discontinuum. *Freshwater Biology*, 47(4):641–660, 2002. ISSN 1365-2427. doi: 10.1046/j.1365-2427.2002.00922.x. URL `http://onlinelibrary.wiley.com/doi/10.1046/j.1365-2427.2002.00922.x/abstract`.

Geoffrey C. Poole and Cara H. Berman. An ecological perspective on in-stream temperature: natural heat dynamics and mechanisms of human-caused thermal degradation. *Environmental Management*, 27(6):787–802, 2001. ISSN 0364-152X, 1432-1009. doi: 10.1007/s002670010188. URL `http://link.springer.com/article/10.1007/s002670010188`.

QGIS Development Team. *QGIS Geographic Information System*. Open Source Geospatial Foundation, 2018. URL `http://qgis.osgeo.org`.

R Core Team. *R: A Language and Environment for Statistical Computing*. R Foundation for Statistical Computing, Vienna, Austria, 2014. URL `http://www.R-project.org/`.

R Core Team. *R: A language and environment for statistical computing*. R Foundation for Statistical Computing, Vienna, Austria, 2016. URL `https://www.R-project.org/`.

Nancy N. Rabalais, R. Eugene Turner, and William J. Wiseman. Gulf of Mexico Hypoxia, A.K.A. "The Dead Zone". *Annual Review of Ecology and Systematics*, 33(1):235–263, 2002. doi: 10.1146/annurev.ecolsys.33.010802.150513.

URL https://doi.org/10.1146/annurev.ecolsys.33.010802.150513. _eprint: https://doi.org/10.1146/annurev.ecolsys.33.010802.150513.

Anthony J. Ranalli and Donald L. Macalady. The importance of the riparian zone and in-stream processes in nitrate attenuation in undisturbed and agricultural watersheds – A review of the scientific literature. *Journal of Hydrology*, 389(3): 406–415, August 2010. ISSN 0022-1694. doi: 10.1016/j.jhydrol.2010.05.045. URL http://www.sciencedirect.com/science/article/pii/S0022169410003306.

Alexander J. Reisinger, Jennifer L. Tank, Timothy J. Hoellein, and Robert O. Hall. Sediment, water column, and open-channel denitrification in rivers measured using membrane-inlet mass spectrometry. *Journal of Geophysical Research: Biogeosciences*, 121(5):1258–1274, 2016. ISSN 2169-8961. doi: 10.1002/2015JG003261. URL https://agupubs.onlinelibrary.wiley.com/doi/abs/10.1002/2015JG003261.

Marc O Ribaudo, Ralph Heimlich, Roger Claassen, and Mark Peters. Least-cost management of nonpoint source pollution: source reduction versus interception strategies for controlling nitrogen loss in the Mississippi Basin. *Ecological Economics*, 37(2):183–197, May 2001. ISSN 0921-8009. doi: 10.1016/S0921-8009(00)00273-1. URL http://www.sciencedirect.com/science/article/pii/S0921800900002731.

J. Richards, R. D. Moore, and A. L. Forrest. Late-summer thermal regime of a small proglacial lake. *Hydrological Processes*, 26(18):2687–2695, 2012. ISSN 08856087. doi: 10.1002/hyp.8360. URL http://doi.wiley.com/10.1002/hyp.8360.

Sylvia C. Schaefer and Merryl Alber. Temperature controls a latitudinal gradient in the proportion of watershed nitrogen exported to coastal ecosystems. *Biogeochemistry*, 85(3):333–346, September 2007. ISSN 1573-515X. doi: 10.1007/s10533-007-9144-9. URL https://doi.org/10.1007/s10533-007-9144-9.

Daniel N. Scott and Ellen E. Wohl. Natural and Anthropogenic Controls on Wood Loads in River Corridors of the Rocky, Cascade, and Olympic Mountains, USA. *Water Resources Research*, 54(10):7893–7909, 2018. ISSN 1944-7973. doi: 10.1029/2018WR022754. URL https://agupubs.onlinelibrary.wiley.com/doi/abs/10.1029/2018WR022754.

Mark C. Scott, Gene S. Helfman, Matthew E. McTammany, E. Fred Benfield, and Paul V. Bolstad. Multiscale influences on physical and chemical stream conditions across Blue Ridge landscapes. *JAWRA Journal of the American Water Resources Association*, 38(5):1379–1392, 2002. ISSN 1752-1688. doi: 10.1111/j.1752-1688.2002.tb04353.x. URL http://onlinelibrary.wiley.com/doi/10.1111/j.1752-1688.2002.tb04353.x/abstract.

D. A. Sear, C. E. Millington, D. R. Kitts, and R. Jeffries. Logjam controls on channel:floodplain interactions in wooded catchments and their role in the formation of multi-channel patterns. *Geomorphology*, 116:305–319, April 2010. ISSN 0169-555X. doi: Sear,D.A. ,Millington,C.E.,Kitts,D.R.andJeffries,R.(2010)Logjamcontrolsonchannel: floodplaininteractionsinwoodedcatchmentsandtheirroleintheformationofmulti-channelpatterns.Ge 116(3-4),305-319.(doi:10.1016/j.geomorph.2009.11.022⟨http://dx.doi.org/10.1016/ j.geomorph.2009.11.022⟩). URL https://eprints.soton.ac.uk/147875/.

S. Seitzinger, J. A. Harrison, J. K. Böhlke, A. F. Bouwman, R. Lowrance, B. Peterson, C. Tobias, and G. Van Drecht. Denitrification across landscapes and waterscapes: a synthesis. *Ecological Applications: A Publication of the Ecological Society of America*, 16(6):2064–2090, December 2006. ISSN 1051-0761.

Sybil P. Seitzinger, Renée V. Styles, Elizabeth W. Boyer, Richard B. Alexander, Gilles Billen, Robert W. Howarth, Bernhard Mayer, and Nico van Breemen. Nitrogen retention in rivers: model development and application to watersheds in the northeastern U.S.A. *Biogeochemistry*, 57-58(1):199–237, April 2002. ISSN 0168-2563, 1573-515X. doi: 10.1023/A:1015745629794. URL https://link.springer.com/article/10.1023/A:1015745629794.

Richard A. Smith, Gregory E. Schwarz, and Richard B. Alexander. Regional interpretation of water-quality monitoring data. *Water Resources Research*, 33 (12):2781–2798, 1997. ISSN 1944-7973. doi: 10.1029/97WR02171. URL https://agupubs.onlinelibrary.wiley.com/doi/abs/10.1029/97WR02171.

Heinz G. Stefan and Eric B. Preud'homme. Stream temperature estimation from air temperature. *JAWRA Journal of the American Water Resources Association*, 29(1):27–45, 1993. ISSN 1752-1688. doi: 10.1111/j.1752-1688.1993.tb01502.x. URL http://onlinelibrary.wiley.com/doi/10.1111/j.1752-1688.1993.tb01502.x/abstract.

Robert S. Stelzer and Lynn A. Bartsch. Nitrate removal in deep sediments of a nitrogen-rich river network: A test of a conceptual model. *Journal of Geophysical Research: Biogeosciences*, 117(G2):G02027, June 2012. ISSN 2156-2202. doi: 10.1029/2012JG001990. URL http://onlinelibrary.wiley.com/doi/10.1029/2012JG001990/abstract.

William D. P. Stewart. Nitrogen fixation by blue-green algae in Yellowstone thermal areas. *Phycologia*, 9(3-4):261–268, December 1970. ISSN 0031-8884. doi: 10.2216/i0031-8884-9-3-261.1. URL https://doi.org/10.2216/i0031-8884-9-3-261.1. Publisher: Taylor & Francis _eprint: https://doi.org/10.2216/i0031-8884-9-3-261.1.

Stream Solute Workshop. Concepts and Methods for Assessing Solute Dynamics in Stream Ecosystems. *Journal of the North American Benthological Society*, 9(2):

95–119, June 1990. ISSN 0887-3593. doi: 10.2307/1467445. URL http://www.journals.uchicago.edu/doi/abs/10.2307/1467445.

Philip G. Taylor and Alan R. Townsend. Stoichiometric control of organic carbon–nitrate relationships from soils to the sea. *Nature*, 464(7292):1178–1181, July 2012. ISSN 1476-4687. doi: 10.1038/nature08985. URL https://www.nature.com/articles/nature08985.

David Tilman, Joseph Fargione, Brian Wolff, Carla D'Antonio, Andrew Dobson, Robert Howarth, David Schindler, William H. Schlesinger, Daniel Simberloff, and Deborah Swackhamer. Forecasting Agriculturally Driven Global Environmental Change. *Science*, 292(5515):281–284, April 2001. ISSN 0036-8075, 1095-9203. doi: 10.1126/science.1057544. URL http://science.sciencemag.org/content/292/5515/281.

E. Tornlund and L. Ostlund. Floating Timber in Northern Sweden: The Construction of Floatways and Transformation of Rivers. *Environment and History*, 8(1):85–106, February 2002. ISSN 09673407, 17527023. doi: 10.3197/096734002129342611. URL http://openurl.ingenta.com/content/xref?genre=article&issn=0967-3407&volume=8&issue=1&spage=85.

U.S. Geological Survey. National Water Information System data available on the World Wide Web (USGS Water Data for the Nation). *https://waterdata.usgs.gov/co/nwis/inventory/?site_no=402114105350101*, 2016. doi: http://dx.doi.org/10.5066/F7P55KJN.

USGS. United States Geological Survey National Elevation Dataset 1/3 arc-second n41w106 1 x 1 degree, July 2015. URL https://www.sciencebase.gov/catalog/item/581d2161e4b08da350d53248. type: dataset.

H. Maurice Valett, Chelsea L. Crenshaw, and Paul F. Wagner. Stream nutrient uptake, forest succession, and biogeochemical theory. *Ecology*, 83(10):2888–2901, October 2002. ISSN 0012-9658. doi: 10.1890/0012-9658(2002)083[2888:SNUFSA]2.0.CO;2. URL http://www.esajournals.org/doi/abs/10.1890/0012-9658(2002)083[2888:SNUFSA]2.0.CO;2.

N. van Breemen, E.W. Boyer, C.L. Goodale, N.A. Jaworski, K. Paustian, S.P. Seitzinger, K. Lajtha, B. Mayer, D. van Dam, R.W. Howarth, K.J. Nadelhoffer, M. Eve, and G. Billen. Where did all the nitrogen go? Fate of nitrogen inputs to large watersheds in the northeastern U.S.A. *Biogeochemistry*, 57(1):267–293, April 2002. ISSN 1573-515X. doi: 10.1023/A:1015775225913. URL https://doi.org/10.1023/A:1015775225913.

Robin L. Vannote, G. Wayne Minshall, Kenneth W. Cummins, James R. Sedell, and Colbert E. Cushing. The river continuum concept. *Canadian Journal of Fisheries*

and Aquatic Sciences, 37(1):130–137, 1980. ISSN 0706-652X. doi: 10.1139/f80-017. URL http://www.nrcresearchpress.com/doi/abs/10.1139/f80-017.

Thomas T. Veblen and Diane C. Lorenz. Anthropogenic Disturbance and Recovery Patterns in Montane Forests, Colorado Front Range. *Physical Geography*, 7(1): 1–24, January 1986. ISSN 0272-3646. doi: 10.1080/02723646.1986.10642278. URL https://doi.org/10.1080/02723646.1986.10642278.

Michael P. Venarsky, David M. Walters, Robert O. Hall, Bridget Livers, and Ellen Wohl. Shifting stream planform state decreases stream productivity yet increases riparian animal production. *Oecologia*, 187(1):167–180, May 2018. ISSN 0029-8549, 1432-1939. doi: 10.1007/s00442-018-4106-6. URL http://link.springer.com/10.1007/s00442-018-4106-6.

Peter M. Vitousek, John D. Aber, Robert W. Howarth, Gene E. Likens, Pamela A. Matson, David W. Schindler, William H. Schlesinger, and David G. Tilman. Human Alteration of the Global Nitrogen Cycle: Sources and Consequences. *Ecological Applications*, 7(3):737–750, August 1997. ISSN 1939-5582. doi: 10.1890/1051-0761(1997)007[0737:HAOTGN]2.0.CO;2. URL http://onlinelibrary.wiley.com/doi/10.1890/1051-0761(1997)007[0737:HAOTGN]2.0.CO;2/abstract.

J. V. Ward and J. A. Stanford. The serial discontinuity concept: Extending the model to floodplain rivers. *Regulated Rivers: Research & Management*, 10(2-4): 159–168, August 1995. ISSN 08869375, 10991646. doi: 10.1002/rrr.3450100211. URL http://doi.wiley.com/10.1002/rrr.3450100211.

Mary H. Ward, Rena R. Jones, Jean D. Brender, Theo M. De Kok, Peter J. Weyer, Bernard T. Nolan, Cristina M. Villanueva, and Simone G. Van Breda. Drinking Water Nitrate and Human Health: An Updated Review. *International Journal of Environmental Research and Public Health*, 15(7):1557, July 2018. doi: 10.3390/ijerph15071557. URL https://www.mdpi.com/1660-4601/15/7/1557. Number: 7 Publisher: Multidisciplinary Digital Publishing Institute.

Dana R. Warren, Emily S. Bernhardt, Robert O. Hall, and Gene E. Likens. Forest age, wood and nutrient dynamics in headwater streams of the Hubbard Brook Experimental Forest, NH. *Earth Surface Processes and Landforms*, 32(8): 1154–1163, July 2007. ISSN 1096-9837. doi: 10.1002/esp.1548. URL https://onlinelibrary.wiley.com/doi/abs/10.1002/esp.1548.

B. W. Webb and Y. Zhang. Spatial and seasonal variability in the components of the river heat budget. *Hydrological Processes*, 11(1):79–101, 1997. ISSN 08856087, 10991085. doi: 10.1002/(SICI)1099-1085(199701)11:1⟨79::AID-HYP404⟩3.0.CO;2-N. URL http://doi.wiley.com/10.1002/%28SICI%291099-1085%28199701%2911%3A1%3C79%3A%3AAID-HYP404%3E3.0.CO%3B2-N.

Jackson R Webster. Changes in water temperature in streams with progressive hemlock mortality at 8 Coweeta Hydrologic Laboratory study sites from 2004 to 2013, 2014. URL http://gce-lter.marsci.uga.edu/public/app/dataset_details.asp?accession=CWT_HYD_3070. itemType: dataset.

E. Wohl and N. Beckman. Controls on the Longitudinal Distribution of Channel-Spanning Logjams in the Colorado Front Range, Usa. *River Research and Applications*, 30(1):112–131, January 2014. ISSN 1535-1467. doi: 10.1002/rra.2624. URL https://onlinelibrary.wiley.com/doi/abs/10.1002/rra.2624.

Ellen Wohl. Threshold-induced complex behavior of wood in mountain streams. *Geology*, 39(6):587–590, June 2011. ISSN 0091-7613, 1943-2682. doi: 10.1130/G32105.1. URL http://geology.gsapubs.org/content/39/6/587.

Ellen Wohl. A legacy of absence: Wood removal in US rivers. *Progress in Physical Geography: Earth and Environment*, 38(5):637–663, October 2014. ISSN 0309-1333. doi: 10.1177/0309133314548091. URL https://doi.org/10.1177/0309133314548091.

Ellen Wohl. Bridging the gaps: An overview of wood across time and space in diverse rivers. *Geomorphology*, 279:3–26, February 2017. ISSN 0169-555X. doi: 10.1016/j.geomorph.2016.04.014. URL http://www.sciencedirect.com/science/article/pii/S0169555X16302082.

Ellen Wohl and Natalie D. Beckman. Leaky rivers: Implications of the loss of longitudinal fluvial disconnectivity in headwater streams. *Geomorphology*, 0, 2011. ISSN 0169-555X. doi: 10.1016/j.geomorph.2011.10.022. URL http://www.sciencedirect.com/science/article/pii/S0169555X11005484.

Ellen Wohl and Kristin Jaeger. A conceptual model for the longitudinal distribution of wood in mountain streams. *Earth Surface Processes and Landforms*, 34(3):329–344, March 2009. ISSN 01979337, 10969837. doi: 10.1002/esp.1722. URL http://doi.wiley.com/10.1002/esp.1722.

Ellen Wohl, Robert O. Hall, Katherine B. Lininger, Nicholas A. Sutfin, and David M. Walters. Carbon dynamics of river corridors and the effects of human alterations. *Ecological Monographs*, 87(3):379–409, 2017. ISSN 1557-7015. doi: 10.1002/ecm.1261. URL https://esajournals.onlinelibrary.wiley.com/doi/abs/10.1002/ecm.1261.

W. M. Wollheim, C. J. Vörösmarty, B. J. Peterson, S. P. Seitzinger, and C. S. Hopkinson. Relationship between river size and nutrient removal. *Geophysical Research Letters*, 33(6):L06410, 2006. ISSN 1944-8007. doi: 10.1029/2006GL025845. URL http://onlinelibrary.wiley.com/doi/10.1029/2006GL025845/abstract.

R.S. Wotton. Temperature and lake-outlet communities. *Journal of Thermal Biology*, 20(1):121–125, 1995. ISSN 03064565. doi: 10.1016/0306-4565(94)00042-H. URL `http://linkinghub.elsevier.com/retrieve/pii/030645659400042H`.

APPENDICES

APPENDIX A

PARAMETERIZATION OF LOGGING EFFECTS

Channel Count and Wetted Width

Our dataset of includes a greater number of observations of bankfull width (n=182) than wetted width (n=115). However, as our simulation models depend on wetted width to calculate the fractional removal of nitrate (3.3), we fit a simple linear model describing the relationship between wetted and bankfull widths for the 115 data points with both metrics

$$W_w = 0.376 + W_b \cdot 0.76634 \tag{A.1}$$

where W_w and W_b are wetted and bankfull widths, respectively. As this model describes a clear and relationship between W_w and W_b, and explains 95% of the observed variation in W_w, we use the fitted relationship to calculate wetted widths for the 67 points with measures of bankfull width but not wetted width, thus expanding our dataset of wetted widths to 182 observations.

We then modeled wetted width as a function of stream drainage area (UAA) and the number of parallel channels of a reach (C_c). Using UAA as a surrogate for stream discharge, we expanded upon the general form of Leopold and Maddock Jr. [1953] to form a relationship between stream width and drainage area which includes a multiplicative effect of C_c:

$$W_w = (\beta_a \cdot UAA^{\beta_b}) \cdot (1 + \beta_c \cdot (C_c - 1)), \tag{A.2}$$

where W_w, UAA, and C_c are the wetted width (m), drainage area (km^2) and number of parallel channels of a stream reach. The first factor in equation (A.2) predicts the wetted width of a single-threaded channel, and the second factor indicates the wetted width of each additional parallel channel as a fixed proportion of the predicted single channel width. As fitted, all terms are highly significant (table A.1), and each channel additional to the first channel is estimated to increase the total wetted width by 67% of the width of a single channel reach. This model explains a substantial portion of the observed variation in wetted with, including many extreme values associated with multi-thread channels (figure A.1). Equations (A.1) and (A.2) were both included in the Monte Carlo analysis described in chapter 4.

Many other explanatory terms are potentially associated with wetted width. However, we consider this model to be sufficient for our application as it provides a reasonable representation of stream widths across the extent of our model domain, and incorporates a major driver of differences between the wetted widths stream reaches in unlogged and logged states. While incorporating additional explanatory terms could improve the accuracy of wetted widths across the simulated networks, only terms that provide greater insight into the effects of historical logging on wetted width would add value to our comparative analysis.

Estimating wetted width across the model scenarios using equation (A.2) requires us to form a quantitative description of the previously identified relationship

Term	Estimate	Std. Error	p value
β_a	2.44963	0.31495	<0.001
β_b	0.30376	0.03386	<0.001
β_c	0.67345	0.05942	<0.001

Table A.1: Fitted values and standard errors for all terms of equation (A.2)

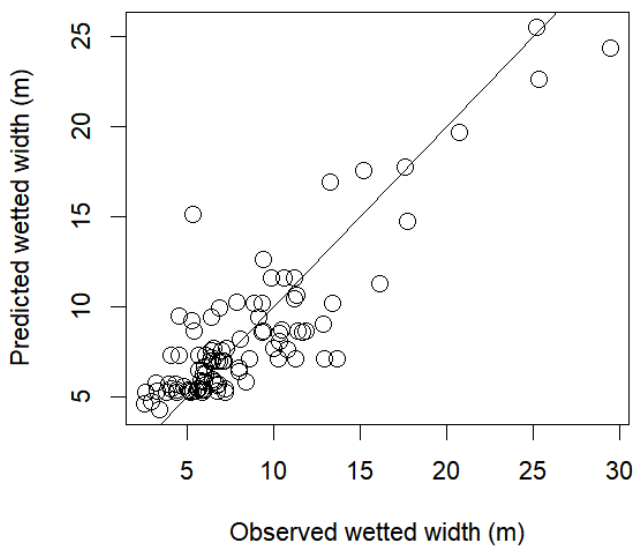

Figure A.1: Alignment between observed and predicted wetted widths

between channel complexity and historical logging [Livers et al., 2017]. Reach scale surveys of channel count (C_c) used in our analysis are comprised of multiple transects surveyed within each reach, therefore reach-scale descriptions of C_c in our dataset do not necessarily take on integer values. Across our dataset, multi-channel reaches are common within unlogged areas, with 49% of reaches (43 of 88) having at more than one channel for at least one transect within the surveyed reach (i.e, $C_c > 1$), and 30% of reaches (26 of 88) having an average of two or more channels across the transects that comprise the surveyed reach (i.e, $C_c > 1.5$). In contrast, only 11% of reaches (6 of 52) within logged areas have any evidence of multiple channels across any of the surveyed transects, and no surveyed reaches have an average of two or more channels.

We attempted to form a statistical model of C_c which accounts for the effect of logging on C_c along with morphologic characteristics of survey reaches which may also influence C_c. However, we were unable to identify specific morphologic factors

in our dataset that provided a statistically significant contribution to such a model. Therefore, we used surveyed data to describe C_c across the unlogged scenario, and applied the median value of 1 for C_c in unlogged areas to all unsurveyed reaches. We then determined the C_c for each simulated reach under the logged scenario by: 1) determining the percentile score for C_c in each reach based on the cumulative frequency distribution of the unlogged data set; and 2) using that percentile to determined the associated C_c from the cumulative frequency distribution of the logged data set (figure A.2). Thus, the simulated wetted widths of modeled reaches varied between unlogged and logged scenarios only for reaches with an unlogged C_c of greater than one.

Uncertainty surrounding the parameterization of C_c for logged scenarios was considered by forming variant parameter sets in which each surveyed reach was assigned a value of C_c that was randomly sampled, with replacement, from the population of observed C_c in logged areas.

Figure A.2: Cumulative distributions of Channel Count for unlogged and logged survey areas. Example equivalences are indicated for the 75th, 90th, and 95th percentiles, where unlogged values of 1.75, 3.6, and 4.8 equate to logged values of 1, 1.12, and 1.25 respectively.

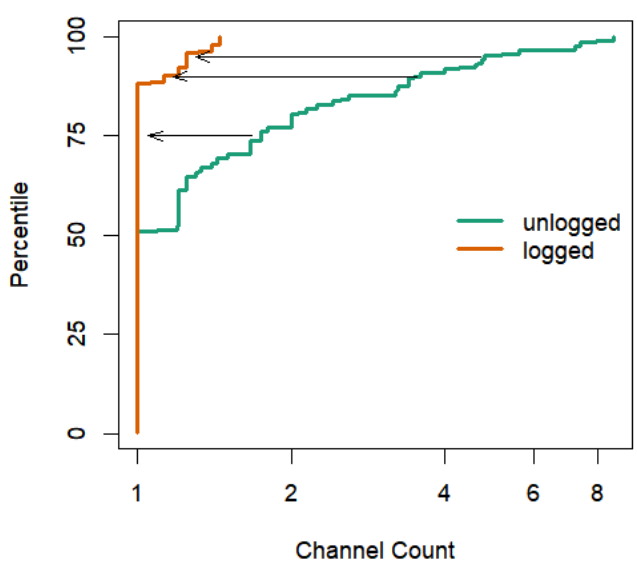

Respiration Rate

We considered stream temperature, stream sediment organic carbon content, jam density, and wood volume per area as hypothesized drivers of aerobic respiration rate. Stream temperature was hypothesized to influence respiration rates by alteration of the chemical activation energy required by aerobic metabolism, as initially described by Arrhenius [1915]. Stream sediment carbon content was hypothesized to influence respiration rates due to the reliance of aerobic heterotrophy on organic carbon as an energy source. Jam density was hypothesized to correlate with respiration rate due to the ability of jams to trap fine suspended particles, including organic particulates. Wood volume was hypothesised to correlate with respiration rate as in-stream wood represents a substantial portion of the total organic carbon contained in a stream, and potentially provides habitat for stream biota in excess of the product of stream reach length and wetted width.

These four hypotheses were tested by matching estimates of whole-stream aerobic respiration taken from Madinger and Hall [2019] with survey data collected by Livers and Wohl [2016], as these survey sites were deliberately co-located with sites for respiration measurements. Of the four hypothesized explanatory variables, only jam density was significantly associated with respiration rate (figure A.3). Further, this relationship appears to show a saturation effect wherein the effect of additional jams on respiration rate is decreased at high jam densities. While this non-linearity is driven by a single point, we consider to be potentially relevant as it is consistent with our perception of the mechanisms relating jam density and respiration rate. Specifically, the ability of an individual jam to trap organic particulates could be limited by the close proximity of upstream jams, which could reduce the supply of suspended organic particulates.

We considered both a linear relationship between respiration rate and jam density:

$$R = 3.91 + 0.053 \cdot D_j, \tag{A.3}$$

as well as a hyperbolic saturation relationship:

$$R = 1.559 + \frac{9.263 \cdot D_j}{21.057 + D_j}, \tag{A.4}$$

where R_i is the respiration rate ($g\ O_2\ m^{-2}\ day^{-1}$) of segment i, and D_j is the jam density of the surveyed reach ($count\ km^-1$). Comparison of the equations (A.3) and (A.4) models using ANOVA suggests that the improved fit of A.4 justifies the added complexity (p=0.03). We therefore accept equation (A.4) as a reasonable representation of the relationship between respiration rate and jam density.

Figure A.3: Relationship between stream respiration rate and temperature, sediment carbon, jam density, and wood volume per area. For the relationship between respiration rate and jam density, the dashed line indicates the linear fit (equation A.3), and the solid line indicates the hyperbolic saturation model (equation A.4)

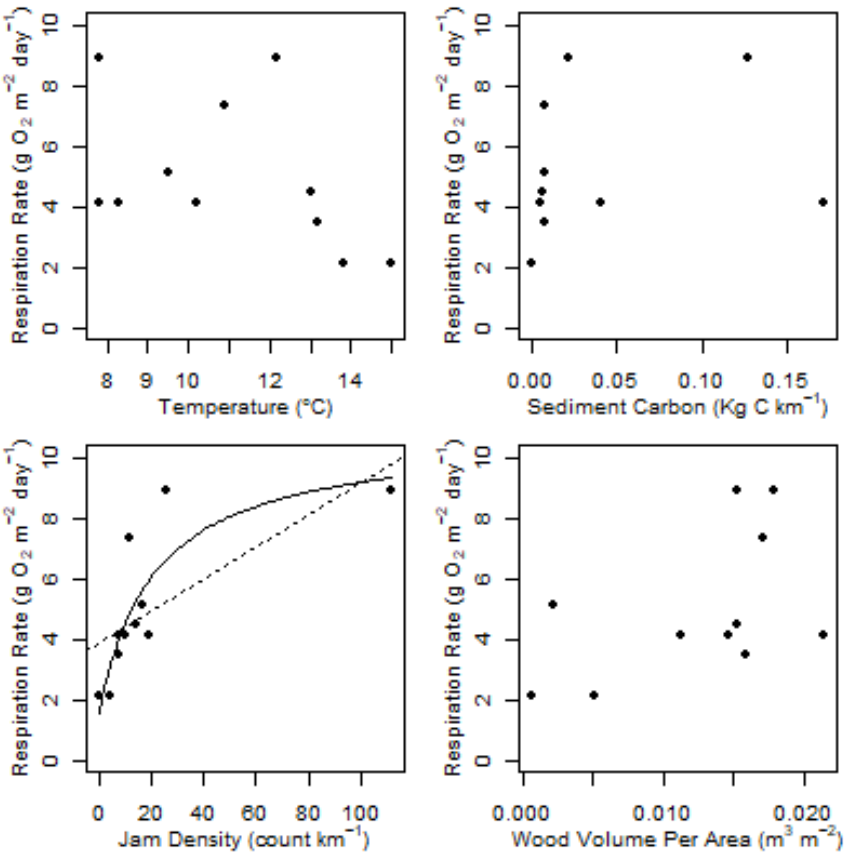

Jam Density

Jam densities were parameterized to represent historically unlogged and logged conditions, with the intention of facilitating a comparison between simulations of the NSV in its current unlogged state, and a logged representation of the NSV. Rather than develop and apply a statistical model to predict jam densities under unlogged and logged states, we parameterized the unlogged scenario directly from survey data, and parameterized the logged scenario by developing a statistical model that estimates the effect of logging on jam density, and applying that effect to observed distributions of jams across the unlogged NSV. This approach avoids injecting error into our parameterization of jams for the unlogged scenario, and also produces a reasonable estimate of jam densities across a logged representation of the NSV.

The NSV network consists of 69.6 km of streams, however, jams do not occur across the whole extent of the network. Streams above treeline do not contain jams,

and small streams with insufficient transport capacity rarely aggregate individual logs into jams [Wohl and Beckman, 2014]. Thus, we define the potentially-jammed area of the NSV as the 26.1 km of streams that are located below 3250 m of elevation, and have drainage areas larger than 4 km^2. Survey data describes jam densities across 22.8 km of stream within this potentially-jammed area, leaving 3.3 km (12%) of potentially jammed stream unsurveyed. For the unlogged scenario, full parameterization of jam density across the potentially-jammed extent of the NSV was achieved by filling in this missing data with the median value for jam density (10.5 jams km^{-1}) observed across the NSV. Jam densities for the logged scenario were then calculated by modifying jam density values from the unlogged scenario in accordance with the estimated effect of logging on jam density.

In order to form an estimate of the effect of logging on jam density, we developed multiple statistical models incorporating an effect of logging as well as effects of other landscape scale drivers on jam density. We consider it necessary to account for variation in other controls on jam density in order to reduce the likelihood of mis-attributing variation in jam density to logging, in cases where other landscape scale drivers may provide a better explanation. Therefore, we include effects of stream UAA, valley confinement, stream gradient, and stream elevation, all previously suggested as landscape-scale drivers of jam density [Abbe and Montgomery, 2003, Wohl and Beckman, 2014, Wohl and Jaeger, 2009].

We also considered incorporating interactions between logging effects and other landscape scale drivers into our analysis. However, incorporating such interactions into the estimation of jam density under logged conditions requires the interactions to be applied across the whole range of the simulated NSV network, potentially extrapolating these terms beyond the bounds of observed data. While our dataset encompasses a substantial range of landscape-scale drivers, the full ranges of stream UAA, gradient, and elevation of the potentially jammed area of the NSV are not are not present in both unlogged and logged surveys (figure A.4). In contrast, survey sites include all categorical combinations of unlogged, logged, unconfined, and confined conditions. Therefore, interactions between logging effects and confinement were allowed, while interactions between logging effects and stream UAA, gradient, or elevation were excluded from our approach.

We formed a 'global' statistical model incorporating the effects of logging stream size, stream elevation, stream gradient, and valley confinement, as well as all allowable

Figure A.4: Ranges of UAA, gradient, and elevation observed in the potentially jammed area of the NSV, as well as in all unlogged and logged surveys. Unlogged survey data does not cover the full range of stream gradients observed within the NSV, and logged survey data do not cover full ranges of stream UAA, gradient, or elevation observed in the NSV. The extent of data across confined and unconfined reaches within logged and unlogged areas is not shown, as it is a comparison between two categorical variables.

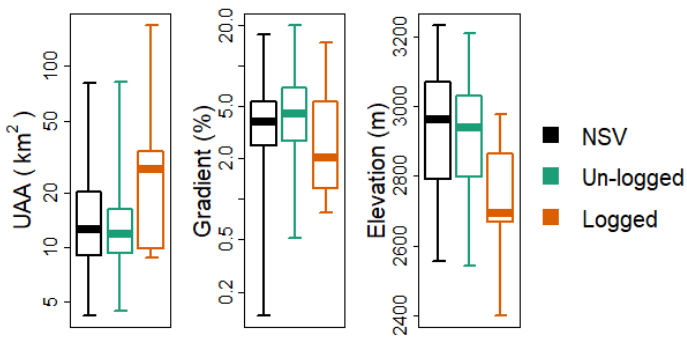

interactions:

$$
\begin{aligned}
C_j \;\approx\; exp\Big(&\alpha + \beta_L Logged + \beta_U log(UAA) + \beta'_U log(UAA)^2 + \beta_E C_E + \beta_G C_G + \beta_C Conf \\
&+ \beta_{UE} log(UAA) \cdot C_E + \beta'_{UE} log(UAA)^2 \cdot C_E \\
&+ \beta_{UG} log(UAA) \cdot C_G + \beta'_{UG} log(UAA)^2 \cdot C_G \\
&+ \beta_{UC} log(UAA) \cdot Conf + \beta'_{UC} log(UAA)^2 \cdot Conf \\
&+ \beta_{EG} C_E \cdot C_G + \beta_{EC} C_E \cdot Conf + \beta_{GC} C_G \cdot Conf \\
&+ \beta_{LC} Logged \cdot Conf \\
&+ offset(log(L_C))\Big)
\end{aligned}
\tag{A.5}
$$

where *Logged* is a boolean description of the logging status, C_E is the channel elevation, and C_G is the channel gradient. This model was fitted as a negative binomial regression, using a natural log linkage between the explanatory and response variables. We use jam count as a response variable, however we include the natural log of channel length (L_C, in km) as an offset term in order to normalize the fitted jam counts to a 1 km reach. The inclusion of the first and second order UAA terms allows for jam densities to be highest at intermediate values of UAA, consistent with previous suggestions of maximum jam densities in streams of intermediate sizes where transport capacity is sufficient to for jams, but insufficient to break them [Wohl and Beckman, 2014].

While this global model (equation A.5) includes all allowable terms and

interactions, it may not represent the optimal combination of terms. As our goal is to produce an accurate estimate of the effect of logging, we favor parsimonious models that include terms sufficient to account for logging effects as well as other factors effecting jam density, without including an excessive number of terms and interactions which could reduce the accuracy of individual terms. Therefore, we ranked all of the possible models by AICc scores, and identified the set of models that are likely to minimize information loss as those models with $\Delta AIC <= 2$. Of the numerous possible models considered by this process, we identify three top-ranked models which meet this criteria (table A.2).

The top ranked model represents the effect of logging on jam density with a single term (β_L), suggesting that the effect of logging in our dataset can be described as causing a consistent, fractional decrease in jam density that does not interact with other factors:

$$\begin{aligned} C_j \approx\ & exp\Big(47.0 - 0.74Logged - 28.8log(UAA) + 4.57log(UAA)^2 - 0.016C_E \\ & - 0.01C_G - 43.6Conf + 0.0108log(UAA) \cdot C_E - 0.0018log(UAA)^2 \cdot C_E \\ & + 59.4log(UAA) \cdot Conf - 11.1log(UAA)^2 \cdot Conf - 0.012C_E \cdot Conf \\ & + 0.79C_G \cdot Conf + offset(log(L_C))\Big), \end{aligned} \tag{A.6}$$

where all terms are consistent with equation (A.5). As this model is fitted using a natural-log linkage between the explanatory and response variables, the density of jams under logged conditions can be calculated as:

$$D_{j,logged} = e^{\beta_L} \cdot D_{j,unlogged}, \tag{A.7}$$

where $D_{j,logged}$ is the expected jam density that would occur given the observed unlogged jam density $D_{j,unlogged}$, and β_L is the fitted coefficient for the effect of logging on jam density. Thus, equation (A.6) indicates that logging reduces jam density to 47.5% of the unlogged value. We note that the 2nd through 4th ranked models show similar logging effects (indicating reductions in jam density to 50.7%, 52.2%, and 42.7% of the unlogged value, respectively), and that, for all of these models, there is no interaction between the effect of logging on jam density and other factors. Uncertainty surrounding this value was incorporated into the Monte Carlo simulations by re-fitting equation (A.6) to a resampled dataset, thus producing variant values for the effect of logging on jam density.

As our intention is to produce a representation of jam densities across the NSV which is typical of jam densities in nearby logged networks, we validated our approach by comparing the simulated jam densities for the logged scenario to observed jam densities. The distribution of simulated jam densities for logged conditions across the NSV aligns closely with the distribution of jam densities across all logged survey

Table A.2: Fitted coefficient values, coefficients of determination, and AICc scores for the 10 most optimal sub-models of equation (A.5), as identified by AICc analysis.

Rank	α	β_L	β_U	β'_U	β_E	β_G	β_C	β_{UE}	β'_{UE}	β_{UG}	β'_{UG}	β_{UC}	β'_{UC}	β_{EG}	β_{EC}	β_{GC}	β_{LC}	R^2	df	ΔAIC
1	47.0	-0.74	-28.8	4.57	-0.016	-0.01	-43.6	0.0108	-0.0018			59.4	-11.1		-0.012	0.79		0.66	14	0.00
2	39.5	-0.68	-28.3	4.71	-0.014	0.92	-40.7	0.0106	-0.0018			59.5	-11.2	-0.00032	-0.013	0.86		0.67	15	0.53
3	60.1	-0.65	-38.2	6.09	-0.020	-0.24	-40.3	0.0136	-0.0022	0.03	0.03	57.0	-10.6		-0.012	0.81		0.68	16	1.11
4	45.8	-0.85	-27.5	4.44	-0.016	-0.01	-69.2	0.0104	-0.0017			49.9	-9.0			0.64		0.64	13	2.30
5	46.9	-0.70	-28.8	4.56	-0.016	-0.00	-40.5	0.0108	-0.0018			53.1	-9.8		-0.010	0.74	-0.79	0.66	15	2.39
6	53.9	-0.61	-37.6	6.21	-0.018	0.52	-38.2	0.0135	-0.0023	-0.01	0.03	57.1	-10.6	-0.00025	-0.013	0.87		0.68	17	2.80
7	46.0	-0.72	-27.9	4.44	-0.016	-0.01	-56.9	0.0105	-0.0017			40.3	-7.1			0.57	-1.63	0.65	14	2.81
8	39.4	-0.63	-28.3	4.69	-0.014	0.92	-37.4	0.0106	-0.0018			53.0	-9.8	-0.00033	-0.012	0.81	-0.82	0.67	16	2.93
9	62.2		-41.1	6.55	-0.021	-0.12	-40.4	0.0146	-0.0024	-0.10	0.06	62.4	-11.7		-0.014	0.84		0.66	15	3.32
10	60.1	-0.60	-38.2	6.07	-0.020	-0.24	-37.1	0.0136	-0.0022	0.03	0.03	50.5	-9.3		-0.011	0.76	-0.84	0.68	17	3.54

sites (figure A.5), with the exception of a small number of simulated reaches with jam densities that exceed the range of jam density observed within logged areas. We examined this discrepancy, and identified two likely causes. Firstly, the number of observations from logged survey sites is much smaller (n=19) than the number of simulated jam densities for all potentially jammed reaches across the NSV (n=51). Thus, the occurrence of larger jam density values in the simulated dataset than in the observed dataset may simply arise from the larger sample, and may not necessarily indicate inaccuracies in the simulated data. Additionally, the high values contained within the simulated data fall within the range of moderate UAA values which corresponds with maximal jam density, a range that is poorly covered by the observational data from logged survey sites (figure A.6). Therefore, it is not possible to determine weather the high values of jam density in some simulated reaches represent conditions which are not present in our observed dataset, or alternatively, if these high values are unreasonable. Given the broad agreement between the distributions of observed and simulated data for logged conditions, we are confident that our method for estimating jam density under logged conditions is appropriate for our heuristic purposes.

Figure A.5: Observed distribution of jam densities under unlogged conditions, along with observed and simulated distributions of jam densities under logged conditions.

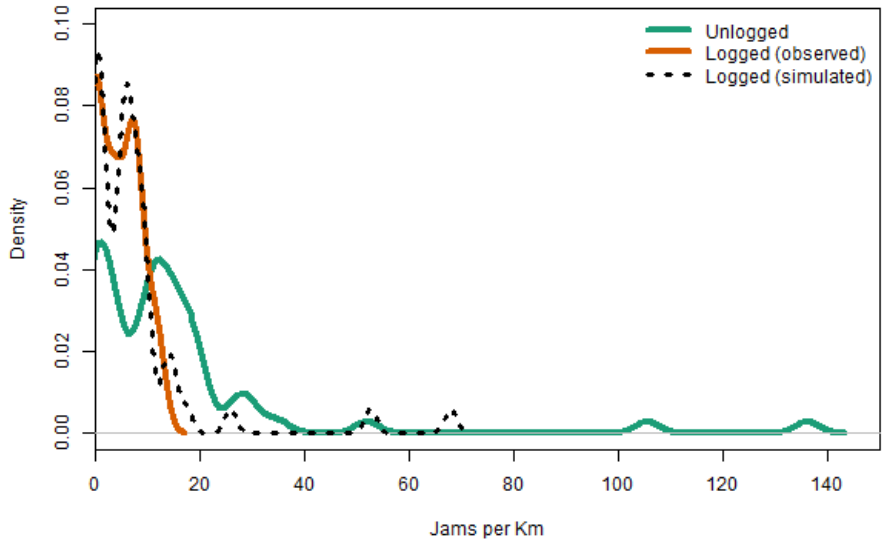

Our empirical model of historical logging on jam density and multi-thread channels comprises a quantitative restatement of previously described findings [Wohl, 2011, Wohl and Jaeger, 2009, Wohl, 2014, Livers et al., 2017]. It was necessary for us to rework these findings in order to provide a quantitative foundation for the

Figure A.6: Relationship between jam density and UAA for observed unlogged and logged survey sites, along with simulated logged conditions

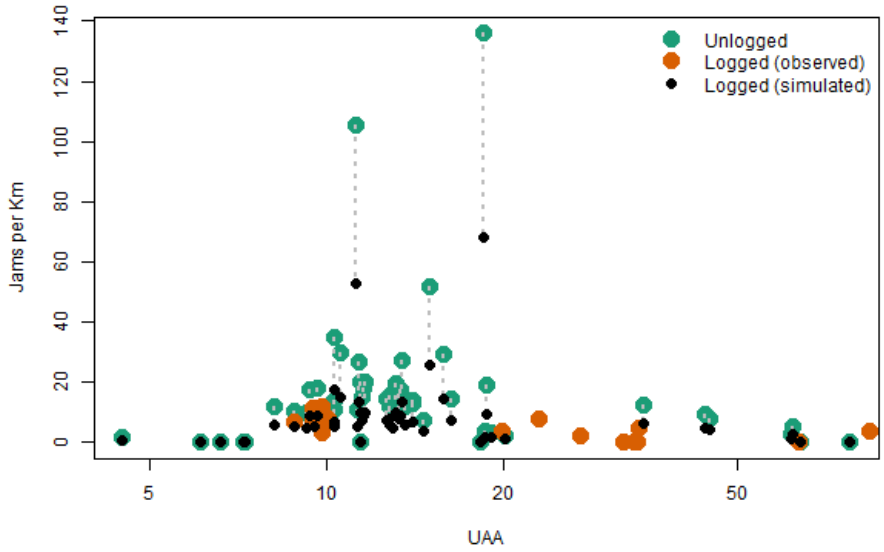

parameterization of our model, however, we emphasize that our findings regarding the effects of historical logging on jam density and multi-thread channels are not novel, nor are they an independent verification of previous findings, as the underlying data are the same.